Experimental Investigations of Surface Magnetism

Harry R. Borsje

Experimental Investigations

of

Surface Magnetism

Experimental Investigations of Surface Magnetism

een wetenschappelijke proeve op het gebied van
de natuurwetenschappen

Proefschrift

ter verkrijging van de graad van doctor aan
de Katholieke Universiteit te Nijmegen,
volgens besluit van het college van decanen
in het openbaar te verdedigen op
woensdag 20 februari 1991,
des namiddags te 3.30 uur

door

Harry Ronald Borsje

geboren op 8 juli 1962 te Rotterdam.

1991
Offsetdrukkerij Haveka B.V.,
Alblasserdam

Promotor: Prof.Dr. J.C. Fuggle, D.Sc.

This work has been supported by the Stichting voor Fundamenteel Onderzoek der Materie (FOM) with financial support from the Nederlandse Organisatie voor Wetenschappelijk Onderzoek (NWO).

CIP-gegevens Koninklijke Bibliotheek, Den Haag

Borsje, Harry Ronald

Experimental investigations of surface magnetism / Harry Ronald Borsje. - [S.l. : s.n.]. - III.
Proefschrift Nijmegen. - Met lit. opg. - Met samenvatting in het Nederlands.
ISBN 90-9003933-3
SISO 535 UDC 537.6(043.3)
Trefw.: magnetisme.

Throughout the history of magnetism experiment, theory and speculation have all played their part. [...] It is the insight and the genius of the few—the great scientific artists—which have made clear the straight paths through the chaos of uncoordinated phenomena; they have conceived and revealed a design running through the whole; but it is the untiring skill and patient labour of the many that have given to their visions significance and reality.

—E.C. Stoner

To Lilian
Stephanie
Dominique

PREFACE

This thesis describes the work I performed in the period of september 1985 until march 1990. The subjects of the various projects I participated in have been quite diverse, but they do have one common feature, which is expressed by the title of this thesis: experimental investigations of surface magnetism.

To clarify and "review" the relevant aspects of magnetism for this work Chapter 1 gives a short account of the historical development in the experimental and theoretical understanding of the phenomena associated with magnetism, as well as a survey of some important experimental techniques that can be applied to investigate these phenomena, mainly from a spectroscopists view. It also tries to indicate which aspects of magnetism are still not completely understood or cannot yet be described adequately by theory, and are therefore in need of further experimental investigation. The development of novel experimental techniques and alternative methods to obtain information on the state and behaviour of magnetic systems is the subject of the remaining chapters.

Chapter 2 describes the implementation of such a novel technique, namely BISCEPS: bremsstrahlung isochromat spectroscopy combined with electrons with polarized spin, designed to study the unoccupied electronic states of magnetic materials. Next to the occupied states, the unoccupied states are also important for the physical properties of magnetic materials. The occupied states can be studied with spin-resolved photoemission and BISCEPS now offers the possibility to study the unoccupied states on the same footing. This technique is at present still quite unique in the world. Therefore, the technical design aspects are enlightened in this chapter. In Chapter 3 two applications of BISCEPS are presented. The spin-resolved unoccupied states of the elemental ferromagnet nickel have been studied at room temperature. These measurements demonstrate the feasibility of BISCEPS. Another application, which is at present still in progress, is the determination of the magnetic coupling between thin ferromagnetic gadolinium overlayers and a nickel substrate at low temperature. This system is representative of an important class of materials and systems currently enjoying great interest all over the world. These applications therefore also serve as examples of what kind of information can be obtained, on which kind of systems, by BISCEPS.

The temperature dependence of the electronic structure of magnetic systems is the subject of Chapter 4. In contrast to the ground-state properties of magnets, the

finite-temperature behaviour—on a microscopic, i.e., not phenomenological scale—is in many cases not well understood. During the last decade much theoretical effort has been put into this subject. Yet, relatively little experimental data has become available. In this chapter we describe the application of an existing technique—photoemission spectroscopy in the Cooper minimum—to extract information on the temperature behaviour of a fundamental property of magnetic systems: the local exchange splitting.

Finally, in Appendix A, measurements are reported with a surface-enhanced implementation of Mössbauer spectroscopy, the 30 years old technique that has had such a large impact on the field of magnetism. These measurements were undertaken in order to establish whether this technique can really be made surface-sensitive on the same scale (inverse) photoemission is. In that case surface Mössbauer spectroscopy would provide additional information on the same sample region, thereby serving as a cross-check for observed effects.

The latter work was performed in collaboration with Zbyszek Stadnik from Dalhousie University (Canada) and Ad Swolfs. The Cooper minimum data were collected during a stay at the BESSY synchrotron in Berlin, together with Ronald Kappert, with assistence from Hendrik Haak and Karsten Horn from the Fritz-Haber Institut, Berlin (FRG). The construction and operation of the BISCEPS system has benefitted from the concientuous efforts of Henk Jongbloets during the design phase, and from the experimental collaboration with Ronald Kappert and Jan Vogel. Also the collaboration with Santos Alvarado and Maurice Campagna, at that time both at the KFA Jülich (FRG), during the initial phase of the BISCEPS project is gratefully acknowledged. The experimental work on gadolinium overlayers on nickel was given impetus during a stay at the ETH Zürich (Switzerland). The hospitality of the ETH and of Martin Landolt, Oliver Paul and others is remembered with gratitude.

There has been numerous discussion, argument and small-talk with my collegues Hugo, Henk, Jeroen, Hans, Pieter, Wiesiek, Ronald, Frank, Miguel, Klaus and Jan as well as with the students and many others of the department of Molecular Spectroscopy. I wish to thank them all. Last, but not least, I thank John Fuggle for offering me a position in his group at the University of Nijmegen, and for stimulating me in my work in his very own way.

Harry R. Borsje
Nijmegen, Februari 1991

CONTENTS

1 Magnetism **1**

1.1 Historical Background 1
1.2 The Magnetic Ground State 2
1.2.1 Insulators 3
1.2.2 Metals 4
1.2.3 Anisotropy 6
1.3 Finite Temperature 6
1.3.1 Excitations 6
1.3.2 The Phase Transition 7
1.3.3 The Paramagnetic Phase 9
1.4 Surface-Induced Effects 10
1.4.1 Band Narrowing 10
1.4.2 Surface States 11
1.4.3 Surface Magnetization 12
1.4.4 Surface Phase Transition 12
1.5 Theoretical Models 13
1.5.1 Ground State Calculations 13
1.6 Experimental Techniques 15
1.6.1 Polarized Electrons 16
1.6.2 Emission Techniques 18
1.6.3 Techniques Involving Scattering 21
1.6.4 Microscopy 24
1.7 Future Prospects 25
1.8 References 27

2 Bremsstrahlung Isochromat Spectroscopy with Spin Polarized Electrons **37**

2.1 Introduction 37
2.2 Technical Description 39
2.2.1 Vacuum Chambers 39
2.2.2 Sample Mounting Facilities 41
2.2.3 The Monochromator 41
2.2.4 X-ray Detection 43

2.2.5 The Spin Polarized Electron Source 44
2.2.6 Electron Optics 48
2.2.7 Measurement Control 49
2.3 Concluding Remarks 49
2.4 References 51

3 Applications of BISCEPS **57**
3.1 BISCEPS of Ni(110) 57
3.1.1 Sample Preparation 58
3.1.2 Experimental Results 58
3.1.3 Comparison with Theory 62
3.1.4 Discussion 68
3.2 Gd Overlayers on Ni(110) 69
3.2.1 Thin Film Preparation 70
3.2.2 BIS Experiments 72
3.2.3 Discussion 75
3.3 Outlook 76
3.4 References 77

4 Finite Temperature Magnetism **83**
4.1 Introduction 83
4.2 Experimental Details 85
4.3 Results and Interpretation 86
4.4 Discussion 89
4.5 Concluding Remarks 91
4.6 References 93

A Surface Mössbauer Spectroscopy **97**
A.1 Introduction 97
A.2 Design Considerations 99
A.3 System Description 100
A.4 System Operation 102
A.5 Discussion 105
A.6 References 108

Summary **111**

Samenvatting **113**

Curriculum Vitae **115**

List of Figures

2.1 BISCEPS apparatus 40
2.2 Johann and Johansson monochromator design 42
2.3 BISCEPS monochromator 43

3.1 Ni(110): total and asymmetry spectrum. 59
3.2 Ni(110): spin-up and spin-down spectrum. 61
3.3 Spin-polarized DOS of Ni: total/asymmetry. 63
3.4 Spin-polarized DOS of Ni: spin up/spin down. 64
3.5 Quasiparticle DOS of Ni. 67
3.6 BIS of 25 Å Gd/Ni(110). 73
3.7 BIS of 3 Å Gd/Ni(110). 74

4.1 Photoemission of disordered binary alloys below and above T_c 87
4.2 Model calculation of Fe impurity LDOS 90
4.3 Model calculation of Ni impurity LDOS 91

A.1 Schematic view of electrostatic spherical analyzer 101
A.2 Electron energy spectrum of ^{57}Co-decay 103
A.3 Conversion electron Mössbauer spectra of ^{57}Fe samples 104

1. MAGNETISM

The general subject of the experimental work described in this thesis is magnetism, especially in the near-surface region of metallic solids, probed with (electron-) spectroscopic techniques. This introductory chapter will review the relevant general aspects of the field, from the spectroscopists point of view.

1.1. Historical Background

Magnetism was first reported in literature about 2800 years ago in Greece,[1,2] although it seems reasonable to assume that the effects of magnetism, i.e., the attraction of iron by magnetite (Fe_3O_4), must have been known to man ever since the Iron Ages. The Greek philosophers, and many others in the centuries that followed, explained the observed phenomena by theories ranging from the idea that magnets posessed a soul to the assumption that magnets emitted invisible particles mediating the presence of a magnet to a piece of iron.[2] It took until the end of the sixteenth century before a more empirical approach was pursued. Magnetism, as did many other fields in physics and chemistry, slowly became a more active field of research, both experimentally and theoretically.

In 1820, Oersted[3] was the first to establish the connection between magnetism and electricity. This marked the start of a host of developments in the new field of electromagnetism, including the formulation of Maxwell's equations. The next landmark was the discovery of the electron at the end of the nineteenth century.[4] Initially, this electron was attributed a discrete charge only. It was not until 1921 that the electron was proposed to possess also a spin and hence a magnetic moment,[5] and it took until 1925 before this could be experimentally proved.[6]

In the meantime, Weiss[7] was the first to present a modern, yet phenomenological theory of magnetism, describing both the ferro- as well as the paramagnetic state by means of a "molecular" or "mean field". A feature of this model that still stands is the Curie-Weiss law[7,8] for the paramagnetic susceptibility of ferromagnetic materials, which, to first order, is obeyed by all known ferromagnets.

As a result of progress made in various fields of physics, including magnetism, the firts decades of the twentieth century witnessed the development of quantum theory with the concepts of quantization, angular momentum, the magneton, etc. This evolved into the description of matter by wave mechanics and the Schrödinger

equation. Around 1928 Heisenberg[9] and Dirac first explained ferromagnetism as the consequence of so-called *exchange interaction*: the interaction between two spins, dependent upon their relative orientation, ultimately driven by electrostatic instead of magnetic forces.

On the experimental side the amount of available data was also expanding fast. Hund postulated his phenomenological rules for the quantummechanical ground state and magnetic moment of free atoms and ions. At the same time, however, measurements of the gyromagnetic ratio showed that in most ferromagnetic metals the angular momentum is largely quenched and primarily the electron spins determine the magnetic moment. It was also known from magnetization measurements that in metallic magnets the magnetic moments per atom are often not integer multiples of the Bohr magneton.

By the year 1930,[10] it was believed that magnetism could be described to satisfaction by the Weiss mean field theory on the macroscopic scale and by the Heisenberg Hamiltonian on the microscopic scale, assigning fixed-amplitude (atomic) magnetic moments to the atoms in a solid on the basis of the Heitler-London approximation.

Then, Bloch[11] showed that, in a Hartree-Fock approximation and under very special circumstances, i.e., extremely low electron density, magnetism could also occur in the nearly-free electron gas, i.e., from electrons described by a band picture, as opposed to the Heitler-London description, which starts out from localized electrons. This opened the way to new theories and led to the development of Stoner's theory of collective-electron magnetism.[12] In this model the magnetic electrons participate directly in the conduction, i.e., they are itinerant, in contrast to the Heisenberg model in which the magnetic electrons are localized and where a different set of electrons accounts for any conduction.

In the years that followed, until this day, both theoretical approaches have had their supporters. More sophisticated theories have been developed on either basis. Nowadays, wide application of large computers allows numerical calculation of complex quantum mechanical systems, and modern experimental techniques, such as (polarized) neutron scattering and photoemission, allow access to the electronic and magnetic structure of solids and surfaces. The available data now seems to confirm what perhaps more open-minded researchers have argued all along, namely that "the true state of affairs is in between" these models [Van Vleck[13]].

1.2. The Magnetic Ground State

In solids, the preference for any (ordered) magnetic ground state is determined by a detailed balance between the energies associated with several interactions in the system. These include the (intra-atomic) Coulomb and exchange interactions, and the hybridization between states on different atoms. Free atoms have magnetic moments for all elements with partially filled shells, i.e., Hund's first rule prescribes that the

electron spins in the outer, partially filled shell order themselves in such a way that the total spin is maximized. The microscopic origin for this phenomenological law is formed by the *electrostatic* or Coulomb interaction between the charged electrons. Electrons with parallel spins will, on the average, be further apart because of the Pauli exclusion principle which requires that the spatial part of their total wavefunction has to be antisymmetric. As a result, the electrostatic interaction energy is lower for parallel-spin electrons than for antiparallel-spin (paired) electrons and a so-called high-spin configuration is energetically favoured. This is the exchange interaction.

In spite of this strong effect, magnetism is not the rule but the exception in solids. This is caused by the the fact that, as the overlap between wavefunctions from neighbouring atoms becomes larger, the electrons become delocalized and the energetically well-defined atomic states broaden into bands. This lowers the total energy of the system. Favouring one spin-subband over the other results in an increase of the total kinetic energy of the electrons occupying these bands, which in most cases more than balances the energy gained by making more spins parallel. In insulators, also crystal field effects can force a system in a low-spin configuration if, for instance, the crystal field splitting between states, that would otherwise have to be occupied, is larger than the gain in exchange energy.

1.2.1. Insulators

In insulators it takes a finite amount of energy to move an electron from one site to another. An actual energy gap can exist when the inter-atomic interactions favour filled bands, like in ionic compounds, but also in strong covalent materials like, e.g., Si. Another mechanism is strong intra-atomic interaction in partially filled bands. In this case the addition of an electron to one site costs more energy than is gained by removing it from another site. Such systems are known as Mott-Hubbard insulators.[14–18] In systems with filled bands it would be necessary to fill states above the gap to obtain a magnetic moment, which often costs more energy than can be gained. In Mott-Hubbard insulators, on the other hand, the hybridization is smaller and the bands are narrower, which enhances the intra-atomic Coulomb and exchange interaction and hence the possibility of an (antiferro-)magnetic ground state.

If magnetic moments are present in an insulator, they are spatially localized to the atomic sites and they have a fixed amplitude. In that case the system can be described by a Heisenberg Hamiltonian of the general form $J\boldsymbol{S}_i \cdot \boldsymbol{S}_j$. The exchange coupling parameters J between the magnetic moment vectors $\boldsymbol{S}$ are very difficult to calculate from an *ab initio* theory. They can be derived from, e.g., neutron scattering measurements of the spin wave dispersion,[19,20] although in some cases insight can also be gained from standard ground state electronic structure calculations.[21] By performing a total energy calculation for the magnetic ground state as well as for

(all) other configurations in which the magnetic moment at one particular site is flipped, the exchange coupling parameters between the magnetic moments can be derived in terms of energy differences. If the J's are known, both the ground state as well as the finite temperature behaviour of the material can be accurately calculated from the Heisenberg Hamiltonian.

In this respect, rare earth metals act very much like insulators. This is caused by the fact that the partially filled $4f$ wavefunctions are very contracted and have very little overlap, if any, with each other and therefore the electrons experience a large Coulomb interaction. The result is that the $4f$ electrons are localized and even show to a large degree atomic behaviour, e.g., in assuming magnetic moments according to Hund's rules. The other partially filled shells, i.e., $5d$ and $6s$, form wide bands and are responsible for the metallic properties. These conduction electrons are polarized by the local moments and thus provide the coupling between the moments on neighbouring sites. This is called indirect exchange interaction.

The ground state configuration of local magnetic moments and the behaviour at finite temperature is influenced not only by the exchange interaction but also by crystal field effects. The crystal field determines the energy associated with the orientation of local orbitals in the electric field caused by the charges in, and with the symmetry of, the lattice. In this way it also influences the preferential orientation of local magnetic moments in the lattice [see Sec. 1.2.3].

1.2.2. Metals

In magnetic metals, other than rare earths, the situation is more complicated. Early experiments[22] already showed that, even in elemental metallic ferromagnets, i.e., Fe, Co, and Ni, the magnetic moment per atom is not an integer multiple of the Bohr magneton.[20] As the orbital contribution to the moment in transition metals is largely quenched, this moment is built up mostly from electron spins, or more precisely, from $3d$-electron spins. The reason why these materials are magnetic lies in a combination of circumstances. The late $3d$ transition metals have a sizeable intra-atomic exchange interaction because, even in the solid state, the $3d$-bands are spatially not very extended, in contrast to s- and p-bands. The second property that is beneficial, related to the first, is the small $3d$-bandwidth.

Whether the $3d$-electrons actually from a band and participate in the conduction has, as a matter of fact, long been an unresolved question, that was not settled until exeprimental data showing the itineracy of the $3d$-electrons became overwhelming. This included specific heat data,[23,24] cohesive energy data,[25,26] and de-Haas-van-Alphen measurements,[27–30] which all showed the presence of $3d$-electrons at the Fermi surface. Valence-band photoemission,[31–33] in conjunction with theoretical bandstructure calculations,[34,35] revealed directly the finite $3d$-bandwidth.

A theory to describe magnetism as a cooperative phenomenon, i.e., one in which

all valence electrons take equal part, was originally developed by Stoner.[12]

The Stoner model is essentially a mean field model in the Hartree-Fock approximation (HFA). The individual magnetic moments, once they exist, constitute a mean magnetic field, just like an external field. This mean field in turn interacts with the electronic structure which has been calculated separately. The electron subbands for each spin direction then shift in energy, according to whether the electron spins are parallel or antiparallel to the magnetic field, resulting in the so-called exchange splitting Δ. The shifting bands result in a redistribution of electrons among the spin-up (= parallel, majority) and spin-down (= antiparallel, minority) states. In order to preserve charge neutrality, the Fermi level has to shift accordingly. The coupled set of equations describing this situation leads to a self-consistent solution with a finite spontaneous magnetization if

$$\mathrm{I} \cdot \mathrm{N}_0(\mathrm{E}_F) > 1 \,. \tag{1.1}$$

Here, I is the intra-atomic (Hund's rule) exchange interaction and $\mathrm{N}_0(\mathrm{E}_F)$ is the paramagnetic density of states at the Fermi level. Equation 1.1 is known as the Stoner criterium. It reflects the condition for which the increase of the energy of the system, due to an infinitessimal and rigid shift of the electronic energy bands, is overcome by the decrease in energy due to the reduction of electron interaction energy. This universal energy argument, which is valid as long as higher order terms in the energy balance are not important, provides a systematic path to search for new magnetic materials, also with the modern calculational techniques.[36–38]

An alternative, macroscopic way to see what happens, is by means of the susceptibility χ, which is the derivative of the magnetization as a function of the externally applied field. Several mechanisms determine the susceptibility of a system and one of them is the Pauli spin susceptibility $\chi_{\mathrm{P}} = \mu_{\mathrm{B}}^2 \mathrm{N}_0(\mathrm{E}_F)$. This describes the response of the conduction electrons in a metal to an external field. With a sizeable value of I, the susceptibility of the system is enhanced over this value by exactly the Stoner factor, reflecting the ease and tendency of the system to accommodate an externally induced magnetic moment by rearranging the electrons at the Fermi level:

$$\chi = \frac{\mu_{\mathrm{B}}^2 \mathrm{N}_0(\mathrm{E}_F)}{1 - \mathrm{I} \cdot \mathrm{N}_0(\mathrm{E}_F)} \,. \tag{1.2}$$

As the enhancement factor becomes larger the susceptibility finally diverges and the system will exhibit a spontaneous magnetization.

Whether the tendency to exhibit a magnetic ground state will express itself in a ferro- or antiferromagnetic configuration depends on an even more subtle energy balance. For instance, when the *d*-band is close to half-filled the intra-atomic exchange stabilization for parallel spins tends to counteract the hopping (delocalization) of electrons if the nearest-neighbour ordering is ferromagnetic. Antiferromagnetic ordering avoids this, as is shown by the antiferromagnetic ground state of Cr and Mn.

1.2.3. Anisotropy

It has already been mentioned that the spatial configuration of magnetic moments can be influenced by crystal field effects. The crystal field is an electric field caused by charges in the lattice. The field therefore has the same spatial symmetry as the crystal. Purely by group-theoretical arguments orbitals with different m_ℓ quantum number, that were initially degenerate, will become split reflecting the different energies associated with their orientation in the crystal field. The size of the splitting and the ordering of the orbitals depends on the chemical and structural details of the material. For materials with L = 0, i.e., with all m_ℓ substates equally populated, there is no net effect. This is the case for, e.g., Gd. Other rare earths and transition-metal compounds do show crystal field effects. If the crystal field is not too strong the occupation of m_ℓ substates will still be governed strictly by Hund's rule, as in many rare earths. The crystal field then perturbes the orientation of the local magnetic moment with respect to the "exchange-only" situation, resulting in exotic spin structures. If the crystal field splittings between m_ℓ substates are comparable to thermal energies temperature will have a large influence on their relative occupation, which in turn is reflected in complicated magnetic behaviour of such a material.[39]

Although in transition metals the orbital moment is not a constant of motion and is quenched, the fact that the gyromagnetic ratio g deviates from the theoretical spin-only value of 2 indicates that crystal field effects might still play a role. It results in preferential crystallographic orientations for the overall magnetization. This is known as magnetic anisotropy.[40]

It is important to note that the surface, by changing the local symmetry, can also change the anisotropy behaviour.[41–44]

1.3. Finite Temperature

As mentioned above, the finite temperature properties of insulator and rare earth magnets, i.e., local moment systems, can be described satisfactory as soon as the exchange coupling constants and crystal field parameters are (experimentally) known. In the following we will therefore focus on itinerant-electron magnetic systems.

1.3.1. Excitations

In Heisenberg systems, the elementary excitations are propagating transverse oscillations of the magnetic moments around their equilibrium direction. These modes, which are analogous to, e.g., phonons, are known as magnons or spin waves. As these magnons obey Bose-Einstein statistics, Bloch[45] already deduced in 1930 the important result that in one or two dimensions no ferromagnetism can exist at non-zero temperature for a system described by an isotropic Heisenberg Hamiltonian.[46]

In other words: *magnetism at finite temperature is only possible in three dimensions or, in lower dimensions (e.g., at surfaces), in the presence of anisotropy.*

Ferromagnetic spin waves obey a quadratic dispersion law at long wavelengths:

$$\hbar\omega(q) = Dq^2 \,. \tag{1.3}$$

D is the spin wave stiffness which can be determined by neutron scattering measurements, which makes it possible to experimentally deduce the exchange coupling parameters for a Heisenberg description of the system.

In Stoner theory the elementary excitations are single-particle spin-flip excitations: an electron at the Fermi level with spin σ is transferred to an empty state with spin $-\sigma$. If there is no net momentum transfer involved in the transition, i.e., $\boldsymbol{q} = 0$, the energy transfer $\hbar\omega$ has to be large enough to exactly overcome the exchange splitting Δ between the σ and $-\sigma$ bands. As $\boldsymbol{q}$ increases the required energy is reduced because of the dispersion of the electronic bands in reciprocal space, and a continuum of excitations exists in a large part of $\boldsymbol{q}$-$\hbar\omega$ space. From simple energetic arguments it is obvious that there also have to be other excitations. Thermal energies, associated with the critical temperatures of metallic magnets, e.g., Fe, are of the order of 100 meV, whereas the exchange splitting is of the order of 2 eV. Spin waves in itinerant magnets have been measured and the associated spin wave stiffness, again for Fe, is $\sim$ 300 at T = 0. By applying dynamical mean field methods, i.e., the random phase approximation RPA, it is possible to incorporate spin waves in Stoner theory, which then, apart from the ground state, is also able to describe the low-temperature properties. In that case, spin waves exist only in that region of phase space that is not occupied by the Stoner continuum, i.e., at both small $\boldsymbol{q}$ and small $\hbar\omega$. In fact, as the behaviour of (long-wavelength) spin waves in itinerant magnetic systems and in Heisenberg systems is identical and because Stoner excitations do not play a large role at low temperatures, one can describe an itinerant magnet by an effective Heisenberg Hamiltonian for temperatures up to about half the critical temperature.[47] The previously mentioned method to deduce exchange coupling parameters from total energy calculations can also be applied to itinerant systems. In that case the size of the magnetic moments, however, depends on the imposed configuration, i.e., the magnetic moments do not have a fixed amplitude, unlike in a real local moment system.[21]

1.3.2. The Phase Transition

As the temperature is increased any physical system will try to increase its entropy, i.e., the degree of disorder. Eventually, this tendency will be strong enough to break up any (long range) order that might exist at low temperature. This is also true for magnetic order. A magnet, i.e., a system which exhibits long range ferro- or ferrimagnetic, or antiferromagnetic order at T = 0, undergoes a second-order phase transition at some critical temperature, T_C or T_N respectively, at which

point the long range magnetic order (LRMO) has dissappeared. Understanding the mechanism which leads to this phase transition has been a major issue in the field of magnetism, and in some respects still is.

For Heisenberg systems the situation is again quite clear. At high temperature more and more spin waves will become thermally excited, reducing the macroscopic magnetization according to a Brillouin function.[48] Eventually the directional long range order is destroyed, whereas the local moments maintain the same amplitude.

For itinerant magnets the original Stoner theory (HFA) predicts that the single-particle excitations reduce the mean field which, in turn, reduces the exchange splitting between the spin-up and spin-down bands. Hence, the macroscopic magnetization reduces proportional to the (local) exchange splitting, until they both become zero at the Stoner temperature. Calculated Stoner temperatures are, however, far too high compared to experiment.[49,50] Incorporation of spin waves by RPA provides no solution as this describes only small deviations from the ground state properly, i.e., at low temperatures. Other methods would be required to incorporate spin waves at higher temperatures. On the other hand, it is also clear that spin waves *alone* cannot describe the magnetization *versus* temperature behaviour properly either.

Several attempts have been made to describe finite-temperature itinerant magnetism by assuming that the magnetic moments nevertheless can be considered to be localized. This can be justified as follows. In itinerant magnets the magnetic electrons are not localized to the atomic sites, hence the magnetic moment, which can be assigned to a specific site, shows very fast quantum fluctuations[51,52,47] on a time scale related to the bandwidth W (≈ 5 *e*V in transition metals) as $t_q \approx h/\mathrm{W} \approx 10^{-15}$ s. When averaged over this characteristic time, each atom has a moment with fixed amplitude. Spin waves then can be considered as transverse fluctuations of these averaged moments as the time scale involved there is only of the order of $t_{sw} \approx 10^{-13}$ s. In certain magnetic systems this paradox, i.e., local moments with itinerant electrons, is resolved quite clearly. The *d* electrons in such systems, e.g., Heusler alloys,[53] transition metal impurities in Pd,[54,55] are itinerant, and form bands several *e*V wide. The majority spin electrons can move freely to all sites. In contrast, the minority spin electrons are selectively expelled from specific atom species, e.g., Mn in the Heusler alloys. In this way the itinerant electrons build up a magnetic moment on these sites, which is, in fact, localized.

Making this assumption means that the magnetic moments do not necessarily vanish at the critical temperature. The phase transition, brought about mainly by the spin waves, is then calculated to be of the order of the experimental values. The main difference between models of this sort is the degree of short range magnetic order (SRMO) above T_c they assume. One limiting case is the local band theory (LBT),[56-60] which assumes that the magnetization varies slowly in space and time with correlated regions of the order of the characteristic length a valence electron

can travel within a thermal scattering time, i.e., of the order of 20–30 Å. The other limit is formed by the disordered local moment model (DLM).[61–64] This model assumes that, in the paramagnetic phase, the lattice sites have a random, time-varying "spin-labelling", analogous to a disordered binary alloy and in the same fashion as in the above mentioned Heusler alloys, and that only electrons with the proper spin visit these sites. Statistical models have been developed that use the amount of LRMO, i.e., the magnetization or the temperature, as well as the amount of SRMO as parameters.[65] Such models serve mainly to interpret experimental data and, although providing a useful interpolation between the limiting models, provide no better understanding of the physical processes underlying the observed phenomena.

As a general concluding remark it can be said that studying the temperature behaviour of physical properties of a system around the phase transition, and the critical exponents associated with a power law description of them,[66–68] provides the ultimate test, if not a straightforward one, of any theory attempting to describe the finite temperature behaviour of that system.[20]

1.3.3. The Paramagnetic Phase

The paramagnetic phase of a system is characterized by the absence of long range magnetic order. In a Heisenberg system the local moments can still orient themselves in an applied field. The susceptibility of a (Heisenberg) system of *non-interacting* local moments, or alternatively at high temperatures, follows the Curie-Weiss law[7,8,48]

$$\chi = \frac{C}{T - T_c} \propto \frac{p_{eff}}{T - T_c} \tag{1.4}$$

with C the Curie-Weiss constant and p_{eff} the effective Bohr magneton number. Corrections to this law, of order $(T - T_c)^{-2}$, allow to determine whether the magnetic ordering will be ferro- or antiferromagnetic, depending on a positive or negative prefactor.

Most magnetic materials, also itinerant systems, show CW behaviour,[20] although the latter generally in a more or less restricted temperature region. From the CW-constant the effective momemt $p_{eff} = p_C(p_C + 2)$ can be determined. For a true local moment system the ratio of p_C and p_s, the saturation moment at T = 0, should be unity. It was demonstrated by Rhodes and Wohlfahrt[69] that, whereas this ratio is close to 1 for magnetic insulators and rare earth metals, it can be much larger (> 5–10) for weakly magnetic systems, which are truly itinerant systems. For the ferromagnetic transition metals the ratio ranges from 1.03 to 1.46, i.e., quite close to 1. For critical temperatures above, say, 500 K, it becomes, however, impossible to distinguish between the type of magnetism on the basis of the susceptibility behaviour

Another important observation in the paramagnetic state is the persistence of spin waves, or at least some sort of magnetic scattering of neutrons. Explanations for

these observations have been given by the aforementioned local band theory (LBT), although it has been argued that this model, which is analoguous to a Heisenberg model with imposed SRMO, in other words, with infinite spin wave stiffness, fails to describe the observed susceptibility behaviour.[70] Another explanation was provided by Moriya[71] on the basis of the self-consistent renormalization (SCR) theory of spin fluctuations. This theory, which is one step beyond the HF-RPA theory (which only works only at low temperature), tries to account for the exchange enhancement of spin fluctuations and was shown to work remarkably well for the weakly magnetic systems, i.e., with small critical temperatures and small magnetic moments like $ZrZn_2$, MnSi, etc. These systems are characterized by the dominance of long wavelength fluctuations, and provide an entirely different mechanism for a CW-like susceptibility. Application of this theory to systems in which also short wavelength fluctuations are important is not straightforward, but might be a fruitful way to come to a theory that describes local moment systems as well as itinerant systems and anything intermediate at all temperatures, i.e., a truly unified theory of magnetism.

1.4. Surface-Induced Effects

The results and effects described so far apply to bulk, or mathematically infinite, solids. The most important perturbation to the physical properties of solids is represented by the surface. The loss of periodicity perpendicular to the surface, the reduction of coordination number for surface atoms, possible relaxation and/or reconstruction at the surface, all these effects affect the electronic structure and by this the physical properties at the surface. The relative importance of these effects is not only related to the sample dimensions (surface effects are especially important for small particles and thin films), but certainly also to the experimental method that is used to probe specific properties. Magnetization or susceptibility measurements, or neutron scattering experiments performed on a bulk sample, i.e., with a small surface to volume ratio, are not influenced by surface effects. A photoemission or electron diffraction experiment performed on the same sample, on the other hand, will always exhibit some surface-related features, no matter high thick the sample is. In this light it is therefore extremely important to know what kind of electronic effects might occur at a surface, and how they relate to the magnetic properties.[72 75]

1.4.1. Band Narrowing

The first effect of the surface on the electronic structure is the phenomenon of band narrowing. When a *d*-band is regarded in a tight-binding description, i.e., with the electron delocalization represented by a hopping matrix element connecting atomic or wannier states on neighbouring sites, the reduction of the number of nearest

neighbours n at the surface results in reduced delocalization, which is reflected in the surface density of states (DOS) by a reduced bandwidth $W \propto \sqrt{n}$. Reducing the dimensionality from three to zero, i.e., the free atom, the DOS narrows even more and finally reduces to the atomic state. This means that reducing the number of nearest neighbours effectively brings the atom somewhat closer to the atomic limit, which clearly also will have implications for the magnetic properties.[76]

In a solid the second atomic layer already has the same coordination number as the bulk, but it interacts with the perturbed surface DOS. In metals, where the conduction electrons can screen local perturbations, the influence of the surface on the local electronic structure extends only a few atomic layers ($\lesssim 10$ Å), unlike for instance in semiconductors where band-bending regions can extend for many hundred ångtroms.

Regarding the effect of band narrowing by itself, the density of states at the Fermi level, which is relevant for magnetism in view of the Stoner factor [Eq. 1.1], will increase for close to half-filled bands (V, Cr, Mn, Fe), i.e., with the Fermi level near the center of the band, and decrease for nearly-filled bands (Ni, Pd, Pt). Especially for a half-filled bcc-DOS (V, Cr, Mn), which generally shows a distinct separation of bonding and antibonding states with reduced weight in the center of the band, band narrowing at the surface can have a large effect on the value of the Stoner factor. However, band narrowing by itself would lead to charging of the surface layer. To preserve charge neutrality either the d-band has to shift with respect to the Fermi level so that it holds the same number of electrons, or charge has to be transferred between the sp-bands and the d-band. Thus, band narrowing can cause a redistribution of electrons at the surface, possibly resulting in either larger (enhanced) or smaller surface magnetic moments. Even so-called "dead" surface layers, i.e., with zero magnetization, are possible. The actual situation is so delicate that it can only be solved theoretically by a rigourous *ab initio* self-consistent calculation, which also takes account of, e.g., structural reconstruction or relaxation effects. Recent calculations predict that, e.g., the Fe(100) surface has a 30% enhanced[77] and the Ni(100) surface a 20% enhanced moment[78,79] in the ground state. These predictions, however, still lack rigorous experimental proof [see the survey of experimental results in Ref. 47].

1.4.2. Surface States

Another effect which can play a role at the surface is the appearance of surface states. These are made up from wavefunctions that are localized at, or even slightly outside the surface. Such states appear at energetic positions that lie within gaps of the bulk bandstructure, and can only exist there because of the lack of periodicity perpendicular to the surface. If a surface state lies above or below the bulk band, i.e., if it is split-off, it removes weight from this band at the surface, thus counteracting

the Stoner criterium for the surface. On the other hand, if a surface state appears exactly at the Fermi level, the surface can exhibit magnetism even if the bulk does not.[80]

1.4.3. Surface Magnetization

Apart from the fact that the magnetization at the surface may have a different zero-temperature value than the bulk it may also show a different temperature behaviour $M_S(T)$. At relatively low temperature, i.e., $T \lesssim 0.5T_c$, the main mechanism that reduces the macroscopic magnetization from its saturation value is the excitation of spin waves. The surface influences spin waves in two ways. First of all by the loss of periodicity normal to the surface: the surface can be regarded as an "open end" boundary condition which results in a larger mean amplitude for spin waves at the surface.[81] Initially, this reduces the magnetization at the surface as $T^{3/2}$, just as the bulk, but with a twice as large prefactor.[82]

The second effect of the surface is a possible renormalization of the (effective) exchange coupling constants. If this happens it can result in the occurrence of explicit surface spin waves. These do not affect the temperature-behaviour. However, if the renormalization results in a so-called softening of the exchange coupling of the surface to the bulk it will have an effect. In the limit of vanishing surface-to-bulk coupling the surface layer becomes magnetically two-dimensional and spin waves will destroy the magnetization for any temperature $T > 0$ [Sec. 1.3.1]. Experimentally the surface magnetization was shown to decrease at least three times faster than the bulk magnetization[83-85] indicating that higher order terms may be important.

For higher temperatures, up to T_c, the magnetization of a bulk Heisenberg system decreases as a Brillouin function. Calculated in a mean field approximation,[86] the surface magnetization on the other hand, decreases linearly. Some of the models that have been developed to deal with finite temperature magnetism of bulk itinerant magnets, in particular the DLM model, have also been applied to surfaces. They, too, predict a surface magnetization which decreases faster than the bulk, with a close-to-linear temperature dependence near T_c.[87,88]

1.4.4. Surface Phase Transition

Related to the above effects is the behaviour of the surface at the magnetic phase transition.[89] Depending on the relative coupling strengths between bulk moments and between the surface and the bulk the surface can undergo a phase transition at the same temperature as the bulk — a so-called ordinary transition, or at a lower temperature — a pure surface phase transition, or even at a higher temperature — a so-called extraordinary phase transition. The latter condition seems to be fullfilled at the surfaces of, e.g., Cr(100)[80] and Gd(0001).[90] Note, that this *apparent* 2-dimensional magnetism implies the presence of (strong) anisotropy at these

surfaces.

Apart from the phase transition at the surface occurring at a different temperature, it can also be of a different order. Bulk magnetic phase transitions are of second order: the order parameter, i.e., the macroscopic magnetization M, goes continuously to zero at T_c. The surface, on the other hand, might well exhibit a first-order transition, indicated by a discontinuity in M at T_c.[89]

1.5. Theoretical Models

Modern theoretical approaches to resolve the electronic structure of magnetic solids and surfaces can be divided into *ab initio*, or parameter-free methods and parameterized models. The former group is formed mainly by the density functional theory (DFT) in its various implementations, capable of determining the spin-resolved ground state electron density. It is also suitable to determine other ground state properties such as lattice structure, lattice spacing, compressibility, magnetic moments, heats of formation, etc.

The DFT formalism is in itself *not* suited to calculate finite temperature or excited state properties, and for that purpose approximate models have to be applied. These form the second group of electronic structure methods. The models that are being used may in themselves be exact, but often can only be solved with more or less severe approximations. The models are applied to real materials by fitting to experimental quantities or to DFT results. Then, such models can help to interpret, e.g., surface effects, finite temperature behaviour, and photoemission data. For *d*-band materials one usually applies a degenerate-band tight-binding (Hubbard) model.

1.5.1. Ground State Calculations

Density functional theory (DFT) was developed in the 1960's by Kohn and Sham.[91] The basic ingredient of DFT is the observation that the ground-state properties of an interacting many-electron system are functionals of the electron density.[92] This holds also for the total energy, and the electron density which minimizes the total energy will then automatically represent the ground state density. The second important ingredient, which makes the method so attractive, is the fact that the density which represents the ground state of the interacting many-electron system also minimises the total energy of an equivalent non-interacting system, which can be described by a set of single-particle, Schrödinger-like equations, the Kohn-Sham equations.[91] A recent account of DFT, its limitations and improvements to it, can be found in Ref. 93.

DFT splits the Hamiltonian of a system in a kinetic energy term, an electrostatic term and a so-called exchange-correlation term. The latter contains all interactions

not included in the other terms. The exchange-correlation part cannot be treated exactly for anything but jellium and therefore has to be approximated. The standard way to do this, nowadays, is to use the local spin density (LSD) approximation: the exchange-correlation potential in a point $\boldsymbol{r}$ with density $n(\boldsymbol{r})$ is assumed to be the same as in the homogeneous electron gas with the same density.[94]

A direct consequence of the fact that DFT does not solve the actual interacting system is that, although the Kohn-Sham theorem ensures that in *exact* DFT the correct ground state electron density will be found, it is *not* true that the single-particle wavefunctions and eigenvalues that are found correspond to observables of the many-body system. According to the theorems of DFT only the highest occupied eigenvalue is correct. The latter statement means that for metals DFT gives the correct Fermi energy (or work function), but not neccessarily the correct Fermi *surface*, and for insulators and semiconductors the correct valence band maximum.[95]

In many cases the agreement between LSD calculations[96] and experimentally determined bandstructures[97] is quite good. In those cases were the discrepancies are more evident, e.g., transition metals with large intra-atomic interactions, the bandgap of semiconductors, they are probably not due to the local approximation for the exchange-correlation potential but rather to the fact that the excited state is too much different from the ground state with respect to the electron-electron interactions. For example, in a semiconductor the experimentally determined band gap is given by the difference between the first ionization energy, which is exact in DFT, and the electron affinity. The latter, however, is determined by an "$n+1$" system in which the extra electron interacts less strongly with the other electrons.

The photoemission process has two effects on the single-particle ground state DOS. The delta functions which make up the DOS suffer so-called lifetime broadening due to the finite lifetime of the created hole. Secondly, the single-particle energies are shifted. This shift need not be a smooth function of the single-particle energy and may even lead to the appearence of additional, so-called satellite or shake-up features in the spectrum. One way to account for these effects is to cast them into a single operator, the self-energy Σ, that works on the single-particle DOS. This self-energy, then, is a non-local, complex, energy-dependent function.

For realistic systems Σ is very difficult to calculate. Only for jellium the exact result is known.[98] For real materials the most successful scheme is the GW-approximation,[99] in which the screened Coulomb interaction, to first order, is included. Implementations of this method can be applied to, e.g., semiconductors[100,101] and simple metals,[102] but not to systems with narrow energy bands.

Another way to look at these phenomena is to accept that DFT can produce the correct ground state for the many-body system, but that it cannot account for the excitations of it. These may, however, be calculated separately, using proper constraints for charge distributions, etc., by the same methods that are used to calculate the ground state. This introduces the concept of occupation-dependent

single-particle energies. A condition is that, as most bandstructure programs require some translational symmetry, the unit cell is chosen large enough to avoid artefacts.[103]

Empirically, one often applies, as a "zero-th order" approximation to self-energy effects a linearly increasing Lorentzian broadening to a single-particle DOS to fit it to photoemission data.[104]

Surface Electronic Structure

Within LSD several implementations are available to treat surfaces. The most successful method is probably the full-potential linearized augmented plane wave scheme (FLAPW),[105] which is specifically applied to slabs: a crystal which is infinite in two dimensions, but which consists of a finite number of lattice planes in the third dimension, and therefore has two surfaces. In order to obtain realistic electronic surface features, as well as the correct "bulk", the number of planes has to be larger than the typical screening length of the material, i.e., 5–13 planes for metallic systems.

With FLAPW exciting predictions regarding surface magnetic structure have been made, like enhanced magnetic moments at surfaces of Fe,[77] Ni[78,79] and Cr,[106] and also regarding the effects of adsorbates and overlayers on the magnetic behaviour at the surface[107,38] The experimentalist, however, should always treat such predictions with caution, bearing in mind the natural limitations of DFT/LSD. Above that, it should be remembered that the result of a computation is always limited by the boundary conditions that are imposed. A calculational unit cell defined to be just equal to a crystallographic unit cell precludes the formation of an antiferromagnetic ground state. Also, if atomic positions or lattice spacings are kept fixed, reconstruction and relaxation at the surface are ruled out. If one then applies such a calculation to distinguish between subtle magnetic effects, inclusion of this structural freedom might lead to completely different conclusions.

1.6. Experimental Techniques

Quite often, experimental methods that probe magnetism at or near surfaces involve either excitation by and/or detection of electrons. The main reason for this is, of course, that electrons, through their spin, are the source of magnetic effects, and also because electrons have a limited probing depth in solids due to their short inelastic mean free path, especially compared to other "particles" like neutrons or photons.

Crudely speaking experimental techniques can be distinguished in those that involve emission of electrons following excitation by some source (and the inverse process), and those that involve scattering of electrons. These techniques are especially

sensitive to magnetic properties when the electron spin polarization is explicitly resolved.

1.6.1. Polarized Electrons

Either by their orbital motion and/or by their spin electrons establish the magnetic moments that, when aligned in a solid, result in a macroscopic magnetization. In itinerant transition metal systems, where the orbital moment L is no longer a constant of motion (it is said to be quenched), the magnetic moments are almost completely due to the spin alone and the magnetization is proportional to the net spin density $(n_\uparrow - n_\downarrow)$. In local moment systems the magnetic moments are determined by the (Hund's rule) coupling between the total spin S and the total orbital moment L.

In view of the importance of the electron spin it is only natural that ever since this property of the electron was discovered in the late 1920's, researchers have tried to observe and exploit it to gain insight in magnetic systems. A major effort therefore, has been to produce and measure spin-polarized free electrons.

Fully spin-polarized beams of alkali atoms could already be made by that time with the Stern-Gerlach method.[108–110] It can be shown,[111] however, that this method, which utilizes an inhomogeneous magnetic field to spatially separate atoms with the spin of the outer valence electron oriented oppositely, cannot work for charged particles which experience a Lorentz force in addition to the interaction of the spin with the magnetic field.

The first unambiguous observation of spin-polarization was made in atomic scattering experiments[112] in 1943, whereas it took until 1967 to observe them in scattering from solids.[113,114] Photoemission, as another principal exponent of experimental techniques involving (spin-polarized) electrons, had already been proposed as a possible source of polarized electrons as early as 1930.[115] The first actual observation of spin-polarized photoelectrons, however, dates only from 1969.[116]

The first spin-polarized photoemission experiments with some energy resolution, i.e., threshold photoyield measurements on Ni, were performed in 1976,[117] but it was only after it was demonstrated that polarization effects could also be observed from suitably shaped samples *without* continuously applying an external magnetic field,[118–120] i.e., in remanence, that actual spin-, energy- (and angle-) resolved photoemission became possible.[121,73,72,75] During the past decade this technique has rapidly developed into an indispensable tool to study exchange and spin-orbit induced effects on the electronic structure of solids.

Polarization in Electron Scattering

In electron scattering experiments the electron spin gives rise to specific phenomena. As scattering occurs also in many other experimental techniques, i.e., secondary

electrons in photoemission, some aspects of the role of the spin in scattering will be outlined.

In spin-dependent scattering one distinguishes between spin-orbit (SO) scattering and exchange scattering. SO-scattering occurs when an incoming electron comes close to the nucleus of a (heavy) target atom and experiences a magnetic field due to its (relativistic) motion in the strong electric field. The electron acquires an effective orbital moment that couples to its spin and gives rise to a different scattering potential depending on their relative angles. Of practical importance is the case of incoming electrons with their spin normal to the scattering plane defined by the electron source, the target and the detector. The scattered intensity under equal angles θ to the left and to the right of the incoming beam then shows an asymmetry $S(\theta)$, the Sherman function. This function is well documented for various heavy target materials, i.e., Hg, Au, Pt, and W, and for a large range of primary electron energies.[111] Although the maxima in the asymmetry occur always close to minima in the total differential scattering cross section, SO-scattering is extensively being used as a polarization detector at high energy (Mott-detector;[111] 30–120 keV) as well as at low energy (SPLEED-detector;[122,73] 50–200 eV).

Exchange scattering occurs as a result of the Pauli exclusion principle which requires that the total wavefunction of an electron system is antisymmetric with respect to exchange of particles. The scattering potential will thus be different for incoming electrons with their spin (anti-)parallel to the net electron spin (if present) of the target. In contrast to the "left-right" asymmetry which characterizes SO-scattering this results in an "up/down" asymmetry.

In general SO and exchange scattering occur simultaneously causing (quantum) interference effects. Using special experimental geometries that exploit the symmetries of the system under investigation it is possible to study the interactions separately, with interference effects appearing at most as small perturbations.[123]

Polarization in Photoemission

In photoemission spin-polarization of the emitted electrons can be caused by several effects. In a single-domain ferromagnet the initial state in photoemission, i.e., the occupied part of the valence band, shows an exchange splitting which lifts the degeneracy of the spin-subbands. The photoelectrons emitted from either subband will retain their polarization, provided no other spin-dependent processes take place simultaneously.

Second, if the initial state and/or the final state shows SO-coupling the optical selection rules for the dipole operator can cause preferential excitation of one spin orientation. The relevant selection rule concerns the quantum number m, and a net effect occurs only for circular polarized light: for right (left) circular light only $\Delta m = -1(+1)$ transitions can take place. This effect lies at the basis of the GaAs

spin-polarized electron source.

Finally, photoelectrons that are excited and pass the surface into the vacuum may experience spin-dependent diffraction at the surface, analogous to LEED [see Sect. 1.6.3]. This effect, which is absent for normal emission (provided the crystal has a center of inversion), depends only on the energy of the electrons relative to the Fermi level. A *caveat* is in order associated with this phenomenon, since the detected polarization vector for off-normal emission no longer has to be directly related to the polarization inside the crystal. In this sense the effect is similar to the effect of surface diffraction on band-mapping experiments.

1.6.2. Emission Techniques

Experimental techniques involving the emission of electrons from a solid are excellently suited to study electronic and magnetic structure.

Photoemission and Inverse Photoemission Spectroscopy

In photoemission spectroscopy (PES) electrons from the solid are excited by light (photons), ranging from ultra-violet (UV) to soft x-ray energies ($10^0 - 10^3$ eV).[121] Due to conservation of energy, the kinetic energy of the E_k of the electron in the vacuum is related to the (apparent) binding energy E_B of the electron in the solid by $E_k = h\nu - E_B$, where $h\nu$ is the energy of the (monochromatic) exciting light. The photoemission process can, with some success, be described by the so-called three-step model.[124] Although this is a conceptually useful procedure it should be kept in mind that it is not strictly valid and can give rise to misleading conlusions. The three-step model separately describes the effects occurring in the actual transition from an occupied electron band, be means of the optical dipole operator, to an unoccupied band, the transport of the hot electron through the solid, and the escape of the electron into the vacuum through the surface. The main ingredients to this theory are the real, i.e., not complex, band structure (generally taken from an LSD calculation), the selection rules dictated by the dipole operator, the finite mean free path of hot electrons in the solid, and the discontinuity at the surface. PES can be divided in two regimes with respect to the energy of the exciting light, i.e., low energy (UV PES, UPS) up to about 10^2 eV, and medium and high energy (x-rays). At low energy, apart from energy conservation, also $\boldsymbol{k}$-conservation can be regarded strict, except for the component perpendicular to the surface $k_\perp$, which is due to the discontinuity at the surface, resulting in a description based on selected direct transitions at any particular energy. At high energy, $\boldsymbol{k}$-conservation is strongly relaxed due to the fact that even small effects (phonon-assisted transitions[125]) are sufficient to make transitions possible for virtually all $\boldsymbol{k}$-vectors at any energy. Thus, for x-ray PES (XPS), the entire initial state DOS is probed. For this situation the three-step model gives generally quite good results.[126] For low energies, when

individual initial-to final state transitions can be discerned and initial state bands traced through $\boldsymbol{k}$-space by varying, e.g., the angle of electron detection (angular resolved UPS, ARUPS), the light energy, or the light polarization, the three-step desription has had some, but limited success.[97]

The modern theory of (UV) photoemission,[127–130] aiming to be quantitative, treats the entire process in a single step: the dipole operator induces direct transitions between an occupied complex band structure (to account for the finite lifetime of the hole-state) and an unoccupied complex band structure (to account for the fact that the system is probed in an excited state, and to account for the fact that near the surface excitation cannot only take place into real bands of the bulk band structure, but also into evanescent waves, which are complex or imaginary eigenstates of the system. The final state is equivalent to a "time-reversed LEED state"[131][Sect. 1.6.3]. Because of this, specific surface related emission features (bandgap emission, photoelectron diffraction, angular distribution effects) can be accounted for. It should be kept in mind, however, that the one-step model makes use of the bulk band structure, i.e., surface induced changes to the band structure (band-narrowing, surface states, etc.) and their associated depth profile are neglected. Partly this is justified by the small range of these effects in metallic systems as compared to the mean free path of most electrons used in ARUPS, but whenever ARUPS is used to explore just these effects their neglect in the theory becomes questionable.

In the photoemission process the electron spin is normally conserved in the transition. This means that, apart from extrinsic effects like spin-flip scattering or spin-dependent surface diffraction (only for off-normal emission), the spin polarization of the detected electrons is the same as it was in the intitial state(s). Spin polarized ARUPS (SPARUPS) has in recent years proven to be a very useful technique,[73,72,132] as it supplies important additional information on materials, e.g., ferromagnets, but also on the photoemission process itself, e.g., the origin of the Ni 6-eV satellite,[133] etc. In this respect SPARUPS of non-magnetic systems,[134] where the spin-polarization effects are strictly due to SO-coupling, has also become an important field. For these materials, but also for magnetic materials, a fully relativistic one-step theory of photoemission has been developed,[135,136] which can describe experimental data extremely well.[137,138]

As extensively described in Sect. 1.5.1 the photoemission process probes the system in an excited, i.e., not ground, state. In the above-mentioned one-step theory for SPARUPS this is included by an empirical self-energy contribution to the potential the electrons feel. The description of XPS (not yet performed with spin resolution) at most includes some lifetime-broadening which is added to the (matrix-element weighed) ground state DOS.

The inverse process of photoemission, i.e., inverse photoemission spectroscopy (IPES), entails the transition of an incident electron from a higher-lying, unoccupied band down to an unoccupied band close to the Fermi level. This represents, in fact,

the only way to probe the unoccupied states between the Fermi level and the vacuum level, except for techniques which provide this information in a highly distorted (XAS) or convoluted (APS) way.

It has been shown[139,140] that PES and IPES are equivalent as far as a theoretical description is concerned, except for the fact that, in contrast to the "$n-1$" state of PES, IPES probes an "$n+1$" state. The exchange of electrons and photons as incoming and emitted particles merely introduces a phase space factor. Hence IPES in the low energy regime (UV) can also be performed with angular or $\boldsymbol{k}$-resolution (KRIPES) to perform band-mapping and to observe, e.g., unoccupied surface states and image states.[141] At high energies, usually referred to as Bremsstrahlung isochromat spectroscopy (BIS), the entire unoccupied DOS is probed, with appropriate weighing due to single-particle matrix elements,[142-144] analogous to XPS.

Electron spin resolution can be obtained when spin polarized electron sources are used. This is a relatively new area, and due to experimental difficulties the amount of data has remained scarce. The most sophisticated spin polarized IPES (SPIPES) results (for Ni) have been recently reviewed.[145] Spin polarized BIS is the subject of Ch. 2 of this thesis.

Auger and Secondary Electron Spectroscopy

Auger electron spectroscopy (AES) is a widely used technique to obtain chemical information on a material (composition, contamination), but also on bonding characteristics and screening effects because of the two-hole final state involved.[146] In principle it is a local probe, i.e., the process, in which an initial core hole is filled by an electron from a higher shell and at the same time another electron with an element-specific kinetic energy is emitted, takes place on one site.[147] Auger electrons from ferro- or ferri-magnetic materials are in general spin polarized. Not only if a valence electron is emitted, but also, through intra-atomic exchange interaction, if core electrons are emitted. Thus, it is possible to obtain element-specific magnetic information if, in a regular AES set-up the electrons are spin-analyzed. Spin polarized AES (SPAES) performed sofar has demonstrated its use in studies of elemental ferromagnets,[148-151] but also for alloy and overlayer systems,[152,153] where it gives information on sublattice magnetization and magnetic coupling behaviour.

When electrons are excited in a material by x-rays or high-energy electrons, scattering processes result in enhanced emission of low-energy electrons created by the cascade, the so-called secondary electrons. Since the scattering processes involve electrons from the valence band it was expected and shown that secondary electrons from ferromagnets are spin polarized.[154,155] Due to spin-flip scattering the polarization at very low energy ($\lesssim 10$ eV) is even much higher than the average band polarization.[148,156,157] As it was shown that this polarization scales with the magnetization, secondary electron emission (SEE) can be used as a magnetometer.

An additional advantage lies in the fact that the secondary electrons have both a (very) high intensity *and* a high (up to 35%) polarization. Exploiting the energy-dependence of the electronic mean free path it is even possible to obtain some depth resolution (5–50 Å, i.e., bulk-like).[158,149] See also Sec. 1.6.4.

Conversion Electron Mössbauer Spectroscopy

With Mössbauer spectroscopy it is possible to obtain information on the hyperfine field acting on the Mössbauer nucleus, mostly ^{57}Fe. This hyperfine field contains a contribution from the s-electron density at the nucleus. As these s-electrons hybridize with the magnetic $3d$-electrons and also experience exchange interaction with them, they are generally polarized and constitute a net magnetic field at the nucleus. Conventional Mössbauer spectroscopy, measuring absorption of 14.4 keV γ-photons, is useful for bulk samples. If, on the other hand one collects the Auger and/or conversion electrons which are emitted when the excited nucleus decays back to the ground state, the method is also useful for the near-surface region. True surface-sensitivity, through energy selection of the emitted electrons, has not been shown feasible [see Appendix A]. Yet, by preparing artificially layered samples, i.e., one Mössbauer-active Fe layer in an otherwise non-active matrix, the method can give depth profiles of the hyperfine field.[159] Extrapolating such results to magnetization depth profiles is, however, dangerous, as the s-electron charge density at the nucleus can also change due to, e.g., surface effects, and thus give a different hyperfine field. Theoretical predictions for the hyperfine field suffer from the fact that the net value is made up from large, partially cancelling contributions.[160]

1.6.3. Techniques Involving Scattering

Low Energy Electron Diffraction

The most prominent representative of (electron) scattering techniques applied to the investigation of surfaces and surface magnetism is low energy (10–500 eV) electron diffraction (LEED). In its rudimentary form LEED is often used to observe the quality of single-crystal surfaces and epitaxial overlayers: the larger the structural coherence (typically with a spot of $\sim 500\mu$A) the sharper the interference spots of diffracted electrons are. Also, it provides a simple test for the presence of surface contamination, especially if this induces surface reconstruction. The more sophisticated use of LEED involves detailed observation of intensity *versus* kinetic energy (I-V) curves of selected diffraction spots.

As a result of the strong interaction of the incoming electrons with the substrate, resulting in a short inelastic mean free path,[161] is that the interpretation of such data involves elaborate relativistic multiple scattering calculations (except in special cases like strongly disordered systems). An important ingredient of such

a dynamic LEED theory is the so-called "LEED-state":[73,131] the total concept of matched incoming electrons, including spin, and diffracted electrons as well as the Bloch states that are excited in the solid. The latter should be taken from the full, complex band structure of the solid to take the finite mean free path of the hot electrons into account. Also purely imaginary wavevectors are then available, i.e., states which dom not propagate but decay exponentially away from the surface. Further, (surface) reciprocal lattice vectors have to be taken into account, as well as the fact that the so-called inner potential inside the solid, due to the ion cores, contributes a certain amount to the wavevector perpendicular to the surface. Concepts developed for band structure calculations are successfully applied to dynamical spin-polarized SPLEED calculations. SO-interactions are always taken into account in a proper description of the LEED process. For magnetic systems, first a non-magnetic relativistic calculation is performed and to the SO-induced asymmetry the exchange-induced asymmetry from a non-relativistic magnetic calculation is added. This is justified by the observation that, at least for nickel, these two contributions can be observed separately, without (significant) interference effects.[123] Now that such calculations are available the detailed influence of, e.g., surface relaxation and magnetization density profiles can be modelled and fitted to experiments.[130]

The behaviour of the intensity asymmetry at a specific energy as a function of temperature is sometimes used as a measure of the magnetization of the (near) surface. From these measurements, e.g., critical exponents have been extracted for nickel,[162,83] and evidence for a magnetic surface phase transition for gadolinium was found.[90,163] However, asymmetry features showing non-monotonous temperature behaviour have also been observed, showing that there is no strict relationship between the magnetization and the SPLEED asymmetry.[164]

The asymmetry in SPLEED intensities has also been successfully applied as a low-energy spin-polarization detector,[122] with efficiency at least comparable to the conventional high-energy Mott detector. The reason for this lies in the fact that, due to constructive interference, asymmetry maxima no longer occur just around intensity minima. This allows to choose a convenient working point, which not only has a high figure of merit, but is also stable against small misalignments, etc. Tungsten was chosen as the scattering target because of its large SO-effects and because its surface can be easily cleaned in ultra-high vacuum.

Electron Energy Loss Spectroscopy

Apart from elastic scattering and diffraction, electrons can also transfer energy and momentum to the solid and undergo inelastic scattering. With electron energy loss spectroscopy (EELS) a wide range of electron-induced excitations of the solid can be probed, ranging from magnons ($\sim 10^{-2}$ eV) and intra-band transitions ($\sim 10^{0}$ eV) to plasmons ($\sim 10^{1}$ eV) and core-electron excitations ($10^{2} - 10^{3}$ eV).[165,166]

Obviously, many of these processes are spin-dependent and with spin-polarized SPEELS, employing both spin-polarized primary electrons and spin-polarization analysis of the scattered electrons, one has access to this information. Observation of spin-flip energy-losses at approximately 0.2 eV in Ni has been interpreted as excitation of Stoner transitions.[167,168,73] It has, however, also been argued that these effects are due to quantum interference between different scattering processes.[169]

Electron Capture Spectroscopy

Probably the most surface sensitive technique to study magnetic phenomena (apart from STM) is electron capture spectroscopy (ECS).[170] Fast (20–150 keV) deuterons (D^+) or protons (H^+) are scattered from the sample surface under extreme grazing incidence (0.2°). During the time of closest approach the ions can capture one or two electrons from the solid. This interaction involves only the exponential tails of the wavefunctions, outside the surface. By hyperfine interaction the spin of the a single captured electron is transferred to the nucleus, which then can be detected by scattering. The net polarization is assumed to be proportional to the electron spin polarization in the solid, which is considered a measure of the surface magnetization. This allows determination of long range magnetic order at the surface. Two-electron capture can only take place if, within the characteristic scattering area (10 20 $Å^2$), two antiparallel spins are available, leading to a singlet D^- (H) ion. The strength of this signal is thus inversely proportional to the amount of short range magnetic order (for a ferromagnetic surface).

ECS can be used to determine whether the surface of a solid or thin film is ferromagnetically ordered or not, and the temperature dependence of both long and short range magnetic order, as well as their field dependence.[171] In spite of interesting observations in recent years, the difficulty of setting up the exerpiment and the lack of a theory to describe the effects have prevented ECS from becoming a widespread technique.

Neutron Scattering

Neutron scattering is a well known alternative to x-ray diffraction to resolve crystallographic structures.[172] Even more so than x-rays, neutrons can penetrate deep into solids. Moreover, neutron scattering is isotope-sensitive and is also sensitive to light atoms. Finally, the magnetic moment of the neutron allows access to, e.g., magnetic moment configurations and magnetic density distributions in all kinds of magnetic solids. Needless to say that neutron scattering only supplies bulk information, except when applied to samples with a large surface-to-volume ratio, i.e., powders, or to artificially layered samples.

With neutron scattering it is also possible to investigate excitations in a solid, in particular of spin waves (magnons). Measurements of the dispersion relation for

spin waves at small momentum transfer yields the spin wave stiffness D [Sec. 1.3.1] which in turn can be related to Heisenberg exchange coupling constants.[20]

In recent years neutron scattering in the paramagnetic state has had a large impact on the understanding of metallic magnetism. The magnetic neutron scattering cross section for momentum transfer $\boldsymbol{q}$ and energy transfer ω is directly proportional to the magnetic correlation cross section $S(\boldsymbol{q},\omega)$. The question of persisting short range magnetic order above the critical temperature can be resolved by observing the behaviour of S for large $\boldsymbol{q}$, i.e., small distance, and low energy, i.e., of order k_BT. If SRMO exists S should have low intensity in this region of phase space. Using polarized neutrons and polarization analysis of the scattered neutrons S can be determined, but usually integrated over some energy range. As a result observations of persisting ("sloppy") spin waves and of local magnetic order (typically over a range of ~12 Å for Fe) have been claimed,[173,174] although these have later been contested by other researchers[175,176] [see also Ch. 4].

1.6.4. Microscopy

One of the aims of modern materials research is to characterize samples on the smallest possible scale. A reason for this lies in the progressive miniaturisation and large scale integration of, e.g., semiconductor components, information storage, senors, etc. Conventional microscopic techniques that involve electrons can be extended with spin-polarization analysis and applied to magnetic materials. Questions that might be addressed are the shape of magnetic domains and domain walls and their behaviour with magnetic field, temperature, etc., but also the interrelation between magnetic, chemical and topographic characteristics.

Scanning Electron/Auger Microscopy

In a conventional scanning electron or Auger microscope (SEM/SAM) imaging is performed by detecting the secondary and/or Auger electrons which are emitted by the sample when it is hit by a well-focussed high energy (5–100 keV) electron beam. These electrons are, however, also spin polarized and can therefore be used to obtain a magnetization image of the sample, with a lateral resolution of ~500 Å or better.[177–183]

With the first implementations of SEM with polarization analysis (SEMPA) promising images have been obtained of domain patterns and also of domain walls themselves (comparable in appeal to STM images, even appearing on the cover of Science[184]). SAMPA, on the other hand, has not yet been implemented, because of the large reduction of signal intensity when the electrons are energy selected.

An additional advantage of SEMPA is that the magnetization image is obtained from the normalized asymmetry of the polarization detector, hence, topographic and chemical information do not interfere with the magnetic information. The

topographic (SEM) or chemical (SAM) information on the *same* sample area is, however, independently available from the total intensity signal.

Scanning Tunneling Microscopy

Since its first demonstration[185] in 1982 scanning tunneling microscopy (STM) has rapidly developed into a widely used technique, not only to study detailed surface topography,[186] but also to perform local electron spectroscopy[187,188] and even to fabricate nanostructures.[189] STM has become one of the most important surface-microscopic techniques, and with unsurpassed spatial resolution.

The potential of STM performed with spin-polarized electrons had quickly been realized by several groups. Only very recently this technique has been demonstrated for the first time.[190] This was made possible through the use of a ferromagnetic CrO_2-tip, a half-metallic ferromagnet, and a special Cr near-(100) surface, which had monoatomic steps with alternating magnetization direction of consecutive terraces, since Cr is "double-lattice" antiferromagnet. The Cr-surface exhibits strongly enhanced surface magnetism due to the presence of a surface state near the Fermi level.[106,191]

For practical applications of spin-polarized STM, like domain-wall imaging or even imaging of antiferromagnetic surfaces, it will be neccessary, especially in the case of rough and alloy-surfaces, i.e., with different chemical species at the surface, to extract the magnetic information from the topographic and chemical information. Even without considering the practical difficulties, it will not do to simply reverse the tip magnetization as the tunneling geometry is not symmetric.

Another way to perform magnetic microscopy with the STM is to use the tip just as a local electron-injector. The secondary electrons which are emitted can then be analyzed with conventional means.[192]

Until now, application of microscopic techniques in the fashion described above has been limited. Obviously the experiments are not easy, but it is to be expected that within the next decade these techniques will be further refined and find increasing applications both in industry as well as in fundamental research.

1.7. Future Prospects

In this Chapter a general review has been given of itinerant magnetism, in relation to surface-sensitive electron spectroscopies. Since the 1930's there has been tremendous progress in experimental techniques, theoretical models, as well as in general concepts. An axample is the concept of persisting local moments in the paramagnetic phase of itinerant systems. This development has been accompanied by appropriate theoretical models and calculational techniques that are able to describe this situation and conform to experimental observations. Eventually, this

may lead to one single theory that is capable of describing both itinerant and local moment magnetism.

The rapid developments in computer technology and calculation schemes have enabled accurate ground state electronic structures and other physical properties to be calculated for a wide range of materials. Recent progress has been made with fully relativistic calculations that incorporate spin-orbit interactions.[193,194]

At the same time it has become accepted that additional calculations are neccessary to allow comparison with experimental data obtained by, e.g., photoemission, that probe an excited state of the system. Such self-energy calculations are now reaching a high level of sophistication.

Progress in experimental techniques has been made in several areas. State-of-the-art sample preparation techniques, like molecular beam epitaxy (non-equilibrium structural phases, modulated structures, etc.), ion-implantation, etc., on the one hand, and adequate surface cleaning and analysis techniques in an ultra-high vacuum environment on the other hand, have the potential to model well-defined prototype structures to study the behaviour of magnetic materials as a function of, e.g., lattice constants, detailed composition and geometry, etc.

Ongoing progress is also being made with measurement techniques. Especially the extension of existing electron-spectroscopy (and -microscopy) techniques with spin polarization analysis is a rewarding achievement, if not always easy. Some spin polarized techniques have already become almost standard tools, e.g., SPARUPS and SPLEED. Others are only just in the development phase.

We do not claim that within a few years these combined efforts will lead to a full understanding of the intricate many-body problem called magnetism. It can be foreseen, however, that our understanding of individual materials, experimentally as well as theoretically, will gradually fill in the blank spots that have existed ever since the ancient Cretan shephard Magnes first stumbled onto a magnetic rock.[1,2]

1.8. References

[1] E.C. Stoner, *Magnetism and Matter.* (Methuen, London, 1934).

[2] D.C. Mattis, *The Theory of Magnetism I*, vol. 17 of *Series in Solid-State Sciences.* (Springer Verlag, Berlin, 1981).

[3] Oersted, 1820.

[4] D.L. Anderson, *The Discovery of the Electron.* (Van Nostrand, Princeton, N.J., 1964).

[5] A.H. Compton, J. Franklin Inst. **192**, 144 (1921).

[6] G. Uhlenbeck and S. Goudsmit, Naturwiss. **13**, 953 (1925).

[7] P. Weiss, J. Physique **6(4)**, 661 (1907).

[8] P. Curie, Ann. Chim. Phys. **5(7)**, 289 (1895).

[9] W. Heisenberg, Z. Phys. **49**, 619 (1928).

[10] *Le Magnétisme, 6$^{\text{th}}$ Solvay Conf.* (Gauthier-Villars, Paris, 1932).

[11] F. Bloch, Z. Phys. **57**, 545 (1929).

[12] E.C. Stoner, Proc. R. Soc. London **A154**, 656 (1936).

[13] J. H. Van Vleck, Rev. Mod. Phys. **25**, 220 (1953).

[14] N.F. Mott, Proc. R. Soc. London **A62**, 416 (1949).

[15] J. Hubbard, Proc. R. Soc. London **A276**, 238 (1963).

[16] J. Hubbard, Proc. R. Soc. London **A277**, 237 (1964).

[17] J. Hubbard, Proc. R. Soc. London **A281**, 401 (1967).

[18] J. Zaanen, G.A. Sawatzky and J.W. Allen, J. Magn. Magn. Mat. **54-57**, 607 (1986).

[19] C.G. Windsor, Physica B **91**, 119 (1977).

[20] E.P. Wohlfahrt, in *Ferromagnetic Materials*, edited by E.P. Wohlfahrt, vol. 1. (North-Holland, Amsterdam, 1980).

[21] J. Kübler, A.R. Williams and C.B. Sommers, Phys. Rev. B **28**, 1745 (1983).

[22] E.C. Stoner, Proc. R. Soc. London **A169**, 339 (1939).

[23] N.E. Philips, Crit. Rev. Solid State Sci. **2**, 467 (1972).

[24] R. Caudron, J.J. Mennier and P. Costa, Sol. St. Commun. **14**, 975 (1974).

[25] J. Friedel and C.M. Sayers, J. Physique **38**, 697 (1977).

[26] F. Kajzar and J. Friedel, J. Physique **39**, 397 (1978).

[27] E. Fawcett and W.A. Reed, Phys. Rev. Lett. **9**, 336 (1962).

[28] A.V. Gold, J. Low Temp. Phys. **16**, 3 (1974).

[29] R.C. Young, Rep. Prog. Phys. **40**, 1123 (1977).

[30] G.G. Lonzarich, in *Electrons at the Fermi Surface*, edited by M. Springford. (Cambridge University Press, 1980).

[31] S. Hüfner, G.K. Wertheim, N.V. Smith and M.M. Traum, Sol. St. Commun. **11**, 323 (1972).

[32] S. Hüfner and G.K. Wertheim, Phys. Lett. **51A**, 299 (1975).

[33] C. Guillot, Y. Ballu, J. Paigné, J. Lecante, K.P. Jain, P. Thiry, R. Pinchaux, Y. Pétroff and L.M. Falicov, Phys. Rev. Lett. **42**, 921 (1977).

[34] C.S. Wang and J. Callaway, Phys. Rev. B **15**, 298 (1977).

[35] J. Callaway and C.S. Wang, Physica **91B**, 337 (1977).

[36] A.R. Williams, V.L. Moruzzi, C.D. Gelatt Jr., J. Kübler and K. Schwarz, J. Appl. Phys. **53**, 2019 (1982).

[37] S. Blügel, *First Principles Calculations of the Electronic Structure of Magnetic Overlayers on Transition Metal Surfaces.* Ph.D. thesis, Neunkirchen/Saar, 1988.

[38] S. Blügel, M. Weinert and P.H. Dederichs, Phys. Rev. Lett. **60**, 1077 (1988).

[39] P. Fulde, in *Handbook on the Phys. and Chem. of Rare Earths*, edited by K.A. Gschneider, Jr. and L. Eyring, vol. 2, p. 295. (North-Holland, Amsterdam, 1979).

[40] U. Gradmann, R. Bergholz and E. Bergter, Thin Solid Films **126**, 107 (1985).

[41] U. Gradmann, J. Korecki and G. Waller, Appl. Phys. **A39**, 101 (1986).

[42] B.T. Jonker and G.A. Prinz, Surf. Sci. **172**, L568 (1986).

[43] D. Pescia, G. Zampieri, M. Stampanoni, G.L. Bona, R.F. Willis and F. Meier, Phys. Rev. Lett. **58**, 933 (1987).

[44] M. Sacchi et al., Phys. Rev. B (1990), (in press).

[45] F. Bloch, Z. Phys. **61**, 206 (1930).

[46] N.D. Mermin and H. Wagner, Phys. Rev. Lett. **17**, 1133 (1966).

[47] J. Mathon, Rep. Prog. Phys. **51**, 1 (1988).

[48] N.W. Ashcroft and N.D. Mermin, *Solid State Physics.* (Holt-Saunders, Philadelphia, 1976).

[49] O. Gunnarson, J. Phys. F **6**, 587 (1976).

[50] O. Gunnarson, Physica B **91**, 329 (1977).

[51] B.L. Gyorffy, A.J. Pindor, J. Staunton, G.M. Stocks and H. Winter, J. Phys. F **15**, 1337 (1985).

[52] H. Capellmann, Ch. 2 of Ref. 72.

[53] A.R. Williams, V.L. Moruzzi, C.D. Gelatt Jr. and J. Kübler, J. Magn. Magn. Mat. **31-34**, 88 (1983).

[54] A. Oswald. Ph.D. thesis, KFA Jülich, 1985.

[55] A. Oswald, R. Zeller and P.H. Dederichs, Phys. Rev. Lett. **56**, 1419 (1986).

[56] V. Korenman, J.L. Murray and R.E. Prange, Phys. Rev. B **16**, 4032 (1977).

[57] R.E. Prange and V. Korenmann, Phys. Rev. B **19**, 4691 (1979).

[58] H. Capellmann, J. Phys. F **4**, 1466 (1974).

[59] H. Capellmann and V. Vieira, Sol. St. Commun. **43**, 747 (1982).

[60] V. Korenman, in *Metallic Magnetism*, vol. 42 of *Topics in Current Physics.* (Springer Verlag, Berlin, 1987).

[61] J. Hubbard, Phys. Rev. B **19**, 2626 (1979).

[62] J. Hubbard, Phys. Rev. B **20**, 4584 (1979).

[63] H. Hasegawa, J. Phys. Soc. Jpn. **46**, 1504 (1979).

[64] H. Hasegawa, J. Phys. Soc. Jpn. **49**, 178 (1980).

[65] R. Clauberg, E. Haines and R. Feder, Z. Phys. B **62**, 31 (1985).

[66] M.E. Fisher, Rep. Prog. Phys. **30**, 615 (1967).

[67] P. Heller, Rep. Prog. Phys. **30**, 731 (1976).

[68] L.P. Kadanoff, W. Götze, D. Hamblen, R. Hecht, E.A.S. Lewis, V.V. Palciauskas, M. Rayl, J. Swift, D. Aspnes and J. Kane, Rev. Mod. Phys. **39**, 395 (1967).

[69] R.R. Rhodes and E.P. Wohlfahrt, Proc. R. Soc. London **273**, 247 (1963).

[70] D.M. Edwards, J. Magn. Magn. Mat. **36**, 213 (1983).

[71] T. Moriya, *Spin Flucuations in Itinerant Electron Magnetism*, vol. 56 of *Series in Solid-State Sciences.* (Springer Verlag, Berlin, 1985).

[72] R. Feder (Ed.), *Polarized Electrons in Surface Physics.* (World Scientific Publishing, Singapore, 1985).

[73] J. Kirschner, Surf. Sci. **162**, 83 (1985).

[74] L.M. Falicov and J.L. Morán-López (Eds.), *Magnetic Properties of Low-dimensional Systems*, vol. 14 of *Proceedings in Physics.* (Springer Verlag, Berlin, 1986).

[75] E. Kisker, in *Metallic Magnetism*, vol. 42 of *Topics in Current Physics.* (Springer Verlag, Berlin, 1987).

[76] M. Weinert and A.J. Freeman, J. Magn. Magn. Mat. **38**, 23 (1983).

[77] S. Ohnishi, A.J. Freeman and M. Weinert, Phys. Rev. B **28**, 6741 (1983).

[78] A.J. Freeman, D.S. Wang and H. Krakauer, J. Appl. Phys. **53**, 1997 (1982).

[79] E. Wimmer, A.J. Freeman and H. Krakauer, Phys. Rev. B **30**, 3113 (1984).

[80] L.E. Klebanoff, *Photoelectron Spectroscopy Studies of Cr(001) Surface Ferromagnetism and Near-surface Antiferromagnetism.* Ph.D. thesis, Lawrence Berkely Laboratory, 1985.

[81] G.T. Rado, Bull. Am. Phys. Soc. II **2**, 127 (1957).

[82] C. Kittel, *Introduction to Solid State Physics.* (Wiley, New York, 5th edition, 1976).

[83] D.T. Pierce, R.J. Celotta, J. Unguris and H.C. Siegmann, Phys. Rev. B **26**, 2566 (1982).

[84] J.C. Walker, R. Droste, G. Stern and J. Tyson, J. Appl. Phys. **55**, 2500 (1984).

[85] J. Korecki and U. Gradmann, Hyp. Inter. **28**, 931 (1986).

[86] T. Wolfram, R.E. Dewames, W.F. Hall and P.W. Palmberg, Surf. Sci. **28**, 45 (1971).

[87] H. Hasegawa, J. Phys. F **17**, 165 (1987).

[88] H. Hasegawa, J. Phys. F **17**, 679 (1987).

[89] K. Binder, Ch. 3 of Ref. 72.

[90] D. Weller, S.F. Alvarado, W. Gudat, K. Schröder and M. Campagna, Phys. Rev. Lett. **54**, 1555 (1985).

[91] W. Kohn and L.J. Sham, Phys. Rev. **140**, A1133 (1965).

[92] P. Hohenberg and W. Kohn, Phys. Rev. B **136**, 864 (1964).

[93] R.O. Jones and O. Gunnarsson, Rev Mod. Phys. **61**, 689 (1989).

[94] D.M. Ceperly and B.J. Alder, Phys. Rev. Lett. **45**, 566 (1980).

[95] R.W. Godby, in *Unoccupied Electronic States*, edited by J.C. Fuggle and J.E. Inglesfield, vol. - of *Tracts in Modern Physics*. (Springer, Berlin, 1991), in press.

[96] V.L. Moruzzi, J.F. Janak and A.R. Williams, *Calculated Electronic Properties of Metals*. (Pergamon, NY, 1978).

[97] F.J. Himpsel, Adv. Phys. **32**, 1 (1983).

[98] L. Hedin and S. Lundqvist, in *Solid State Physics*, edited by H. Ehrenreich, D. Turnbull and F. Seitz, vol. 23. (Academic, NY, 1969).

[99] L. Hedin, Phys. Rev. **139**, A796 (1965).

[100] R.W. Godby, M. Schlüter and L.J. Sham, Phys. Rev. Lett. **56**, 2415 (1986).

[101] W. von der Linden and P. Horsch, Phys. Rev. B **37**, 8351 (1988).

[102] J.E. Northrup, M.S. Hybertsen and S.G. Louie, Phys. Rev. Lett. **59**, 819 (1987).

[103] P.J.W. Weijs, G. Wiech, W. Zahorowski, W. Speier, J.B. Goedkoop, M. Czyżyk, J.F. van Acker, E. van Leuken, R.A. de Groot, G. van der Laan, D.D. Sarma, L. Kumar, K.H.J. Buschow and J.C. Fuggle, Phys. Scr. **41**, 629 (1990).

[104] D. van de Marel, G.A. Sawatzky, R. Zeller, F.U. Hillebrecht and J.C. Fuggle, Sol. St. Commun. **50**, 47 (1984).

[105] E. Wimmer, H. Krakauer, M. Weinert and A.J. Freeman, Phys. Rev. B **24**, 864 (1981).

[106] C.L. Fu and A.J. Freeman, Phys. Rev. B **33**, 1755 (1986).

[107] C.L. Fu, A.J. Freeman and T. Oguchi, Phys. Rev. Lett. **54**, 2700 (1985).

[108] O. Stern, Z. Phys. **7**, 249 (1921).

[109] O. Stern and W. Gerlach, Z. Phys. **8**, 110 (1922).

[110] O. Stern and W. Gerlach, Z. Phys. **9**, 349 (1922).

[111] J. Kessler, *Polarized Electrons*, vol. 1 of *Series on Atoms and Plasmas.* (Springer Verlag, Berlin, second edition, 1985).

[112] C.G. Shull, C.T. Chase and F.E. Myers, Phys. Rev. **63**, 29 (1943).

[113] W. Eckstein, Z. Phys. **203**, 59 (1967).

[114] R. Loth, Z. Phys. **203**, 66 (1967).

[115] E. Fues and H. Helman, Phys. Z. **31**, 465 (1930).

[116] G. Busch, M. Campagna, P. Cotti and H.C. Siegmann, Phys. Rev. Lett. **22**, 597 (1969).

[117] W. Eib and S.F. Alvarado, Phys. Rev. Lett. **37**, 444 (1976).

[118] E. Kisker, G. Baum, A.H. Mahan, W. Raith and B. Reihl, Phys. Rev. B **18**, 2256 (1978).

[119] R.J. Celotta, D.T. Pierce, G.-G. Wang, S.D. Bader and G.P. Felcher, Phys. Rev. Lett. **43**, 728 (1979).

[120] E. Kisker, W. Gudat, E. Kuhlmann, R. Clauberg and M. Campagna, Phys. Rev. Lett. **45**, 2053 (1980).

[121] H.C. Siegmann, F. Meier, M. Erbudak and M. Landolt, Adv. El. El. Phys. **62**, 2 (1984).

[122] H. Oepen, Ber. KFA Jülich **1970** (1985).

[123] S.F. Alvarado, R. Feder, H. Hopster, F. Cicacci and H. Pleyer, Z. Phys. B **49**, 129 (1982).

[124] C.N. Berglund and W.E. Spicer, Phys. Rev. **136**, A1030, A1044 (1964).

[125] N.J. Shevchik, Phys. Rev. B **16**, 3428 (1977).

[126] W. Speier, J.C. Fuggle, P. Durham, R. Zeller, R.J. Blake and P. Sterne, J. Phys. C **21**, 2621 (1988).

[127] J.B. Pendry, Surf. Sci. **57**, 679 (1976).

[128] G. Thörner and G. Borstel, Phys. Status Solidi B **126**, 617 (1984).

[129] J. Braun, G. Thörner and G. Borstel, Phys. Status Solidi B **130**, 643 (1985).

[130] R. Feder, Ch. 4 of Ref. 72.

[131] P.J. Feibelman and D.E. Eastman, Phys. Rev. B **10**, 4932 (1974).

[132] E. Kisker, K. Schröder, W. Gudat and M. Campagna, Phys. Rev. B **31**, 329 (1985).

[133] R. Clauberg, W. Gudat, E. Kisker, E. Kuhlmann and G.M. Rothberg, Phys. Rev. Lett. **47**, 1314 (1981).

[134] A. Eyers, F. Schäfers, G. Schönhense, U. Heinzmann, H.P. Oepen, K. Hünlich and J. Kirschner, Phys. Rev. Lett. **52**, 1559 (1984).

[135] B. Ackermann and R. Feder, J. Phys. C **18**, 1093 (1985).

[136] B. Ackermann and R. Feder, Sol. St. Commun. **54**, 1077 (1985).

[137] E. Tamura, W. Piepke and R. Feder, J. Phys.: Condens. Matter **1**, 6469 (1989).

[138] E. Tamura, R. Feder, B. Vogt, B. Schmiedeskamp and U. Heinzmann, Z. Phys. B **77**, 129 (1989).

[139] J.B. Pendry, Phys. Rev. Lett. **45**, 1356 (1980).

[140] J.B. Pendry, J. Phys. C **14**, 1381 (1981).

[141] N.V. Smith, Rep. Prog. Phys. **51**, 1227 (1988).

[142] J.K. Lang, Y. Baer and P.A. Cox, J. Phys. F **11**, 121 (1981).

[143] W. Speier, J.C. Fuggle, R. Zeller, B. Ackermann, K. Szot, F.U. Hillebrecht and M. Campagna, Phys. Rev. B **30**, 6921 (1984).

[144] J.C. Fuggle and J.E. Inglesfield (Eds.), *Unoccupied Electronic States*, vol. - of *Tracts in Modern Physics.* (Springer, Berlin, 1991), (in press).

[145] M. Donath, V. Dose, K. Ertl and U. Kolac, Phys. Rev. B **41**, 5509 (1990).

[146] J.C. Fuggle, in *Electron Spectroscopy*, edited by C.R. Brundle and A.D. Baker, vol. 4. (Academic, London, 1981).

[147] P.W. Palmberg, G.E. Rich, R.E. Weber and N.C. MacDonald, *Handbook of Auger Electron Spectroscopy.* (Physical Electronics Industries, Inc., Edina, Minnesota, 1972).

[148] M. Landolt, Ph. Niedermann and D. Mauri, Phys. Rev. Lett. **48**, 1632 (1982).

[149] R. Allenspach and M. Landolt, Surf. Sci. Lett. **171**, L479 (1986).

[150] M. Taborelli, R. Allenspach and M. Landolt, Phys. Rev. B **34**, 6112 (1986).

[151] R. Allenspach, D. Mauri, M. Taborelli and M. Landolt, Phys. Rev. B **35**, 4801 (1987).

[152] M. Taborelli, R. Allenspach, G. Boffa and M. Landolt, Phys. Rev. Lett. **56**, 2869 (1986).

[153] S. Toscano. *Magnetismus dünner Gd-Filme auf Ni(110) untersucht mit Spinpolarisierter Sekundärelektronen-Spektroskopie.* Master's thesis, ETH, Zürich, 1988.

[154] G. Chrobok and M. Hofmann, Phys. Lett. **57A**, 257 (1976).

[155] J. Unguris, A. Seiler, R.J. Celotta, D.T. Pierce, P.D. Johnson and N.V. Smith, Phys. Rev. Lett. **49**, 1047 (1982).

[156] E. Kisker, Rev. Sci. Instrum. **53**, 114 (1982).

[157] H. Hopster, C. Raue, E. Kisker, G. Güntherodt and M. Campagna, Phys. Rev. Lett. **50**, 70 (1983).

[158] D. Mauri, R. Allenspach and M. Landolt, J. Appl. Phys. **58**, 906 (1985).

[159] J. Korecki and U. Gradmann, Phys. Rev. Lett. **55**, 2491 (1985).

[160] A.J. Freeman, C.L. Fu, S. Ohnishi and M. Weinert, Ch. 1 of Ref. 72.

[161] M.P. Seah and W.A. Dench, Surf. Interf. An. **1**, 2 (1979).

[162] S.F. Alvarado, M. Campagna, F. Cicacci and H. Hopster, J. Appl. Phys. **53**, 7920 (1982).

[163] D. Weller, S.F. Alvarado, M. Campagna, W. Gudat and D.D. Sarma, J. Less-Common Metals **111**, 277 (1985).

[164] J. Kirschner, Phys. Rev. B **30**, 415 (1984).

[165] H. Ibach and D.L. Mills, *Electron Energy Loss Spectroscopy and Surface Vibrations.* (Academic, NY, 1982).

[166] H. Ibach, J. Vac. Sci. Technol. **A5**, 419 (1987).

[167] H. Hopster, R. Raue and R. Clauberg, Phys. Rev. Lett. **53**, 695 (1984).

[168] J. Kirschner, D. Rebenstorff and H. Ibach, Phys. Rev. Lett. **53**, 698 (1984).

[169] D.L. Mills, Phys. Rev. B **34**, 6099 (1986).

[170] C. Rau, J. Magn. Magn. Mat. **30**, 141 (1982).

[171] C. Rau, 1989, (preprint).

[172] L.A. Feigin and D.I. Svergun, *Structure Analysis by Small Angle X-ray and Neutron Scattering.* (Plenum, 1987).

[173] H.A. Mook, J.W. Lynn and R.M. Nicklow, Phys. Rev. Lett. **30**, 556 (1973).

[174] J.W. Lynn, Phys. Rev. B **11**, 2624 (1975).

[175] G. Shirane, Y.J. Uemura O. Steinvoll and J. Wicksted, J. Appl. Phys. **55**, 1887 (1984).

[176] J. Callaway, Phys. Lett. **112A**, 67 (1985).

[177] K. Koike and K. Hayakawa, Appl. Phys. Lett. **45**, 585 (1984).

[178] K. Koike and K. Hayakawa, J. Appl. Phys. **57**, 4244 (1985).

[179] K. Koike, H. Matsuyama, H. Todokoro and K. Hayakawa, Jpn. J. Appl. Phys. **24**, L542 (1985).

[180] K. Koike, H. Matsuyama, H. Todokoro and K. Hayakawa, Jpn. J. Appl. Phys. **24**, 1833 or 1078 (1985).

[181] J. Unguris, G.G. Hembree, R.J. Celotta and D.T. Pierce, J. Microscopy **139**, RP1 (1985).

[182] J. Unguris, D.T. Pierce and R.J. Celotta, Rev. Sci. Instrum. **57**, 1314 (1986).

[183] J. Unguris, G.G. Hembree, R.J. Celotta and D.T. Pierce, J. Magn. Magn. Mat. **54–57**, 1629 (1986).

[184] R.J. Celotta and D.T. Pierce, Science **234**, 249 (1986).

[185] G. Binnig, H. Rohrer, Ch. Gerber and E. Weibel, Phys. Rev. Lett. **49**, 57 (1982).

[186] See, e.g., *Proc. 4th Int. Conf. Scanning Tunneling Microscopy/Spectroscopy*, J. Vac. Sci. Technol. A **8**, 153 (1990).

[187] G. Binnig, K.H. Frank, N. Garcia, B. Reihl, H. Rohrer, F. Salvan and A.R. Williams, Phys. Rev. Lett. **55**, 991 (1985).

[188] N. Garcia, B. Reihl, K.H. Frank and A.R. Williams, Phys. Rev. Lett. **54**, 591 (1985).

[189] M.A. McCord, D.P. Kern and T.H.P. Chang, J. Vac. Sci. Technol. B **6**, 1877 (1988).

[190] R. Wiesendanger, H.-J. Güntherodt, G. Güntherodt, R.J. Gambino and R. Ruf, Z. Phys. B **80**, 5 (1990).

[191] L.E. Klebanoff, S.W. Robey, G. Liu and D.A. Shirley, Phys. Rev. B **30**, 1048 (1984).

[192] M. Landolt and R. Allenspach, private communication.

[193] O. Eriksson, L. Nordström, A. Pohl, L. Severin, A.M. Boring and B. Johansson, Phys. Rev. B **41**, 11807 (1990).

[194] O. Eriksson, B. Johansson, R.C. Albers, A.M. Boring and M.S.S. Brooks, Phys. Rev. B **42**, 2707 (1990).

2. Bremsstrahlung Isochromat Spectroscopy with Spin Polarized Electrons[†]

This chapter describes the design considerations and technical realization of a new experimental technique, which we designate by the acronym BISCEPS — Bremsstrahlung Isochromat Spectroscopy Combined with Electrons with Polarized Spin. The technical details are described at some length to give a justification of the chosen operating parameters as well as for future reference.

2.1. Introduction

With BISCEPS we can probe the unoccupied electronic states of solids in a spin-resolved fashion, which is evidently useful for the study of magnetic systems. The technique can alternatively be regarded as spin-resolved inverse photoemission (IPES) at x-ray energies. To explain its relevance we therefore refer to photoemission spectroscopy (PES), which is a widespread and well understood technique that holds a prominent place in studies of solid state electronic structure.[1-3] In PES, core or valence electrons are emitted from the solid following excitation by monochromatic photons. In practice, PES is generally classified with respect to the energy range of the photons, i.e., ultra-violet photoemission spectroscopy (UPS, 10–50 eV) and x-ray photoemission spectroscopy (XPS, 1000 eV and higher). Although the increasing application of synchrotron radiation, which covers the entire range from optical up to hard x-ray energies, seems to render this classification somewhat out of date, it is still useful to make this distinction for, as far as valence band photoemission is concerned, UPS and XPS differ fundamentally from each other with respect to, among other things, the variation of transition matrix elements[4] and probing depth[5] but most of all with respect to the degree of momentum conservation.

The dipole induced transition conserves the crystal momentum or wave vector $\boldsymbol{k}$ of the electron in the solid. This yields an electron kinetic energy distribution that reflects the joint density of states (JDOS) of points in reciprocal space connected by vertical transitions in the reduced zone scheme. Due to several mechanisms a

[†]Parts of this Chapter have been published in Rev. Sci. Instrum. **61**, 765 (1990).

one to one correspondence with the JDOS will in practice be distorted by the time the excited electrons are detected. Among these are: the finite analyzer acceptance angle, the broken symmetry at the surface, the finite mean free path (mfp) of the excited electrons[6] and phonon assisted transitions.[7] At medium and high kinetic energies these mechanisms result in considerable averaging over momentum space. Together with the fact that the density of available final states, especially at high energies, is very large and smooth,[6] the spectrum will essentially represent a more or less uniform average of initial states from arbitrary points in the Brillouin zone (BZ). This means then, that even for monocrystalline samples, PES in the x-ray range, i.e., XPS, reflects the total initial density of states (DOS) of the solid (distorted by matrix element effects). At low kinetic energies, on the other hand, these averaging mechanisms have a greatly reduced influence. One can even consider the component of $\boldsymbol{k}$ parallel to the surface to be strictly conserved. This is exploited in experiments on single crystals to trace energy bands through $\boldsymbol{k}$-space, i.e., band-mapping, for instance by varying the electron escape angle (angular resolved UPS, ARUPS).[8]

For polycrystalline samples UPS spectra also represent a uniform sampling of the BZ, but due to the restricted number of available and allowed final states at a given energy the spectra in general still do not correspond to the total DOS. Roughly speaking, UPS probes more directly the $\boldsymbol{k}$-resolved bandstructure (BS) of a solid, whereas XPS reflects the total initial DOS. Over the past two decades both XPS and UPS, separately and in comparative studies, have greatly increased our understanding of the electronic structure of solids such as metals, alloys and semiconductors, and adsorbates.

For a more complete investigation of the valence bands of magnetic systems it has proven to be very useful to extend PES with spin polarization analysis of the emitted photoelectrons. Especially with the advent of high-intensity dedicated synchrotron radiation sources, spin polarized UPS (SPUPS or SPARUPS)[3,9,10] has become a relatively standard experimental technique that has stimulated research, both experimentally and theoretically, in magnetism in general and magnetism at surfaces in particular.[11]

PES cannot directly assess the unoccupied electronic states, which of course are also important for the physical properties of a solid, except strongly convoluted with the occupied states. These states *can* be probed, however, by the inverse process: incoming electrons undergo a radiative transition and are captured in the solid. As with PES, this technique can also be performed in the UV range and in the x-ray range. The former is generally referred to as inverse photoemission (IPES)[12,13] and the latter,mainly for historical reasons, as bremsstrahlung isochromat spectroscopy (BIS).[14–17] The differences between both methods are essentially the same as between UPS and XPS. The overall picture of the valence bands that can be obtained by combining PES and IPES enables one to determine physical parameters such as the dispersion of bands crossing the Fermi level (UPS/IPES), or the effective Coulomb

interaction in highly correlated systems (XPS/BIS), that cannot be derived so easily by other experimental techniques.

Following the discovery and development of intense and convenient spin polarized electron sources,[18] also inverse photoemission has been extended to include analysis of spin resolved features. Several investigations in the UV range on elemental ferromagnets and the influence of adsorbates on surface magnetism have been performed with spin polarized IPES (SPIPES).[19–23] The system we describe here, and the measurements performed with it which are presented in the next chapter, is the first ever implementation of the x-ray counterpart: BISCEPS.

2.2. Technical Description

2.2.1. Vacuum Chambers

The UHV system, as shown schematically in Fig. 2.1, consists of four interconnected chambers. For the large measurement and preparation chambers, separated from each other by a large viton-sealed UHV-valve,[24] liquid-nitrogen-trapped oil diffusion pumps[25] are used. These pumps have the advantage of high pumping speed for all residual gasses, including light and noble gasses. A disadvantage is the risc of oil contamination of the vacuum system. This risc, however, has been minimized by the special construction of the pumps with nitrogen cooled baffles preventing direct line of sight. To further minimize the risc the pumps are equipped with built-in pneumatic valves that will close automatically in case of system leaks or pump failure. The measurement chamber is also fitted with a titanium sublimation pump[26] that further reduces H_2, H_2O and CO_2 partial pressures. The base pressure of these chambers, as measured by ionization gauges,[27] is below 5×10^{-11} mbar.

The monochromator chamber, which also houses the x-ray detector, is separated from the measurement chamber by a thin polycarbonate foil.[28] This foil allows the x rays from the sample to pass practically without attenuation. Stray electrons, however, cannot penetrate the monochromator and reach the detector. Also, this foil separates the vacuum of both chambers, at least in the low pressure range. The monochromator chamber is pumped by a small diode ion getter pump.[29] To prevent charged particles to escape from the pump and reach the detector an electrically floating grid is fitted in front of it.

The source chamber can be operated independently from the rest of the system by closing a viton-sealed UHV-valve.[30] This valve incorporates a sapphire window that allows the photocathode to be irradiated by the laser even with the valve closed. The small source chamber is also pumped by a diode ion getter pump.[29] Pressure is measured by a cold cathode gauge.[31] This was chosen instead of an ionization gauge because, firstly, a hot filament can produce CO which is lethal to the photocathode and, secondly, because the O_2 used to activate the photocathode could burn out

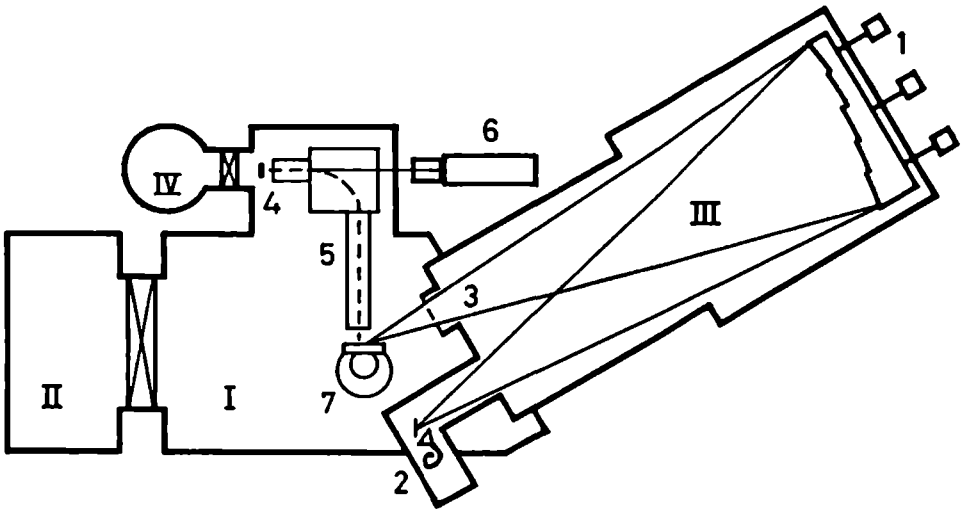

Figure 2.1: Schematic representation of the BISCEPS system: I. measurement chamber; II. preparation chamber; III. monochromator chamber; IV. source chamber; 1. monochromator mirror with adjustment micrometers; 2. x-ray detector; 3. polycarbonate foil; 4. photocathode; 5. electron optics; 6. laser and Pockels cell; 7. sample mounted on weak iron yoke.

the filament. The base pressure in this chamber is well below 5×10^{-10} mbar, the lowest reading of the gauge controller. The entire system can be baked out with high-power resistive heaters after it has been up to atmospheric pressure placing isolating shrouds around it. The bake-out temperature is limited to about 150 °C because of several viton parts. The preparation chamber can be baked separately with resistive heaters strapped around the flanges. This is important, for the pressure during a bake-out can rise to 10^{-7}–10^{-6} mbar which is again incompatible with proper photocathode operation. Changing the sample or evaporator material, etc., in the preparation chamber can thus be done independent of the rest of the system. The measurement chamber is further equipped with standard surface characterization tools such as a reverse-view LEED[32] (low-energy electron diffraction) to check surface structure, and a hemispherical electron analyzer[33] and electron gun[34] for AES (Auger electron spectroscopy) to check surface contamination. The preparation chamber also houses an inert-ion sputter gun[35] to clean the sample surface and a Knudsen cell evaporator[36] and quartz-crystal layer thickness monitor[37] to prepare (epitaxial) overlayers with controllable, slow evaporation rates.

2.2.2. Sample Mounting Facilities

The sample to be investigated is mounted on a high-precission XYZ-manipulator[38] which can travel between the various preparation positions and the measurement position. Presently, this manipulator is equipped with a copper sample holder on which the sample, measuring $10 \times 5 \times 1$ mm^3, is strapped onto a small weak-iron yoke, which is electrically isolated from ground, by two thermocouple wires. The sample can be magnetized by a pulse- or DC-current through a wire wrapped around the yoke. Heating can be achieved by a grounded heater situated just behind the sample. When the sample itself is raised to a high voltage of about 1 kV flash-heating can be performed to temperatures up to 1300 K within minutes. Temperature is monitored by the chromel and alumel wires which hold the sample into place. The manipulator is equipped with a liquid nitrogen (flow) cooling facility. Thermal contact to the sample is provided through a 2-mm sapphire disc by two 5-mm-diameter copper wires that are clamped to the yoke. The lowest sample temperature obtained is approximately 115–120 K. The electrical connections are shielded by a molybdenum plate, only exposing the sample surface. This prevents ceramics to become metal coated during evaporation of overlayers. All electrical connections to the manipulator are plug-in type, hence exchanging samples can be done simply by exchanging the entire sample holder. Also, mechanically sensitive samples, e.g., iron which is notorious for its magnetic anisotropy behaviour under stress, can be mounted and tested by, for instance, MOKE (magneto-optical Kerr effect), before mounting in the UHV system.

2.2.3. The Monochromator

The x-ray monochromator is a crucial element of the BISCEPS system. It determines both the maximum attainable resolution as well as the signal strength, which is expected to be relatively low with the spin-polarized electron source. It also determines the "Isochromat" energy at which the "Bremsstrahlung" is detected in a BIS experiment. In a combined XPS/BIS apparatus the detection energy is fixed by the demand that, first of all, the monochromator has to be suited for Al Kα radiation at 1486.7 eV. This is not the case for the present BISCEPS apparatus in which no (monochromatized) XPS is planned.

The most suitable type of monochromator, which combines the demands of high resolution and high intensity, is the Johann design[39] depicted on the left hand side of Fig. 2.2. This design consists basically of a crystal, bent into a *radius* R, which, together with the source and the detector, is located on a Rowland circle of *diameter* R. Fullfilment of the Bragg condition for constructive interference leads to focussing of monochromatized radiation from a point source onto the detector. However, if the crystal is made larger (distance 'x' in Fig. 2.2) the focus and the transmitted energy distribution become progressively wider. A refinement of this design, depicted on

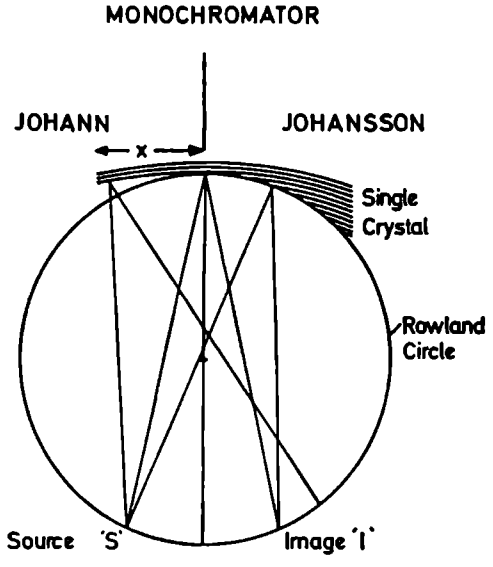

Figure 2.2: Schematic Johann monochromator design (on the left) and Johansson design (on the right) defining the Rowland circle and the positions of source and detector ("image"). Taken from Ref. 40.

the right hand side of Fig. 2.2, avoiding these problems is due to Johansson,[41,42] but this is much more difficult to implement as it requires spherically polished instead of plane crystals. As the monochromator is rotationally invariant around the source-detecor axis (if the mirror surface is toroidal) there is no inherent limit on the crystal size in the direction perpendicular to the Rowland circle. Still, a large acceptance angle only seems possible with a large reduction of the resolution. A solution to this problem is given by the observation that the shift of the energy for which the Bragg condition is satisfied for a point away from the center of the mirror can be compensated by shifting the reflecting crystal accordingly closer to or further away from the source–detector line. In practice, one shifts macroscopically sized crystals in discrete steps so as to minimize the total deviation from the central energy, per crystal. In fact, this configuration mimics the Johansson design. The resulting design of our monochromator[43] is shown in Fig. 2.3.

The monochromator mirror consists of 40 quartz crystals[44] measuring $40 \times 40 \times 0.4$ mm^3, with the (100) Bragg planes (Y-cut, $d = 4.25$ Å) parallel to the surface. With the angle of incidence set at 84.7° this fixes the energy at 1463.0 eV. The crystals are bent into a radius of 600 mm and cemented onto a spherical 280-mm-diameter stainless steel backplate.[45] This procedure did result in cracks in some of the crystals, but as long as their surface follows the shape of the backplate this is not a problem. The backplate is cut into five 40-mm-wide segments which are shifted with respect to each other according to ray-tracing minimization of the aberrations. The acceptance angle of the monochromator adds up to 0.14 sterad. The experimental

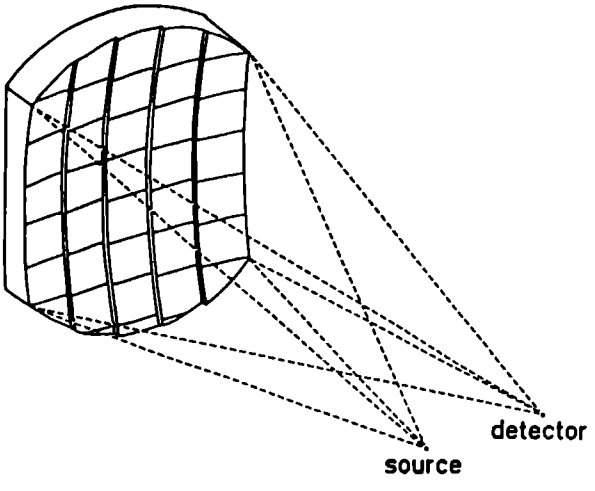

Figure 2.3: BISCEPS monochromator in perspective.

configuration is such that the monochromator "sees" the sample, which represents the source of x-rays, under an angle of 15°–30°. The circular focus of the electron beam on the sample is thus transformed into an elliptical shape which also helps to reduce aberrations caused by the finite source dimensions. The calculated geometry-related resolution for a point source is $\sim$0.1 eV. The actual resolution depends also on the quality of the quartz crystals (rocking curve) and possible contributions due to strain. The experimentally determined resolution of the monochromator alone, deduced by taking the 10%–90% width of the Fermi edge of clean nickel, amounts to 0.65 eV. This value, although not significantly better than achieved in other systems, combined with the exceptionally large solid angle, makes the monochromator excellently suited for BISCEPS experiments.

2.2.4. X-ray Detection

The detector which measures the monochromatic x-ray intensity also has to be as efficient as possible. For subsequent signal processing the x-ray intensity is converted into current pulses. These can then be converted into voltage pulses, discriminated, and shaped into TTL-pulses, which can be counted by some logic device. To achieve this we followed the design by Lang and Baer.[14] The detector consists first of all of a grounded stainless steel disc onto which a 5000 Å CsI film is evaporated. This material was shown to produce, with high efficiency, low-energy secondary electrons when irradiated by soft x rays. An alternative to the use of CsI, which has a broad but still relatively low response characteristic, would be to use a material with a resonant absorption line at the right energy. In our case this would be some thullium salt. A salt, because an insulator prevents hot electrons from recombining before they can escape into the vacuum, and thullium because it has an absorption line

exactly at 1463.0 *e*V. The secondary electrons emitted by the CsI are accellerated to the input cone of a single channel electron multiplier[46] (channeltron) by a 200 V potential difference. The channeltron is operated at 2800 V. To prevent stray charged particles from entering the channeltron the entire assembly is mounted inside a grounded stainless steel shield. A 20-mm-diameter opening, covered by a 1-μm aluminum foil,[47] allows the x rays to illuminate the CsI. Together with the floating grid in front of the ion getter pump this maintains the background count rate at less than 0.3 c/s. Thanks to the foil, blocking electrons that scatter from the sample during measurements, the total background intensity in the spectra does not significantly increase above this value. The detection system, consisting of monochromator and detector, produces a net count rate of more than 10 c/s per μA sample current from the empty nickel states just above the Fermi level.

2.2.5. The Spin Polarized Electron Source

General Considerations

Spin sensitive spectroscopies using incident electrons can only be performed if spin polarized electron beams can be produced with sufficient intensity, preferably comparable to unpolarized sources. Such a source has become available since it was demonstrated in 1976[18] that a GaAs photocathode not only emits spin polarized electrons when it is irradiated with circularly polarized light, but that it also exhibits all characteristics of a good electron source. Before that, other sources were available (for a comparative list, see Ref. 18), but none combining the same brightness with the ease of operation of a GaAs spin polarized electron source.

The use of heavily *p*-doped GaAs as a photoemitter has been known since 1965.[48] GaAs is a direct-gap semiconductor with a gap of 1.52 *e*V. Electrons that are excited to the conduction band can only escape into the vacuum if their energy is high enough to overcome the electron affinity, the difference between the vacuum level and the bottom of the conduction band, which is of the order of 4–5 *e*V for the clean surface. Adsorption of an electropositive metal, e.g., cesium, on the surface lowers the work function to about 1.4 *e*V above the Fermi level. This layer also induces downward band-bending at the surface. If a semiconductor is *p*-doped the Fermi level is located near the bottom of the gap. In a heavily doped material the band-bending region becomes very small, i.e., smaller than the escape depth for excited electrons. Combining all these effects leads to a situation where the bottom of the conduction band *in the bulk* is about equal in energy to the work function at the surface. Adding not only cesium but also oxygen to the surface was later found to lower the work function even more so that the vacuum level becomes lower than the bottom of the bulk conduction band. This is known as negative electron affinity (NEA).[49] The exact mechanism which is responsible for the reduction of the work function when oxygen and cesium are adsorbed is, however, still unknown, in spite

of extensive ongoing research.[50-55]

A net spin polarization of the electrons excited into the conduction band is accomplished using optical orientation. Since the direct gap of GaAs is located at the high-symmetry Γ-point, i.e., the center of the Brillouin zone, the states to be considered in threshold excitation of electrons from the valence band into the conduction band have well-defined total angular momenta J. Hence, it is straightforward to calculate relative transition probabilities for dipole-induced excitations. It follows that if the exciting light is circularly polarized the electrons in the conduction band have a net polarization of + or −50%, depending on wether the light is of σ^+ or σ^- helicity. The polarization is defined as the normalized difference between the number of electrons with spin parallel or antiparallel to the incoming light, i.e.,

$$P_0 = \frac{N_\uparrow - N_\downarrow}{N_\uparrow + N_\downarrow}. \tag{2.1}$$

The theoretical value of 50% holds only if the exciting light matches the gap exactly. If the light has higher energy there will also be transitions away from the Γ-point. Also, if transitions can be made from the spin-orbit split band, located 0.34 eV below the top of the valence band, the net polarization vanishes identically. Apart from these intrinsic effects, also spin-flip scattering, especially in the activating Cs:O-layer,[18] can reduce the polarization. For light ranging from 1.52–1.86 eV, i.e., in the near infra-red, a polarization of up to 45% has been obtained from NEA GaAs photocathodes. Nowadays light sources in this range are readily available in the form of solid state diode lasers. Before that, and also to avoid the experimental difficulties of working with IR radiation, it was proposed to use materials with similar bandstructure but with a larger gap than GaAs. For this purpose $GaAs_{1-x}P_x$[56-58] and $Al_xGa_{1-x}As$[59] have been investigated. For GaAsP the gap remains direct up to $x = 0.49$ and for AlGaAs up to $x = 0.45$. In both cases the maximum direct gap is ∼2 eV. It was shown that these systems indeed show similar behaviour to plain GaAs, however, with slightly reduced polarization. As, at the time this project started, laser diodes of sufficient power were not yet available, we decided to use $Al_xGa_{1-x}As$ with an Al-concentration $x = 0.32$. This material has a gap of 1.9 eV,[59] to fit the energy of our 25-mW HeNe-laser.[60] For this combination a polarization of approximately 30% has been reported.[59] It should be noted here that, given a particular laser/photocathode-combination, the polarization tends to decrease if the electron yield is increased by further lowering of the work function, presumably by depolarization in the Cs:O-layer. Hence, the highest yield is not generally accompanied by the highest polarization.

The AlGaAs photocathodes were prepared by metalorganic chemical vapour deposition (MOCVD). Heavily p-doped (∼10^{19} Zn/cm^3) layers of 5000 Å thickness were grown on a GaAs(100) substrate.[61] One aspect of the use of AlGaAs as photocathode material needs some attention. Due to the high Al-content these crystals

tend to oxidize very rapidly. Transferring the crystal from the MOCVD system to the BISCEPS system is impossible if the surface is not protected from oxidation. *In situ* ion sputtering of the photocathode surface has been applied[58] but surface damage is likely to occur.[62] Several other schemes have been used, especially in molecular beam epitaxy (MBE), like growing a thick GaAs[63] or InAs[64] capping layer on top of the AlGaAs. Such a layer can be heated off *in situ*, but only in the presence of a considerable As background pressure. Another possibility, which we preferred to apply, is to adsorb an amorphous As capping layer. This had been shown to work for MBE-grown AlGaAs.[62,65,66] The As capping layer can easily be heated off at relatively low temperature, of the order of 100–200 °C. It turned out that it is indeed possible to make such a capping layer in an MOCVD system, but that there is no guarantee that the capping is closed or of homogeneous thickness.

A quite recent development, that applies equally to both MBE and MOCVD, is to grow a thin, ~100 Å GaAs layer on top of the AlGaAs. This layer provides the desired protection from oxidation. It has been shown[67] that the emission from this thin layer, which is essentially unpolarized when irradiated with a HeNe-laser, is much smaller than that from the AlGaAs which has almost unchanged polarization and emission characteristics. Such a heterostructure combines the advantages of AlGaAs and GaAs photocathodes. We have used such a AlGaAs/GaAs photocathode, grown by MBE,[68] and found it to exhibit about the same properties as the MOCVD-grown AlGaAs/As photocathodes.

Recently, we adapted the optical system to accommodate also plain GaAs photocathodes, i.e., we incorporated a laser diode[69] and special broad band mirrors[70] that are suited for the laser diode as well as the HeNe laser. Experience with this system, however, is just beginning to accumulate.

A spin polarized electron beam is obtained by illuminating the activated photocathode with circularly polarized light. This is achieved by passing the linearly polarized laser beam through a Pockels cell[71] in $\lambda/4$ mode. Reversing the Pockels cell voltage polarity by means of a high-voltage logic switch changes the sign of the light helicity and thereby the sign of the polarization of the emitted electrons with respect to the quantization axis, which is defined by the laser beam illuminating the cathode.

Operating Procedure

The AlGaAs and GaAs photocathodes we use measure $12 \times 8 \times 0.3$ mm^3 and are mounted on a ceramic holder, which is in turn attached to a Z-translator, by means of tantalum clamps. Preparation of the photocathodes is performed in the source chamber. The surface is cleaned by passing a DC current (~ 0.5 A/6 V) directly through the crystal. The maximum temperature, measured by a chromel/alumel thermocouple behind the crystal, is ~450 °C for AlGaAs and ~600 °C for GaAs.

At the same time the pressure is never allowed to rise above 1×10^{-9} mbar during the cleaning procedure and is mostly well below 5×10^{-10} mbar. The cathode is activated to NEA[18,72–75] by applying cesium from a dispenser[76] to the surface, at an approximate rate of one monolayer (ML) per 15 minutes, and adding small amounts of oxygen[77] by means of a leak valve at a partial pressure of 1×10^{-8} mbar to a total dose of 5 to 10 Langmuir (L; $1\text{L} = 1 \times 10^{-6}$ Torr s $= 0.75 \times 10^{-6}$ mbar s). During the activation procedure the photocathode is set at a moderate potential (−45 V battery) and irradiated by the laser. Thus, the emission current can be monitored by a picoammeter.[78] We found that applying the oxygen continuously (after the first emission maximum with cesium-only is reached) or in a "yo-yo" fashion gave identical results.

Following activation the cathode is moved in front of the electron optics. There, another cesium dispenser is mounted. For large initial currents the emission tends to decrease very fast. This is due to the combined effects of contamination of the activating layer and to cesium depletion. The latter can occur either via direct electron stimulated desorption, "sputtering" by positive ions that are desorbed from other parts by fast electrons, or by resistive heating of the semiconductor surface. It turned out that adding small amounts of cesium,[74] at intervals or continuously, increased the decay time by several orders of magnitude to a $1/e$ time-constant of 10 to 20 hours. Cooling of the photocathode (with water or liquid nitrogen) may have a positive effect on the decay time as well as on the attainable polarization.[18]

Whenever the emission current has degraded too much the cathode can be heat cleaned again and reactivated. This procedure can be repeated several times[59] before replacement of the crystal becomes necessary.

The maximum emission currents we obtained, with an incident light power of 20–25 mW, were around 50–80. μA, decreasing with every successive activation, especially the first few. From extrapolation of literature values it was expected that emission up to a few hundred microamperes should have been possible. The exact reason for this discrepancy is unclear. Apart from the possibility that the reported values are too optimistic, it may be that a linear extrapolation is no longer valid at high currents. Previous photocathode studies have often been performed at quite low emission currents. Another possible explanation could be found in the quality of the photocathode crystals. It has been observed by other groups[75] that the performance of GaAs photocathodes depends strongly on the individual crystal quality. The fact that we found no distinct differences between the MOCVD-grown AlGaAs and the MBE-grown AlGaAs/GaAs photocathodes, however, seems to rule out this effect as the main cause of the low emission. It also invalidates the assumption that the AlGaAs is already oxidized before the intitial heat clean, because especially the GaAs overlayer should be quite effective in protecting the AlGaAs. The most likely explanation, as far as we see, is that the heat cleaning procedure either damages the crystal structure or stoichiometry at the surface, or, alternatively, that during the

heat clean the surface becomes poisened with CO. Either mechanism would result in a surface that exhibits "dead" spots or spots that can no longer be activated to NEA. In fact, we did see some improvement when we kept the pressure during the heat cleaning below 1×10^{-9} mbar, and also when we kept the maximum heat clean temperature well below 450 °C. It should be noted that the emitted electrons can also produce CO by stimulated desorption from the vacuum chamber walls and the entrance aperture of the electron optics. The only real solution to this problem is to have ample pumping capacity in the source chamber and to take great care that all parts in the neighbourhood of the photocathode do not become contaminated with CO (or hydrocarbons). In the course of time we did see some improvement, perhaps caused by the fact that all parts near the cathode became covered with cesium.

2.2.6. Electron Optics

The kind of electron gun generally applied in BIS-experiments, i.e., the Pierce type,[79,80] is designed to use highest possible, space-charge-limited current densities.[14,81] For BISCEPS, in the present configuration, this concept is not applicable because the electrons, which leave the photocathode with longitudinal polarization, have to hit the sample with transverse polarization (parallel to the in-plane sample magnetization). This can be achieved by electrostatic deflection.[82] The electron optical system further has to able to accelerate the electrons to the required kinetic energy (~ 1460 eV) without large variations in the throughput and with a focus size of the order of 1–3 mm diameter. We used an electron optical system developed at the KFA Jülich[83] which, although actually designed for use at low energies ($\sim$100 eV), fulfills our requirements.

The electrons are accelerated from the photocathode to the entrance aperture of the electron optics to 500 eV kinetic energy. With this energy they subsequently pass through a 90° spherical deflector and are accelerated (or decelerated) to the required kinetic energy by a four-element electrostatic zoom lens. The high pass energy was chosen to be able to use high current densities without reaching the space charge limit, but it implies that no monochromatization of the electrons takes place. This is no drawback as a photocathode with the gap properly matched to the exciting light, produces a very small energy spread. From elastic scattering experiments we estimate the energy spread to be 0.25 ± 0.04 eV (full width at half maximum) under normal experimental conditions. Also "low-temperature" thermal emitters, like indirectly-heated impregnated BaO cathodes,[84] produce a low enough energy spread to be used instead of the photocathode. To reduce disturbing effects from stray magnetic fields the entire electron optical system is enclosed in a mu-metal shielding.

The custom-built electrical supply for the electron optical system consists of high stability high-voltage modules[85] with additional feedback circuitry to further

decrease ripple and drift. The kinetic energy supply can be set with a precision of 30 mV to the required energy by a 16-bit DA-converter, either manually or remote. Adjustment of the pass energy, the voltage on the 90°-deflector, and small corrections to the beam path by means of built-in X- and Y-deflection plates, is provided by frontpanel controls. The supply and electron optical system can be used either with the photocathode for BISCEPS and spin-polarized electron energy loss (SPEELS) experiments or with a BaO cathode for (unpolarized) BIS, EELS or AES measurements.

2.2.7. Measurement Control

Measurements are controlled by a custom-built 68000-based microprocessor system, which drives the DAC of the electron optics HV-supplies, the Pockels cell HV-supply, and (eventually) the magnetization pulser. It also serves as storage device for the counts from the x-ray detector.

Prior to measurements the sample is usually remanently magnetized by a ($\sim$ 40 A) current pulse through the 8-turn coil wound around the weak-iron yoke. Energy scans are made in fixed steps of 50–200 meV. At each point the signal for both light helicities, i.e., for both voltage polarities on the Pockels cell, is stored in two subspectra during a constant dwell time, which is usually of the order of 0.5 seconds. The energy scans over a range of 10–20 eV are repeated until a good signal-to-noise ratio is obtained, or (in case of low signals) as long as the contamination level is still acceptable. For nickel this amounts to about 2 hours at a pressure of $\sim 10^{-10}$ mbar. In order to check and correct for apparatus asymmetry or other, non-exchange-induced asymmetry in the spectra, the measurements are repeated for reversed magnetization. Adding appropriate subspectra together isolates the exchange-induced asymmetry.[86]

Up to 8 measurements can be programmed and executed consecutively. Upon completion, they can be transferred to a central computer system for further processing. An identical microprocessor system controls the electron analyzer HV-supply for AES and EELS measurements.

2.3. Concluding Remarks

The above described system houses all the tools required to perform BISCEPS experiments on well characterized, clean single-crystal surfaces. Possible extensions and/or improvements of the system one might conceive of include additional sample characterization tools. In order to check the magnetization characteristics of bulk samples, as well as of thin overlayers on non-magnetic substrates,[87] one could add an *in situ* MOKE set-up. It would also be advantageous to be able to perform XPS, instead of AES, for chemical characterization of the sample. With XPS one

can probe core levels as well as the valence band, and the results may be easier to interpret in terms of, e.g., bonding characteristics, than AES results. Apart from that, XPS also completes the picture of the valence band that results from BISCEPS, even when it is not spin polarized.

Possible improvements to the photocathode system have already been mentioned. This includes the possible benefit one might draw from cooling the cathode holder assembly with water or even liquid nitrogen. Changing from AlGaAs- to GaAs-crystals is one possibility which is already being implemented.

2.4. References

[1] M. Cardona and L. Ley (Eds.), *Photoemission in Solids*, vol. I and II of *Topics in Applied Physics, Vols. 26 and 27.* (Springer Verlag, Berlin, 1978).

[2] C.R. Brundle and A.D. Baker (Eds.), *Electron Spectroscopy*, vol. 1 and 2. (Academic, London, 1977).

[3] B. Feuerbacher, B. Fitton and R.F. Willis (Eds.), *Photoemission and the Electronic Properties of Surfaces.* (Wiley, New York, 1978).

[4] J.J. Yeh and I. Lindau, At. Data and Nucl. Data Tables **32**, 1 (1985).

[5] M.P. Seah and W.A. Dench, Surf. Interf. An. **1**, 2 (1979).

[6] P.J. Feibelman and D.E. Eastman, Phys. Rev. B **10**, 4932 (1974).

[7] N.J. Shevchik, Phys. Rev. B **16**, 3428 (1977).

[8] F.J. Himpsel, Adv. Phys. **32**, 1 (1983).

[9] U. Heinzmann and G. Schönhense, Ch. 11 of Ref. 11.

[10] E. Kisker, Ch. 12 of Ref. 11.

[11] R. Feder (Ed.), *Polarized Electrons in Surface Physics.* (World Scientific Publishing, Singapore, 1985).

[12] V. Dose, Surf. Sci. Rep. **5**, 377 (1985).

[13] N.V. Smith, Rep. Prog. Phys. **51**, 1227 (1988).

[14] J.K. Lang and Y. Baer, Rev. Sci. Instrum. **50**, 221 (1979).

[15] P.A. Cox, J.K. Lang and Y. Baer, J. Phys. F **11**, 113 (1981).

[16] J.K. Lang, Y. Baer and P.A. Cox, J. Phys. F **11**, 121 (1981).

[17] W. Speier, J.C. Fuggle, R. Zeller, B. Ackermann, K. Szot, F.U. Hillebrecht and M. Campagna, Phys. Rev. B **30**, 6921 (1984).

[18] D.T. Pierce and F. Meier, Phys. Rev. B **13**, 5484 (1976).

[19] J. Unguris, A. Seiler, R.J. Celotta, D.T. Pierce, P.D. Johnson and N.V. Smith, Phys. Rev. Lett. **49**, 1047 (1982).

[20] H. Scheidt, M. Glöbl, V. Dose and J. Kirschner, Phys. Rev. Lett. **51**, 1688 (1983).

[21] A. Seiler, C.S. Feigerle, J.L. Pena, R.J. Celotta and D.T. Pierce, J. Appl. Phys. **57**, 3638 (1985).

[22] L.E. Klebanoff, R.K. Jones, D.T. Pierce and R.J. Celotta, Phys. Rev. B **36**, 7849 (1987).

[23] M. Donath, Appl. Phys. A **49**, 351 (1989).

[24] Type 10744-CE01 bakeable gate valve, VAT, Haag, Switzerland.

[25] Edwards EO4K diffusion pump with polyphenylether fluid and CCT100 liquid nitrogen trap, supplied by VG Instruments (UK).

[26] ST22, VG Instruments (UK).

[27] VIG17, VG Instruments (UK).

[28] Bayer (FRG).

[29] PID 50, MECA-2000, supplied by VG Instruments (UK).

[30] GV28SW gate valve with 6.4-mm-diameter sapphire window, VG Instruments (UK).

[31] IKG011, Balzers (Liechtenstein).

[32] 640-2 RVL reverse view, VG Instruments (UK).

[33] EA10/100, Leybold Heraeus (FRG).

[34] EQ11/35, Leybold Heraeus (FRG).

[35] AS10, Vacuum Science Workshop (UK).

[36] Radak I, Luxel Corp., 515 Tucker Ave., Friday Harbor, Washington, USA.

[37] IL100, Intellemetrics (UK).

[38] HPLT600, VG Instruments (UK).

[39] H.H. Johann, Z. Phys. **69**, 185 (1931).

[40] J.C. Fuggle (unpublished).

[41] T. Johansson, Naturwiss. **20**, 758 (1932).

[42] T. Johansson, Z. Phys. **82**, 507 (1933).

[43] Custom-built by Vacuum Science Workshop, Warwick Road South, Old Trafford, Manchester, UK.

[44] Dr. Steeg und Reuter GmbH, Bernerstrasse 109, Frankfurt, FRG.

[45] Manufactured from SS420 by Zeiss, Oberkochen, FRG.

[46] Type 959BL, Philips Elcoma.

[47] Goodfellows Metals (UK).

[48] J.J. Scheer and J. van Laar, Sol. St. Commun. **3**, 189 (1965).

[49] R.L. Bell, *Negative Electron Affinity Devices.* (Clarendon, Oxford, 1973).

[50] B.J. Stocker, Surf. Sci. **47**, 501 (1975).

[51] C.Y. Su, W.E. Spicer and I. Lindau, J. Appl. Phys. **54**, 1413 (1983).

[52] D.C. Rodway and D.J. Bradley, J. Phys. D **17**, L137 (1984).

[53] D.C. Rodway, Surf. Sci. **147**, 103 (1984).

[54] D.C. Rodway and M.B. Allenson, J. Phys. D **19**, 1353 (1986).

[55] R. Cao, K. Miyano, T. Kendelewicz, I. Lindau and W.E. Spicer, Phys. Rev. B **39**, 12655 (1989).

[56] J.S. Escher and G.A. Antypas, Appl. Phys. Lett. **30**, 314 (1977).

[57] D. Conrath, T. Heindorff, A. Hermanni, E. Ludwig and E. Reichert, Appl. Phys. **20**, 155 (1979).

[58] J. Kirschner, H.P. Oepen and H. Ibach, Appl. Phys. A **30**, 177 (1983).

[59] F. Ciccacci, S.F. Alvarado and S. Valeri, J. Appl. Phys. **53**, 4395 (1982).

[60] GLG5700, NEC.

[61] AlGaAs photocathodes were grown by MOCVD by X. Tang, Solid State Physics Department, University of Nijmegen, The Netherlands.

[62] M. Campagna, S.F. Alvarado and F. Ciccacci, AIP Conf. Proc. **95**, 566 (1983).

[63] H. Tanaka, M. Mushiage, Y. Ishida and H. Fukada, Jpn. J. Appl. Phys. **24**, L89 (1985).

[64] Y.-J. Chang and H. Krömer, Appl. Phys. Lett. **45**, 449 (1984).

[65] P. Etienne, P. Alnot, J. Rochette and J. Massies, J. Vac. Sci. Technol. **B4**, 1301 (1986).

[66] S. Sinharoy, Y.F. Lin and J.H. Rieger, J. Appl. Phys. **61**, 1655 (1987).

[67] F. Ciccacci, H.-J. Drouhin, C. Hermann, R. Houdré and G. Lampel, Appl. Phys. Lett. **54**, 632 (1989).

[68] Heterostructure AlGaAs/GaAs photocathodes were grown on GaAs(110) by MBE by H. Meier, IBM Rüschlikon, Zürich, Switzerland.

[69] Philips collimated laser diode, type CQL72A/D, 25 mW, 820 nm.

[70] Melles Griot, external protected silver.

[71] PC18, Electro Optic Developments (USA).

[72] D.T. Pierce, R.J. Celotta, G.-C. Wang, W.N. Unertl, , A. Galejs, C.E. Kuyatt and S.R. Mielczarek, Rev. Sci. Instrum. **51**, 478 (1980).

[73] F. Meier and B.P. Zacharchenya (Eds.), *Optical Orientation*, vol. 8 of *Modern Problems in Condensed Matter Sciences.* (North-Holland, Amsterdam, 1984).

[74] F.C. Tang, M.S. Lubell, K. Rubin, A. Vasilakis, M. Eminyan and J. Slevin, Rev. Sci. Instrum. **57**, 3004 (1986).

[75] U. Kolac, M. Donath, K. Ertl, H. Liebl and V. Dose, Rev. Sci. Instrum. **59**, 1933 (1988).

[76] CS/NF/3.9/12 FT 10+10, SAES-getters, Via Gallerate 215, Milano (Italy).

[77] Purity 4N8 O_2, Messer Griesheim.

[78] Type 485 picoammeter, Keithley.

[79] J.R. Pierce, J. Appl. Phys. **11**, 548 (1940).

[80] J.R. Pierce (Ed.), *Theory and Design of Electron Beams.* (Van Nostrand, Princeton, 1954).

[81] F U. Hillebrecht, J. Keppels and R. Otto, Rev. Sci. Instrum. **58**, 776 (1987).

[82] J. Kessler, *Polarized Electrons*, vol. 1 of *Series on Atoms and Plasmas.* (Springer Verlag, Berlin, second edition, 1985).

[83] R. Rochow. *Ein neuartiges Elektronenspektrometer zur Energieverlust-spektroskopie spinpolarisierter Elektronen.* Master's thesis, KFA Jülich, 1984.

[84] Type 134 tungsten dispenser cathode, Spectra-Mat, 1240 Highway 1, Watsonville, California (USA)

[85] PM series, Wallis Electronics (UK).

[86] S.F. Alvarado, R. Feder, H. Hopster, F. Cicacci and H. Pleyer, Z. Phys. B **49**, 129 (1982).

[87] S.D. Bader and E.R. Moog, J. Magn. Soc. Jpn. **11S1**, 7 (1987).

3. Applications of BISCEPS[†]

In this chapter we describe two applications of BISCEPS. The first concerns the clean surface of Ni(110). This experiment is intended to demonstrate the feasability of the method itself, as well as provide insight in the physics of the magnetic phenomena in this prototype ferromagnetic material. We furthermore propose to use Ni as a reference probe to determine the polarization of the electron beam in future experiments.

The second application is more ambitious and in fact is not completed yet. This experiment deals with thin overlayers of the rare earth metal Gd on the Ni(110) surface. It should provide more insight into the magnetic (next to crystal field) effects playing a role in this system, which in some respects could be regarded a prototype of rare earth-transition metal intermetallics. The results obtained sofar deal mainly with the structural and chemical characterization of the system.

3.1. BISCEPS of Ni(110)

The choice of material to perform the first BISCEPS experiments on is governed by a few basic requirements, mainly concerning the effort to keep the experiment as simple as possible as far as the sample is concerned. First of all, of course, it has to be (ferro)magnetic. It also has to have a substantial magnetization at room temperature to avoid having to cool the sample. Finally, it preferably has to be a mono-atomic material so it can be easily (sputter-)cleaned without risk of changes in surface stoichiometry. These requirements reduce the possibilities to the $3d$-transition metals (TM): Fe, Co, and Ni. Co and Ni are so-called strong ferromagnets,[1] meaning that there are only holes present in the minority spin d-band. This provides the possibility to determine the incident electron beam polarization in a self-calibrating fashion, as will be described later. Furthermore, Ni has the easiest accessible Curie temperature (631 K, as opposed to 1044 K for Fe and 1390 K for Co) which may be advantageous in studies of the phase transition, it does not undergo a structural phase transition at high temperature as does Fe, and in the literature there are no indications that Ni presents difficulties with respect to magnetic anisotropy changes at the surface, which again is the case for Fe. Theoretically, Ni is by far the most investigated material, with excellent calculations (in the correct crystal structure)

[†]Parts of this Chapter have been published in Rev. Sci. Instrum. **61**, 765 (1990).

readily available, as well as many (model) calculations on finite temperature and self-energy effects. It will be obvious that the choice was made for Ni.

3.1.1. Sample Preparation

The sample we used was a (110)-oriented Ni single crystal.[2] This crystal was spark-cut[3] and mechanically polished,[4] the final polish using 0.25 μm diamond paste. Subsequently it was annealed in a glass tube furnace at 650 °C, first for 12 hours under a 5×10^{-4} mbar H_2 flow to reduce sulphur contamination, and then for 12 hours under a 1×10^{-7} mbar vacuum. Once mounted in the UHV system the sample was cleaned by Ar sputtering at room temperature (500 eV, $\sim 10\mu A/cm^2$, 45°–80° incidence) followed by flash heating by electron bombardment to 800 °C. This procedure resulted in reproducibly clean and well-ordered surfaces. The AES spectra showed no sulphur or oxygen contamination and only very small carbon signals. LEED showed sharp spots on a low background from $\sim$35 eV up to $\sim$600 eV on the entire surface, with no traces of facetting or reconstruction.

The [111]-axes are the easy magnetization directions of Ni. The (110) surface orientation was chosen so that the crystal could be cut with the long side parallel to a [111]-axis which then coincides with the quantization axis of the system as defined by the electron source. Magnetizing the crystal along an easy axis, together with the favourable shape, helps to keep the remanent magnetization in the surface plane. In the (110) surface plane there are, however, two [111] axes, making an angle of approximately 70°. From magneto-optical Kerr effect (MOKE) tests on similar crystals we found that there may be domains oriented along the wrong axis in the surface plane, even when the driving magnetizing field had been applied along the long side. This means that the magnetization, projected along the quantization axis, can be considerably reduced. Probably this phenomenon is related to the sample history. Recent MOKE tests seem to indicate that the best treated samples still only have a remanent magnetization of $\sim$80% of the saturation value at room temperature. We were not yet able to perform MOKE tests on this particular sample.

3.1.2. Experimental Results

The BISCEPS spectrum of this Ni(110) sample is shown in Fig. 3.1. The total spectrum shows a peak up to 1.5 eV above the Fermi level, derived from the 3d-band of Ni. This peak is superimposed on a rather smooth signal derived from s- and p-bands. These show a structure at about 6 eV above E_F corresponding to a so-called critical point in the bandstructure. Furthermore, the spectrum shows a progressively increasing background due to inelastically scattered electrons. The asymmetry data show a distinct peak at the same energy as the 3d-signal in the total spectrum. The maximum value of this asymmetry peak amounts to $-10 \pm 1\%$.

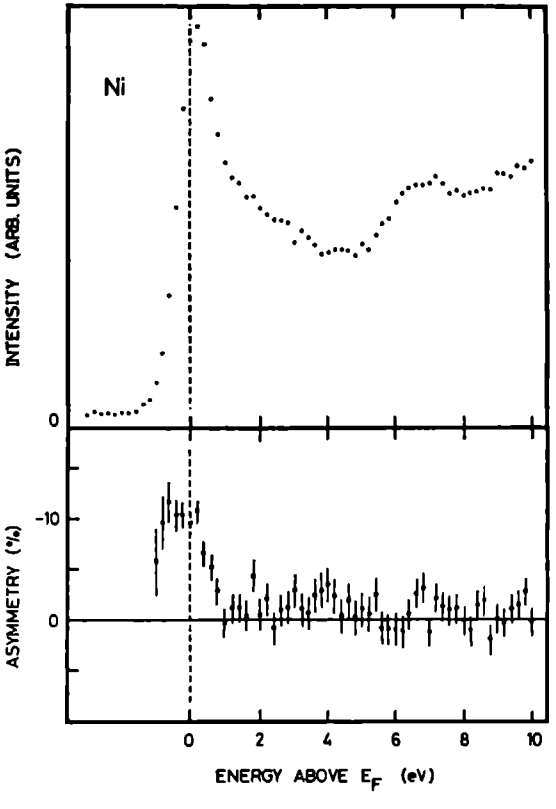

Figure 3.1: BISCEPS of Ni(110). Top: total (unpolarized) intensity N_T. Bottom: normalized asymmetry N_A. The error bars represent one standard deviation.

Due to the incomplete polarization P_0 of the electron source the spectra for positive and negative helicity, N_+ and N_- respectively, constitute a mixture of pure spin up and spin down contributions. Also, as mentioned in the previous section, the presence of wrongly oriented domains would result in such a mixing. The parameter involved is the reduced magnetization, $m \equiv M_z/M_0$, where M_0 is the saturation magnetization at zero temperature and M_z is the net (remanent) magnetization along the spin quantization axis defined by the electron source. From the measured spectra we calculated the total intensity, $N_T \equiv N_+ + N_-$, and the normalized asymmetry, $N_A \equiv (N_+ - N_-)/N_T$. The total spectrum corresponds to the usual BIS measurement with unpolarized electrons, and compares to the best published data.[5] The asymmetry, which represents the new information provided by BISCEPS, is, as far as its shape is concerned, not influenced by P_0 nor m. The absolute value, on the other hand, is related to the actual asymmetry, $A \equiv (N_\uparrow - N_\downarrow)/(N_\uparrow + N_\downarrow)$, between up- and down-spin spectra, $N_\uparrow$ and $N_\downarrow$ respectively, by $N_A = |m| \times |P_0| \times A$. This means, that when the (*ad hoc*) parameter $\alpha \equiv |m| \times |P_0|$ is known, the $N_\uparrow$ and $N_\downarrow$ spectra can be calculated from N_T and N_A.

The formulae according to which the actual spin up and spin down spectra can be calculated are:

$$N_{\uparrow} = \frac{N_T}{2}(1+\frac{N_A}{\alpha}) = \frac{N_T}{2}(1+A)\,, \qquad (3.1)$$

$$N_{\downarrow} = \frac{N_T}{2}(1-\frac{N_A}{\alpha}) = \frac{N_T}{2}(1-A)\,.$$

The procedure is now to insert a reasonable value for α in Eq. 3.1, i.e., $0 \leq \alpha < 0.50$, and to observe the resulting spin-up and spin-down spectra.[6,7] Since Ni is a strong ferromagnet, there are nominally no $3d$ majority (up) spin holes. Of course, due to s-d hybridization some holes with d character will be present anyway. However, for the majority-spin spectrum we expect only a smooth sp-signal, quite similar to a copper BIS spectrum, where the $3d$-band is completely below the Fermi level for both spins. This means that we vary α until the $3d$-derived peak at the Fermi level is just removed from the majority spin spectrum. If α is increased over this value, too much spectral weight is removed from this spectrum and an unphysical dip at the Fermi edge results. With this procedure, the resulting spectra are actually quite sensitive to the value of α. The value we deduced in this way, in accordance with the criteria mentioned above, is $\alpha = 0.22 \pm 0.02$. The majority and minority spectra are shown in Fig. 3.2. The error bars include the statistical uncertainty in the measured data as well as the estimated error in α.

At this point it might be useful to discuss the influence of various experimental conditions on the obtained result for α.

Whether the inherent spin polarization maximum of 50% can be obtained in the bulk of the photocathode is determined by the degree of circular polarization of the laser beam, which we estimate to be at least 95%, and the match of laser wavelength and gap energy. In this case we expected for the electron beam in vacuum $P_0 \approx 30\%$, being aware of the fact that the actual polarization might be lower, because of enhanced depolarization in the Cs:O activation layer, if the photocathode is activated for maximum emission. As long as the obtained emission currents do not allow for the possibility to activate the cathode only partially, this cannot be verified to be the case here. On the other hand, we found, within experimental error, different cathodes to yield about the same α and are therefore inclined to believe that this is not the main effect here.

Next in line is the alignment of the laser optical axis, defining the spin quantization axis, and the magnetization axis of the sample. Because of the cosine-dependence on the relative angle this will only have a minor influence.

We then have to consider the possibility of depolarization of the incoming electrons as they enter and traverse the solid before they undergo the (BIS-) transition. Several investigations have shown that depolarization of slow electrons by spin-selective scattering in a ferromagnet can be quite strong.[9-11] On the other hand, it

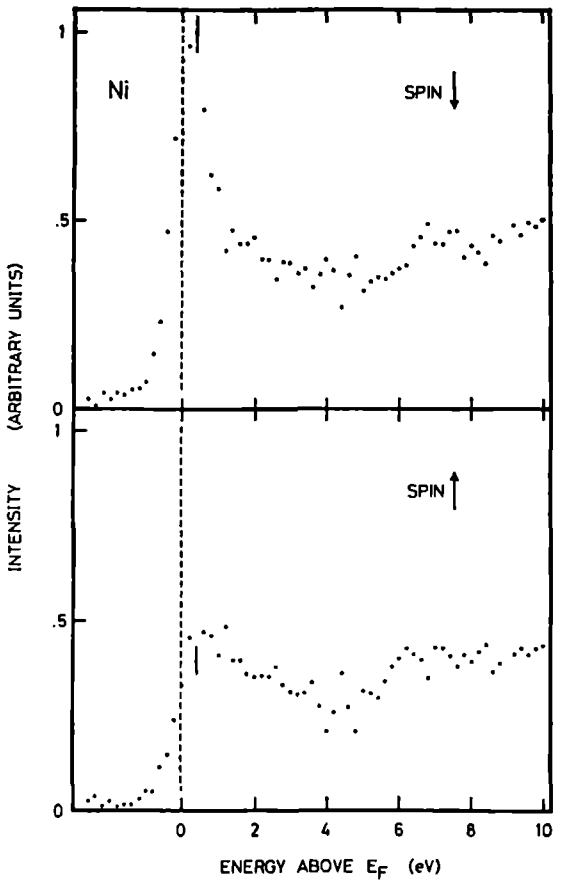

Figure 3.2: BISCEPS of Ni(110). Top: spin-down intensity. Bottom: spin-up intensity. The error bars represent one standard deviation.

has also been shown that the cross section for such (spin-flip) scattering processes is strongly energy-dependent[12,13] and becomes negligible at the high energy we are using.

The occurrence of a spin-flip in the BIS-transition itself has also been proposed.[14] Either by spin-orbit coupling or by interaction with the electromagnetic field. Model calculations have shown that such processes make up a fraction $\hbar\omega/mc^2 \approx 2 \times 10^{-3}$ (at 1500 eV) of the total number of transitions.[15] Therefore, they should in this case be negligible. This means, in fact, that for a theoretical description of the BIS-process a non-relativistic dipole approximation suffices.

Concluding, we believe that the spin-polarization of the electrons which are responsible for the BISCEPS-signal will certainly be of the right order, say, 0.30 ± 0.05. This means that the remaining discrepancy will then have to be accounted for by a reduction of the reduced magnetization m from unity.

The measurements were performed at room temperature, i.e., at $\sim 0.5 T_c$, implying that the magnetization will not be saturated. Bulk magnetization curves yield a magnetization at 0.5 T_c of approximately 95% of the zero-temperature value.[16] On the other hand, it is of course by no means neccesary for the surface to follow the same magnetization curve,[17] or even to have the same zero-temperature magnetization.[18] On account of calculations,[19] and also because of the relatively large probing depth involved in BISCEPS (10–20 Å or 4–8 Ni layers[20]), we nevertheless expect this effect to be small.

As the measurements were performed in magnetic remanence, the presence of wrongly oriented domains does represent a likely cause for a drastic reduction of m. We realize this will have to be checked with MOKE on this particular sample as soon as possible. MOKE tests performed on a sample prepared under comparable conditions indicate that a remanent magnetization of only 70 80% of the saturation magnetization is not unlikely, which would comply perfectly with the α we find.

Finally, it should be mentioned that spectra are also influenced by accumulated contamination of the sample surface. Prolonged single measurements, i.e., without cleaning the surface periodically, have shown that a reduction of α by a factor of 2 can occur, without significant changes in the total intensity spectrum, i.e., as would be measured by BIS. This may be explained by strong spin-flip scattering at the surface even in the presence of only a limited amount of impurities. In that case the total intensity spectrum would not change much, but the polarization of the incoming electrons would be reduced considerably before they can contribute to the BISCEPS signal deeper in the solid. By retaining only measurements taken in sufficiently short counting times and after careful cleaning of the surface, we believe the reported data represent the BISCEPS spectrum of the clean Ni(110) surface.

Concluding, we believe that the α-value we find is quite reasonable under the given (sample) conditions. Moreover, we propose that BISCEPS of Ni could even be used as a reference for other samples, in other words, to employ it as an *in situ* polarization detector. A (polycrystalline) Ni sample, properly attached to an electromagnet, or even just a permanent magnet, and cleaned by Ar sputtering or scraping would suffice. Just to determine the polarization of the electron beam, it would be enough to measure the asymmetry in the energy region around 0.25 eV above the Fermi level Even with low beam currents it would then take relatively little time to determine the beam polarization.

3.1.3. Comparison with Theory

The motivation to develop a new, elaborate experimental technique, such as BISCEPS, was that it would provide additional, important information on the electronic structure of magnetic materials, i.e., more than its unpolarized counterpart BIS, that could help resolve some of the still open questions in the field of magnetism. To

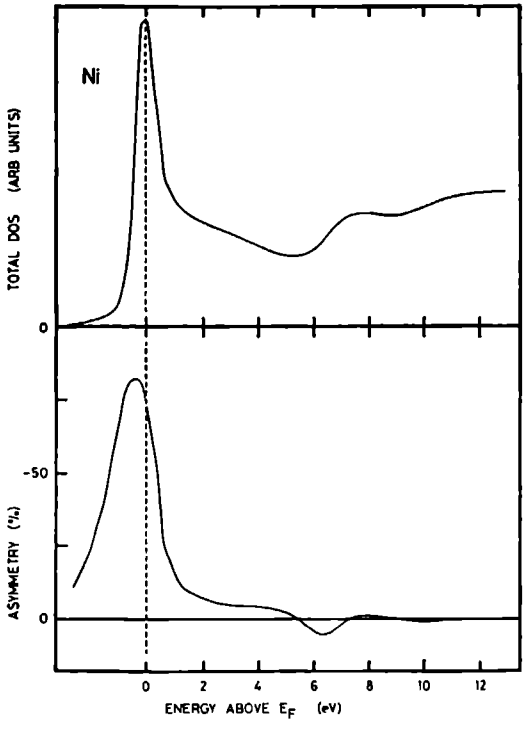

Figure 3.3: Calculated spin-polarized density of states of Ni, including matrix element effects and instrumental (Gauss: FWHM 0.6 *e*V) and lifetime (Lorentz: FWHM 0.1(E - E_F) *e*V) broadening. Top: total DOS. Bottom: asymmetry. From Ref. 23

illustrate this, we are aware of the fact that nickel is not the most perfect example. We even used some of the knowledge we already had, i.e., that nickel is a strong ferromagnet, to determine the polarization of the incoming electron beam and proposed to use nickel as a reference material. Still, a closer comparison of the experimental results with a theoretical bandstructure calculation may serve to illustrate the possibilities *and* difficulties that are associated with the application of so-called high-energy spectroscopies to determine the electronic structure of solids.

It was noted before [see Ch. 1] that the density of states (DOS) that results from a one-electron (single-particle) ground state calculation does not represent the quasiparticle DOS as is probed by (inverse) photoemission. Yet, in many cases it has been observed that the self-energy corrections to the one-electron DOS are limited to straightforward shifts and broadenings, which can easily be simulated to fit theory to experiment. Without, of course, providing insight into the background of the effects. When also solid state effects, i.e., matrix elements, are included in the calculations even better agreement between calculated single-particle densities of states and XPS/BIS data can be obtained.[21,22] Applying this scheme to the unoccupied spin-polarized DOS of Ni results in the curves shown in Figs. 3.3 and 3.4. Comparing this result with experiment [Figs. 3.1 and 3.2] several features attract

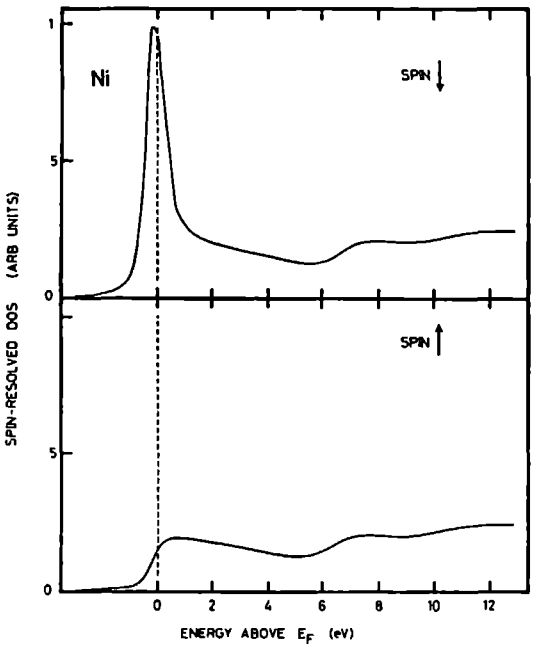

Figure 3.4: See Fig. 3.3. Top: spin down DOS. Bottom: spin up DOS.

attention. The most important discrepancy is the very different peak-to-background ratio of the 3*d*-derived peak at the Fermi level in the total DOS with respect to the unpolarized spectrum [see also Ref. 22]. Note, that this discrepancy is independent of our polarization estimate. As a result of this apparent overestimation of the spin-down *d*-intensity also the maximum asymmetry comes out wrong: ~80% from the calculation (slightly dependent on the applied broadening) *versus* ~45% from experiment (corrected for $\alpha = 0.22$). Also, the energy position of the critical point is found experimentally at ~ 0.4 *e*V, or 7.5% higher energy. Finally, the experimental spectra show a monotonically increasing background, whereas the theoretical spectra level off.

The small energy shift, which could alternatively be regarded as an expansion of the energy scale, is not unlike is found also for, e.g., *s*-band metals, and is a common manifestation of the limitations of LSD-theory applied to (inverse) photoemission.[5]

The increasing background is also easy to account for. It is due to electrons undergoing inelastic collisions before they contribute to the BISCEPS-signal. In view of the arguments given above, regarding electron energy loss transitions including a spin-flip, the inelastic background should be related to each spin direction separately, i.e., without intermixing of the opposite spin signal. In other words, the inelastic background should contribute to the asymmetry at higher energies. The signal-to-noise (S/N) ratio of the experimental spectra at present does not allow for this effect

to be observable, but would provide a direct verification of the small contribution of spin-flip transitions at these energies.

The S/N ratio also interferes with a clear interpretation of the asymmetry around the critical point. Theory predicts that the DOS around this point shows a net asymmetry, caused by the small induced exchange splitting of the *s*-bands. This splitting is very small ($\sim$ 0.3 *e*V) and is only visible at this point because the *s*-bands reach the boundary of the Brillouin zone and therefore have a vanishing dispersion. Although a structure in the experimental asymmetry can be observed at the right energy and of the right (relative) sign and size ($\sim$ 10% corrected), we cannot be certain that it is not just a statistical fluctuation.

The large discrepancy in the minority 3*d*-intensity thus seems to be more fundamental. At the energy we used the Ni 3*d* matrix elements are somewhat larger than the *s* and *p* matrix elements, especially at the top of the *d*-band.[21] The excitation-energy dependence of the matrix elements, as can be seen applied to Ni in Figs. 1 and 2 of Ref. 22, largely agrees with experiment: when the 3*d* matrix elements are much larger (at lower energy) or much smaller (at higher energy) than the *s* and *p* matrix elements the agreement becomes better. However, if for some reason, the 3*d* matrix elements would be smaller by about 30–40% the agreement at this energy would improve without very much affecting the agreement at lower or higher energies.

On the other hand, there are many indications that suggest that applying LSD to (inverse) photoemission data of especially Ni is not straightforward. Valence band photoemission data[24] shows the Ni 3*d*-band at the Fermi level, but much narrower than calculated,[25,26] and a resonant satellite structure some 6 *e*V below the Fermi level. Spin-polarized photoemission experiments[27] have shown that this structure has a high spin polarization. Furthermore, the exchange splitting between spin-up and spin-down bands[28] is about a factor of 2 smaller than calculated.[25,26] It is generally accepted that these discrepancies are caused by considerable intra-atomic electron interaction effects. The reason why these effects are so strong in Ni, and can to a large extent be neglected in, e.g., Fe, lies in the fact that with increasing atomic number the spatial extent of the *d*-band becomes smaller, while at the same time it holds more electrons. Thus, not only the exchange interaction increases, but also the (unscreened) Coulomb interaction. The extent to which these effects are important is governed by the ratio of effective Coulomb interaction and bandwidth. The bandwidth W is a measure of the spatial overlap, or hopping probability, between wavefunctions from different atoms — for free atoms the bandwidth is zero. Upon decreasing the interatomic distance the bandwidth increases and the electrons are more and more free to arrange themselves in such a way as to minimize the Coulomb interaction energy. If $U/W \ll 1$, i.e., either U is small or W is large, the effects can be neglected (or treated as a perturbation). If, on the other hand, $U/W \gtrsim 1$ the effects will be important. Theory predicts for Ni a bandwidth of 3.6 *e*V,[29] whereas

U is estimated to be of the order of 4 eV.[30] It is therefore to be expected that for Ni self-energy effects have to be taken into account explicitly.

In photoemission, self-energy effects can be observed as severe peak distortions in systems with narrow energy bands that, in the excited state, contain more than one hole. For Ni this is the case, but for closed shell materials, such as Cu, there is just one hole present in the excited state, hence self-energy effects are not observed but for a shift of the entire band. The question rises to what extent these effects will be observable in inverse photoemission of Ni, as the excited state will either have the $3d$ band completely filled, or have the extra electron in the sp bands, i.e., delocalized.

As it is impossible to calculate the self-energy exactly, several approximate models have been applied to Ni.[31–34] These attempts aimed at reproducing the bandnarrowing, the reduced exchange splitting and the 6 eV-satellite and its polarization as found in photoemission experiments. With these models the physical background of the spectral features could be identified, but the approximations used were quite crude. Other methods have been developed over the years to calculate self-energies [see Ref. 35 Sec. VI and references therein]. One important method is the so-called GW approximation[36] that has been applied to a variety of materials and has been particularly successful in calculating band gaps of semiconductors.[37] A drawback of present implementations of this method (with pseudopotentials and a plane wave basis set) is that it cannot be applied to d-band materials.

A recent calculation, based on a generalized Hubbard model, of the electronic structure, magnetic properties and spectral distribution of Ni seems to give quite realistic and accurate results.[38,39] The method starts out with a paramagnetic parametrized tight binding DOS calculation, that reproduces an LSD DOS. This is put into a many-body Hamiltonian containing all relevant interactions. The (two) free parameters of the model are fit to obtain the experimental zero-temperature magnetic moment. The model then reproduces quite accurately the experimental critical temperature, magnetization curve and paramagnetic susceptibility. For the present discussion it is important to note that the spectral distribution, or quasiparticle DOS, which is directly observed by (inverse) photoemission, reproduces the 6 eV satellite (and a second satellite), its spin polarization, the bandnarrowing and the reduced exchange splitting.

Comparing their quasiparticle DOS with the LSD single-particle DOS [Fig. 3.5] it appears first of all that also in the paramagnetic state the many-body corrections to the single-particle DOS are quite large — the satellites still appear and across the entire band weight has shifted. Also, the area under the curve above the Fermi level, or chemical potential has changed. Judging from their results the d-intensity in a BIS experiment would be reduced by about 30–40% compared to what would be expected from the single-particle DOS. The sp-states were not included in the many-body calculation, but were just taken from the single-particle DOS, justified

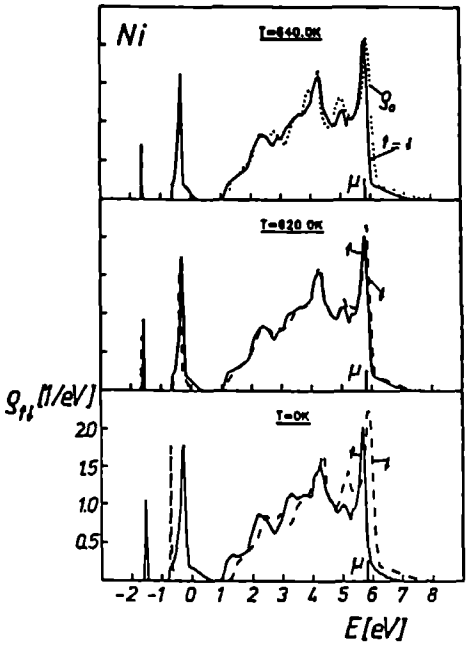

Figure 3.5: Total quasiparticle d-DOS of Ni for three different temperatures. Solid curves: spin up. Dashed curves: spin down. Dotted curve: single-particle DOS. The chemical potential μ is marked by a bar. Reproduced from Ref. 39.

by the assumption that self-energy effects in these extended bands can be neglected. This means that this calculation would probably give excellent agreement with the observed BISCEPS spectra.

If indeed this model calculation reproduces correctly the BIS(CEPS) *and* XPS spectra of Ni, while it already gives a proper description of the macroscopic physical properties, then it seems that all the important interactions have indeed been taken into account properly. This then also has important consequences for the interpretation of the finite temperature properties of Ni which, however, lies beyond the scope of this thesis.

Concluding, we have shown that a comparison of (inverse) photoemission data with theory is not straightforward. In those cases were the electron interactions are very different from the homogeneous electron gas, e.g., insulators, semiconductors, narrow band metals, one must keep the limitations of the method in mind. On the other hand, experimental spectra can be used successfully to test model calculations that allow determination of the quasiparticle DOS, and thus the interplay between theory and experiment can finally lead to a complete understanding of the physical interactions determining material properties.

3.1.4. Discussion

As we have pointed out in the Introduction to Ch. 2, combining the results obtained from different spectroscopies can provide an understanding of specific physical phenomena that would be impossible or very difficult to obtain from any single spectroscopic technique. In this respect BISCEPS is most closely related to spin polarized XPS because of the similar way spectra can be interpreted. Unfortunately, no attempts have been made, as far as we know, to perform genuine XPS, i.e., at energies above, say, 1000 eV, including spin analysis. Such experiments could be performed with existing beamlines at synchrotrons that are presently used for SPARUPS, provided the employed monochromator extends to high enough energy with sufficient intensity.

On the other hand one can also take advantage of the entirely different energy regimes that apply to BISCEPS and SPIPES to gain a better insight into spin resolved electronic structure and the way it is probed by spectroscopy.

We mentioned before that it is possible to perform angular resolved (SP)IPES and scan the Brillouin zone for allowed transitions, thus mapping the detailed bandstructure. This is nicely demonstrated by Donath *et al.*[40] Their data can mostly be described by $\boldsymbol{k}$-conserving transitions. Yet, some contribution to the spectra from DOS-like features cannot be ignored and this interferes with any attempt to a quantitative description of such results. BISCEPS, on the other hand, can be explained exclusively in terms of the total DOS, sampling all available final states, irrespective of the angle of incidence. It has been shown that with valence band XPS and BIS it is in many cases, i.e., whenever self-energy effects can be ignored, possible to obtain excellent quantitative agreement with theoretical DOS calculations when the energy- and symmetry-dependent transition matrix elements are taken into account. For such systems spin polarized BIS enables us to go an important step further and apply this scheme also to the spin resolved DOS of magnetic systems. For systems that do show large self-energy effects, such as Ni and the rare earths, BISCEPS can provide important additional information that can help identifying the important interactions in these systems.

Finally, such studies can be performed on polycrystalline and amorphous samples on the same quantitative footing as monocrystalline samples. This is an important practical advantage of BISCEPS.

The data presented here show that it is possible to perform BISCEPS experiments. Increase of the polarized electron current by a factor of at least 10 should be possible. The consequent decrease of the data acquisition time, which is at present still a drawback, thus will extend the practical range of candidate systems to be investigated in the future. We thus believe BISCEPS will prove to be an important experimental technique to study systems ranging from elemental ferromagnets and binary ferrimagnets to overlayer/substrate systems and amorphous alloys with

respect to magnetic order, exchange coupling, surface effects, etc.

3.2. Gd Overlayers on Ni(110)

An active field of current research deals with the interactions between atoms of different species. Such interactions, can be studied in bulk systems, i.e., alloys, but nowadays much of the state-of-the-art work is performed on ultrathin overlayer films of a metal on a metallic substrate.[41,42] This has several reasons, the most important one being that overlayers on surfaces are perfect model systems for (surfaces of) alloys. Secondly, the modern experimental techniques that are suited to study such interactions, like photoemission, electron diffraction and other related techniques, are all more or less surface sensitive. Finally, surface effects themselves are inherently interesting because of their importance for, e.g., catalysis.

Overlayer systems are also well suited to study magnetic interactions between different elements. Apart from modelling a perfect interface, overlayers also provide the possibility to prepare non-equilibrium epitaxial structures and determine the influence this has on the magnetic properties.[43–50]

Ferrimagnetic rare earth-transition metal (RE-TM) alloys[51] represent a class of materials that has gained importance in recent years because of (possible) applications for hydrogen storage, catalysts, permanent magnets and high-density magneto-optical recording, but also to answer more fundamental questions, such as the behaviour of the Coulomb interaction energy and crystal field effects. These systems are therefore also more and more studied by the overlayer approach. However, it seems that most studies of RE-overlayers on TM-substrates are either concerned with the structural and chemical properties or with the magnetic properties. The result is that there are many excellently characterized overlayer/substrate systems on the one hand, which are less suitable for magnetic studies, and magnetically characterized systems on the other hand, without a clear characterization of the structural and chemical properties.

Structure and chemistry have been investigated on: Nd on Cu(100)[52,53] and on Cu(111),[54] Sm on Cu(100)[55,56] and on Mo(110),[57,58] Eu on W(211),[59] Gd on Ni(111),[60] on Cu(100),[61] and on W(110)[62–64] Tb on W(211)[59] and on W(110),[64–66] Yb on Ni(100),[67–70] on Ni(110),[71] and on Mo(110).[58] Magnetic investigations have been performed on Nd, Gd, Tb and Dy on Fe(100) and on Ni(110). The RE/Fe(100) systems have all been investigated by SPARUPS[72,73]. The first was Gd/Fe(100), which before that had already been investigated by SPAES.[74] The Gd/Ni(110) system has also been investigated by SPAES,[75] whereas the other RE/Ni(110) systems have (preliminary) been studied by MXD by our group.[76–78] With BISCEPS we set out to investigate Gd/Ni(110). The choice for Ni(110) as the substrate was obvious. The main reason to choose for Gd was that the half-filled (or half-empty) $4f$-level forms a fairly narrow single peak at about 4.4 eV above the Fermi level.[79] Hence, the

Gd-signal, which consists of the dominant $4f$-peak on a small, smooth $5d6s$ background, is well separated from the Ni-signal [Fig. 3.1]. In general, for spin-polarized spectroscopies the RE's have the advantage that the (magnetic) $4f$-levels do not directly participate in the bonding, because of their spatial localization. The RE magnetic moments are almost entirely an atomic property, the solid environment merely determining the relative orientation of neighbouring $4f$ moments by indirect exchange and crystal field effects, and the size of the induced $5d$ magnetic moment. This means that, with a predetermined quantization axis, the polarization or asymmetry of the $4f$-level is directly related to the macroscopic magnetization along that axis.

Another reason to investigate Gd/Ni(110) with BISCEPS were the promising results obtained with SPAES (and SPARUPS) for Gd/Fe(100). In these investigations it was shown that the Gd magnetic moment couples antiferromagnetically to the Fe moments, with an extrapolated zero-temperature polarization of -100%. Furthermore, it was shown that the critical temperature T_c of thin Gd overlayers is much higher than for bulk Gd (293 K), although smaller than for the Fe substrate (1043 K). It had even been possible to determine the magnetic correlation length over which the Fe-Gd interaction extends.

Following these results we then collaborated with the research group of Landolt at the ETH, Zürich (Switzerland) in a SPAES investigation of Gd/Ni(110). The result of this study was that the Gd-Ni coupling is also antiferromagnetic, as in the meantime was also concluded from an LSD calculation for a Gd monolayer on a Fe(100) and a Ni(100) surface.[80] It seemed therefore justified to expect from a monolayer-range Gd overlayer on Ni(110), a BISCEPS spectrum consisting of a negative Ni-$3d$-induced asymmetry at the Fermi level [Sec. 3.1.2] and a positive Gd-$4f$-induced asymmetry 4–5 eV above the Fermi level which, when properly normalized to the Gd-coverage, should extrapolate to $+100\%$ at $T = 0$ (for a fully polarized electron beam).

3.2.1. Thin Film Preparation

Deposition

We prepared the Gd overlayers on the cleaned Ni substrate (see Sect. 3.1.1) by thermal evaporation[81,82] from a Knudsen cell,[83] chosen for its reproducible and controllable evaporation rate, homogeneous vapour distribution and for ease of operation. The K-cell was outgassed at 1500 °C before loading with 99.99% pure Gd.[84] We evaporated the Gd (and also Tb, Dy and Nd) from alumina crucibles. Later, we used molybdenum crucibles placed inside the alumina crucible, which then provided the electrical insulation from the heater filament. This gave some improvement in the quality of the deposited layers with respect to contamination, most likely because of the possibility that at elevated temperatures RE materials reduce alumina

to aluminum metal and RE-oxide [Ref. 51, p. 1184].

Deposition took place at cell temperatures of 1150–1250 °C[85] at a rate of 1–2 Å/min, as measured by the quartz-crystal layer thickness monitor. The absolute error in layer thickness, e.g., by assuming bulk density and equal sticking coefficients for the substrate and the quartz crystal, is of the order of ±50%. The relative error, for layers of the same material, is much smaller because most error sources are systematic. The relative error, which could be estimated from the Gd-4*f* to Ni-3*d* intensity ratio in the BIS spectra, is about ±10% or 0.5 Å.

One of the problems in working with RE materials is their susceptibility to hydrogen uptake. We observed that, when heating the K-cell up to the deposition temperature, at ~ 350° large amounts of H_2 were released ($\sim 5 \times 10^{-9}$ mbar), which had probably been adsorbed on Gd-covered parts. During deposition the pressure in the preparation chamber was $3\text{–}6 \times 10^{-10}$ mbar. This was achieved by water-cooled copper shielding around the K-cell and by opening the large valve to the main chamber and the titanium sublimation pump which has a particularly high pumping speed for H_2. Residual gas analysis showed that H_2 was still the most abundant species, followed by CO (from the hot filament of the K-cell). Recent investigations have suggested that the reactivity of clean RE surfaces with H_2 may be lower than generally believed [Ref. 86, p. 675], but it should be emphasized that although the presence of H_2 on or in the sample surface cannot be detected by conventional means, i.e., AES, XPS, etc., it can have dramatic influence on the surface magnetic properties.[87 89]

In the following, depositions were performed with the substrate held at room temperature (RT), unless explicitly specified otherwise.

LEED

The (110)-surface of Ni, which has the fcc crystal structure, has a rectangular unit cell of 2.49×3.52 Å^2. Bulk Gd metal has the hcp crystal structure with an *a*-axis of 3.64 Å and a *c*-axis of 5.78 Å. Except for very small coverages, no epitaxial growth is therefore to be expected.

In the following, (nominal) layer thicknesses are given as indicated by the layer thickness monitor, i.e., $c/2 = 2.9$ Å corresponds to a single Gd(0001) monolayer (ML), or 0.87×10^{15} atoms/cm^2. Note, that the Ni(110) surface contains 1.14×10^{15} atoms/cm^2. In other words, 1 ML Gd corresponds to a coverage of only 0.76 in terms of the number of Ni atoms at the surface. In principle, for coverages corresponding to 0.5 times the number of Ni atoms at the surface, i.e., for coverages up to 0.7 ML Gd, it is possible to arrange the Gd adatoms on the Ni(110) surface in such a way that every second surface unit cell contains a Gd atom in an ordered way. Such ordering would give rise to a superimposed c(1×1) LEED overlayer pattern. We have not observed this to occur as the surface mobility at room temperature is

probably too low. The sharp LEED pattern of the Ni(110) substrate was, however, found to disappear at Gd coverages of the order of 2 Å, or 0.7 ML. This is in agreement with previous investigations[75] and indicative of uniform, but non-epitaxial growth, without islanding.

AES

From our AES spectra,[90] taken with a primary energy of 2 keV, we found that a contamination-free Ni-surface, right after deposition of a Gd overlayer, showed considerable amounts of oxygen- and to a lesser degree carbon-contamination. This contamination level increased by a factor of 2 over a period of ~4 hours.

The high-energy Ni AES-peaks (800–850 eV) were found to decrease with increasing Gd coverage, although we were unable to calibrate this dependence. Maybe because of the low primary energy we did not observe the low-energy Gd AES-peaks (100–140 eV) and the high-energy peaks (900-1000 eV) only for the highest coverages, i.e., more than 10 monolayers. It has been observed that for Gd layers deposited onto a Ni substrate at room temperature the Ni AES signal did not vanish, even for very thick layers.[91] This could mean that either alloying takes place, or that the system can reduce the thermodynamic surface energy by maintaining (some) Ni at the surface. We would expect that this can be suppressed by deposition onto a cooled substrate. Other investigations have indeed shown that up to at least 250 K no (additional) intermixing takes place, for several hours, when the layer is deposited at 80 K.[75]

3.2.2. BIS Experiments

BIS proved to be a very sensitive probe of the (chemical) state of the Gd overlayer. To enhance the sensitivity to the Gd overlayer we could rotate the substrate around an axis perpendicular to the incoming electron beam up to 40° off-normal incidence without affecting the performance of the BISCEPS system. Because the effective mean free path is then reduced by $\cos 40° = 0.77$ the surface sensitivity is increased by the inverse of this factor, i.e., 1.3. The Gd $4f$ peak can then already be observed at a layer thickness of $\lesssim 1$ Å. The Ni $3d$ peak at the Fermi level could be discerned up to about 15 Å coverage.

The relative energy position of the $4f$ levels in XPS and BIS is, among other things, determined by the effective Coulomb interaction U, i.e., the bare Coulomb interaction screened by the chemical environment. To exploit this effect fully one should perform both experiments. Any changes in the chemical environment can not only change U but also shift the XPS and BIS peaks simultaneously, analogous to core level shifts, due to charge transfer between the $5d6s$ valence bands and the environment. Such experiments are currently planned. For now, we will relate our overlayer BIS data to XPS/BIS data of bulk alloys.

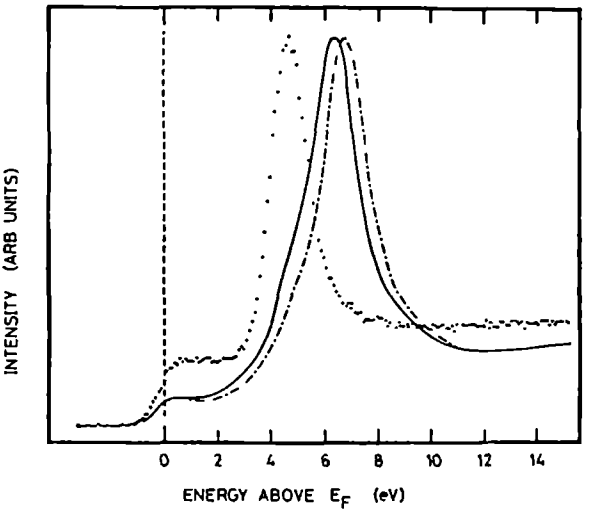

Figure 3.6: BIS spectrum of a 25 Å Gd overlayer on Ni(110) at room temperature, taken under an angle of incidence of 40° with respect to the surface normal. Dotted curve: freshly deposited; full curve: 66 hours after deposition; dot-dashed curve: the aged overlayer exposed to 14 L of O_2.

The BIS spectrum of freshly deposited thick Gd layers [Fig. 3.6] corresponds to previously published bulk Gd BIS data.[79] a single $4f$ peak at ~4.6 eV on a smooth, slowly increasing background. We find a peak width of 1.6 eV (FWHM), which is about 50% larger. In part this is due to the experimental resolution. It could, however, also be related to the previously mentioned phenomenon that some Ni, insufficient to show up in the BIS spectrum, remains close to or at the surface. If a substantial part of the Gd atoms interacts with Ni atoms this could result in shifts of the $4f$ peak position leading to an overall broadening of the line.

As the overlayers aged the $4f$ peak shifted exponentially to higher energy [Figs. 3.6 and 3.7]. The maximum peak shift was about 2.8 eV, i.e., the final peak position was in all cases ~7.4 eV. The time constant depended on the nominal layer thickness and ranged from ~2.5 hours for 1 ML to several tens of hours for 10 ML films. This can be understood if the process taking place occurs only at the surface or at the interface and from there penetrates the bulk of the Gd layer. At intermediate times the $4f$ peak was indeed broader than for freshly deposited layers. If the same experiment was performed with the substrate held at 125 K, instead of at room temperature, the time constants increased consistently with a factor of ~1.6.

These data were derived from a series of spectra taken continuously with an electron beam current of ~50 μA. If, on the other hand, RT spectra were taken at large intervals, i.e., without the 1460 eV-electron beam continuously hitting the surface to simulate lower beam curents, the time constants increased by a factor of ~3.5. This leads to the conclusion that whatever process is taking place, although exhibiting some temperature dependence, is greatly enhanced by the electron beam. At this point there are two possibilities. Either Gd and Ni are slowly forming an

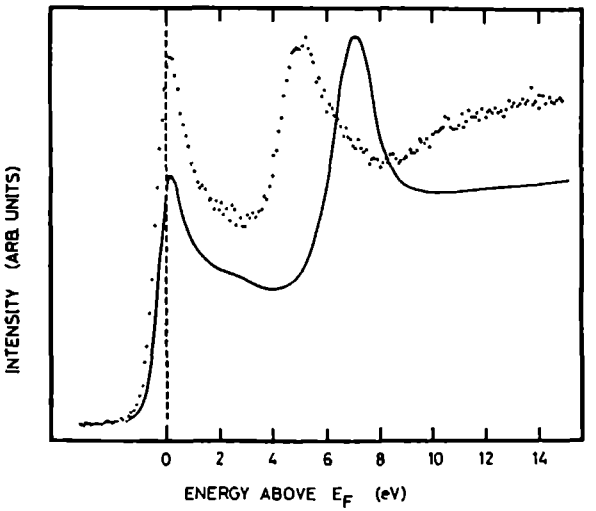

Figure 3.7: Normal-incidence BIS spectrum of a 3 Å Gd overlayer on Ni(110) at room temperature. Dotted curve: freshly deposited; full curve: 17 hours after deposition.

alloy, i.e., massive interdiffusion takes place, or the Gd overlayer is oxidizing. To decide which process is taking place we performed several test experiments.

First, we note that the temperature dependence we find, can be related to a diffusion activation energy E_D. An expression for the rate of diffusion, which is the inverse of the time constant, is

$$1/\tau = R = De^{-E_D/kT}, \tag{3.2}$$

where D is the diffusion constant. Solving this equation for T = 300 K and T = 125 K, we find a diffusion constant of 1.4 and an activation energy of 100 K or 8.6 meV, independent of layer thickness. If this is correct it means that, with an incident electron beam current of ~50 μA at 1460 eV, diffusion takes place at all practical temperatures. What remains to be explained in that case is the electron beam dependence. If, on the other hand, the process taking place is in fact electron-stimulated oxidation, the temperature dependence can be explained by the simple fact that, with the sample cooling in operation, the pressure in the vacuum chamber decreases.

Annealing freshly deposited layers for a short time up to 700 K produced no shift of the $4f$ peak, i.e., no significant decrease in time constant. This is consistent with the above derived activation energy, which predicts only 15-20% reduction of τ. From comparable experiments with other rare earths on Ni(110)[92] we know that such a treatment is, however, sufficient to greatly increase the crystallographic/topographical order of the overlayers with respect to low temperature and room temperature conditions

An XPS/BIS study of bulk Tb-Ni alloys[93] (and Gd-Ni alloys; in progress) was initiated by these observations. Of all transition metals, Ni most readily froms alloys with rare earths.[51] Formation of such bulk alloys, according to the phase diagram, requires temperatures of the order of 800 K.[94] The power dissipated in the sample during measurements was about 75 mW, which increased the sample temperature by 10 degrees. Directly under the beam the temperature could be higher than this, but certainly not sufficient for a bulk reaction to take place. Of course, it is possible that a surface reaction requires a lower temperature.

For Tb-Ni alloys with compositions 3:1, 1:1, 1:3, 1:5, and 2:17[95] the hybridization between Ni $3d$ and Tb $5d6s$ states results in an increasing charge transfer from Tb to Ni with increasing Tb content, until the $3d$ band is filled and moves completely below the Fermi level. The filled $4f$ levels, i.e., in the XPS spectra remain stationary. The unfilled levels, however, shift to higher energy with respect to the pure Tb metal with increasing Ni content, up to 0.9 eV for the 2:17 alloy. This is interpreted as an increase in the effective Coulomb interaction U upon dilution of Tb with Ni, at least for the stoichiometric alloys. Such behaviour has also been found for La-Ni alloys[96] and seems to be also the case for the Gd-Ni alloys, i.e., the peak shift we find for the overlayers, although much larger, is compatible with these results.

The decisive experiment was then to deliberately oxidize the overlayers in order to obtain the BIS spectrum of Gd oxide. We found that, upon adding 10–15 Langmuir of oxygen to freshly deposited *and* partly aged overlayers, we instantly obtained the same final peak position and overall spectrum as before [see also Fig 3.6].

3.2.3. Discussion

The (careful) conclusion drawn from these experiments is that the Gd overlayers show strong electron-stimulated oxidation. The observed time constants impose that the RT spectrum of a clean overlayer should be obtained within, maybe, half an hour after deposition. With a beam current of 50 μA this presents no real problem. For BISCEPS, with much lower currents, and also as these measurements will be performed at low temperature, the time constants involved will be longer. It will, however, probably be neccessary to add spectra obtained from several deposition cycles, thus introducing additional uncertainty in the evaluation of the data. We note that, in view of the experimental circumstances, i.e., with only $\sim$10 μA beam current and the sample cooled down to 80 K, the SPAES data[75] are consistent with these conclusions.

Early depositions of thick Gd overlayers (35 Å) occasionally showed no peak shifts with time, nor with exposure to 100 L of oxygen. An explanation for this effect could be that large H_2 uptake blocks the oxidation process. Experiments to test this effect under controlled conditions are planned, as are XPS/BIS experiments on the overlayers in order to assess the behaviour of the filled levels.

A few BISCEPS measurements have been performed on early depositions of Gd onto the Ni(110) substrate which was held at 125 K. The results obtained sofar are, however, highly inconsistent. In some spectra the $4f$ signal exhibited some asymmetry, although certainly not extrapolating to -100%. In some spectra the Ni $3d$ asymmetry was reversed with respect to the clean surface, indicative of the presence of antiferromagnetic interactions at the surface. In other spectra no asymmetry was found at all.

In view of the results obtained since then this behaviour is perhaps not surprising. Whether oxidation or alloying takes place, the resulting compound may well have a very low, even antiferromagnetic, ordering temperature, if any. Also, crystal field effects, which have been neglected sofar, could obscure purely magnetic effects.

We feel that, with the deposition process and layer characterization under control, only now we are capable of obtaining reliable BISCEPS data of the Gd/Ni(110) system.

3.3. Outlook

In this Chapter we have demonstrated that BISCEPS is an experimentally feasible technique by measurements on the elemental ferromagnet Ni. These data also served to indicate some aspects of the interpretation of (inverse) photoemission data and how BISCEPS might be useful in this respect. The preliminary measurements on the alledged antiferromagnetic overlayer system Gd/Ni(110) represent a different type of experiment, which is primarily concerned with the microscopic magnetic properties of the system, rather than with the electronic properties.

Under proper conditions many other systems might prove to be excellent candidates to be studied with BISCEPS. Prerequisites are that the interesting electronic features are accessible with the present experimental resolution of 0.65 eV, and that the region of interest is located near the surface. Samples do not have to be monocrystalline.

Systems of fundamental as well as technological importance that come to mind are, of course, magnetic overlayers on a magnetic substrate (RE/TM, TM/TM, RE/RE), but also non-magnetic overlayers on a magnetic substrate (Ag/Fe, etc.) and *vice versa* (Fe/Cu, Gd/W, etc.), multilayer systems (Co/Cu/Co/..., etc.), and magnetic alloys. Of the latter class of systems so-called half-metallic ferromagnets[97] (NiMnSb, CrO_2, etc.) are especially challenging.

3.4. References

[1] L. Hodges, Phys. Rev. **152**, 505 (1966).

[2] L & K, Geilenkirchen (FRG).

[3] Ni crystals were oriented and cut by L. Schreurs, Physics Department, University of Nijmegen, The Netherlands.

[4] Ni crystals were polished by J. Hermsen, Physics Department, University of Nijmegen, The Netherlands.

[5] W. Speier, R. Zeller and J.C. Fuggle, Phys. Rev. B **32**, 3597 (1985).

[6] U. Kolac, M. Donath, K. Ertl, H. Liebl and V. Dose, Rev. Sci. Instrum. **59**, 1933 (1988).

[7] M. Donath, Appl. Phys. A **49**, 351 (1989).

[8] R. Feder (Ed.), *Polarized Electrons in Surface Physics.* (World Scientific Publishing, Singapore, 1985).

[9] R.K. Nesbet, Phys. Rev. B **32**, 390 (1985).

[10] D.L. Abraham and H. Hopster, Phys. Rev. Lett. **58**, 1352 (1987).

[11] F. Meier, Ch. 10 of Ref. 8.

[12] S. Modesti, F. Della Valle, R. Rosei, E. Tosatti and J. Glazer, Phys. Rev. B **31**, 5471 (1985).

[13] S. Modesti, F. Della Valle and G. Paolucci, Phys. Scr. **T19**, 419 (1987).

[14] P.M. Platzman and M. Campagna, Sol. St. Commun. **36**, 449 (1980).

[15] T.E. Feuchtwang, P.H. Cutler and D. Nagy, Surf. Sci. **75**, 490 (1978).

[16] C. Kittel, *Introduction to Solid State Physics.* (Wiley, New York, 5th edition, 1976).

[17] K. Binder, Ch. 3 of Ref. 8.

[18] J. Mathon, Rep. Prog. Phys. **51**, 1 (1988).

[19] E. Wimmer, A.J. Freeman and H. Krakauer, Phys. Rev. B **30**, 3113 (1984).

[20] M.P. Seah and W.A. Dench, Surf. Interf. An. **1**, 2 (1979).

[21] W. Speier, J.C. Fuggle, P. Durham, R. Zeller, R.J. Blake and P. Sterne, J. Phys. C **21**, 2621 (1988).

[22] W. Speier, J. Phys. C **21**, L1183 (1988).

[23] W. Speier (unpublished).

[24] L.C. Davis, J. Appl. Phys. **59**, R25 (1986).

[25] C.S. Wang and J. Callaway, Phys. Rev. B **15**, 298 (1977).

[26] V.L. Moruzzi, J.F. Janak and A.R. Williams, *Calculated Electronic Properties of Metals.* (Pergamon, NY, 1978).

[27] R. Clauberg, W. Gudat, E. Kisker, E. Kuhlmann and G.M. Rothberg, Phys. Rev. Lett. **47**, 1314 (1981).

[28] K.-P. Kämper, *Die spinaufgespaltene Bandstruktur von Ni entlang der Γ-L Linie in Abhängigkeit von Temperatur und Schichtdicke.* Ph.D. thesis, RWTH Aachen, 1989.

[29] O.K. Andersen and O. Jepsen, Physica B and C **19**, 317 (1977).

[30] E. Antonides, E.C. Janse and G.A. Sawatzky, Phys. Rev. B **15**, 1669 (1977).

[31] A. Liebsch, Phys. Rev. Lett. **43**, 1431 (1979).

[32] A. Liebsch, Phys. Rev. B **23**, 5203 (1981).

[33] D.R. Penn, Phys. Rev. Lett. **42**, 921 (1979).

[34] G. Treglia, F. Ducastelle and D. Spanjaard, J. Physique **41**, 281 (1980).

[35] R.O. Jones and O. Gunnarsson, Rev. Mod. Phys. **61**, 689 (1989).

[36] L. Hedin, Phys. Rev. **139**, A796 (1965).

[37] R.W. Godby, M. Schlüter and L.J. Sham, Phys. Rev. Lett. **56**, 2415 (1986).

[38] W. Nolting, W. Borgieł V. Dose and Th. Fauster, Phys. Rev. B **40**, 5015 (1989).

[39] W. Borgieł and W. Nolting, Z. Phys. B **78**, 241 (1990).

[40] M. Donath, G. Schönhense, K. Ertl and V. Dose, Appl. Phys. A **50**, 49 (1990).

[41] P.A. Dowben, M. Onellion and Y.J. Kime, Scanning Micros. **2**, 177 (1988).

[42] C. Argile and G.E. Rhead, Surf. Sci. Rep. **10**, 277 (1989).

[43] A. Amiri Hezaveh, G. Jennings, D. Pescia, R. Willis, K. Prince, M. Surman and A. Bradshaw, Sol. St. Commun. **57**, 329 (1986).

[44] H.I. Starnberg, M.T. Johnson, D. Pescia and H.P. Hughes, Surf. Sci. **178**, 336 (1986).

[45] A.S. Arrott, B. Heinrich, S.T. Purcell, J.F. Cochran and K.B. Urquhart, J. Appl. Phys. **61**, 3721 (1987).

[46] D. Pescia, G. Zampieri, M. Stampanoni, G.L. Bona, R.F. Willis and F. Meier, Phys. Rev. Lett. **58**, 933 (1987).

[47] Z.Q. Wang, Y.S. Li, F. Jona and P.M. Marcus, Sol. St. Commun. **61**, 623 (1987).

[48] C. Carbone, G.S. Sohal, E. Kisker and E.F. Wassermann, J. Appl. Phys. **63**, 3499 (1988).

[49] J.R. Dutcher, B. Heinrich, J.F. Cochran, D.A. Steigerwald and W.F. Egelhoff Jr., J. Appl. Phys. **63**, 3464 (1988).

[50] D.A. Steigerwald, I. Jacob and W.F. Egelhoff Jr., Surf. Sci. **202**, 472 (1988).

[51] K.H.J. Buschow, Rep. Prog. Phys. **40**, 1179 (1977).

[52] R.M. Nix and R.M. Lambert, Surf. Sci. **186**, 163 (198).

[53] R.M. Nix, R.W. Judd and R.M. Lambert, Surf. Sci. **215**, L316 (1989).

[54] R.M. Nix, R.W. Judd and R.M. Lambert, Surf. Sci. **203**, 307 (1988).

[55] A. Faldt and H.P. Myers, Phys. Rev. B **30**, 5481 (1984).

[56] J.N. Andersen, I. Chorkendorff, J. Onsgaard, J. Ghijsen, R.L. Johnson and F. Grey, Phys. Rev. B **37**, 4809 (1988).

[57] A. Stenborg and E. Bauer, Surf. Sci. **185**, 394 (1987).

[58] A. Stenborg and E. Bauer, Surf. Sci. **189/190**, 570 (1987).

[59] J. Kolaczkiewicz and E. Bauer, Surf. Sci. **154**, 357 (1985).

[60] D. LaGraffe, P.A. Dowben and M. Onellion, 1989, (preprint).

[61] D. LaGraffe, P.A. Dowben and M. Onellion, Phys. Rev. B **40**, 3348 (1989).

[62] D. Weller, S.F. Alvarado, W. Gudat, K. Schröder and M. Campagna, Phys. Rev. Lett. **54**, 1555 (1985).

[63] D. Weller and S.F. Alvarado, J. Appl. Phys. **59**, 2908 (1986).

[64] J. Kolaczkiewicz and E. Bauer, Surf. Sci. **175**, 487 (1986).

[65] C. Rau and C. Jin, J. Physique **49**, 1627 (1988).

[66] C. Rau, C. Jin and M. Robert, Phys. Lett. A **138**, 334 (1989).

[67] J.N. Andersen, J. Onsgaard, A. Nilson, B. Eriksson, E. Zdansky and N. Mårtenson, Surf. Sci. **189/190**, 399 (1987).

[68] A. Nilsson, B. Eriksson, N. Mårtensson, J.N. Andersen and J. Onsgaard, Phys. Rev. B **36**, 9308 (1987).

[69] J.N. Andersen, J. Onsgaard, A. Nilson, B. Eriksson and N. Mårtenson, Surf. Sci. **202**, 183 (1988).

[70] A. Nilsson, B. Eriksson, N. Mårtensson, J.N. Andersen and J. Onsgaard, Phys. Rev. B **38**, 10357 (1988).

[71] I. Chorkendorff, J. Onsgaard, J. Schmidt-May and R. Nyholm, Surf. Sci. **160**, 587 (1985).

[72] C. Carbone and E. Kisker, Phys. Rev. B **36**, 1280 (1987).

[73] C. Carbone, R. Rochow, L. Braicovich, R. Jungblut, T. Kachel, D. Tillmann and E. Kisker, Phys. Rev. B **41**, 3866 (1990).

[74] M. Taborelli, R. Allenspach, G. Boffa and M. Landolt, Phys. Rev. Lett. **56**, 2869 (1986).

[75] S. Toscano. *Magnetismus dünner Gd-Filme auf Ni(110) untersucht mit Spinpolarisierter Sekundärelektronen-Spektroskopie.* Master's thesis, ETH, Zürich, 1988.

[76] J.B. Goedkoop, *X-ray Dichroism of Rare Earth Materials.* Ph.D. thesis, University of Nijmegen, 1989.

[77] J.B. Goedkoop, M. Grioni and J.C. Fuggle. submitted to Phys. Rev. B, 1990.

[78] R.J.H. Kappert, M. Sacchi, J.B. Goedkoop, M. Grioni and J.C. Fuggle. submitted to Surf. Sci., 1990.

[79] J.K. Lang, Y. Baer and P.A. Cox, J. Phys. F **11**, 121 (1981).

[80] S. Blügel, *First Principles Calculations of the Electronic Structure of Magnetic Overlayers on Transition Metal Surfaces.* Ph.D. thesis, Neunkirchen/Saar, 1988.

[81] M. Gasgnier, Phys. Status Solidi B **57**, 11 (1980).

[82] F.P. Netzer and E. Bertel, in *Handbook on the Physics and Chemistry of Rare Earths*, edited by K.A. Gschneidner, Jr. and L. Eyring, vol. 5, p. 217. (North-Holland, Amsterdam, 1982).

[83] Radak I, Luxel Corp., 515 Tucker Ave., Friday Harbor, Washington, USA.

[84] Reacton, Johnson Matthey Chemicals (UK).

[85] Type 820 PID controller, Eurotherm (UK).

[86] F.P. Netzer and J.A.D. Matthew, Rep. Prog. Phys. **49**, 621 (1986).

[87] L.N. Liebermann, D.R. Fredkin and H. Shore, Phys. Rev. Lett. **22**, 539 (1969).

[88] L.N. Liebermann, J. Clinton, D.M. Edwards and J. Mathon, Phys. Rev. Lett. **25**, 232 (1970).

[89] M. Weinert and J.W. Davenport, Phys. Rev. Lett. **54**, 1547 (1985).

[90] J.C. Rivière, G. Strasser, G. Rosina, F.P. Netzer and J.A.D. Matthew, J. Electron Spectr. and Rel. Phen. **36**. 331 (1985).

[91] S.F. Alvarado, private communication.

[92] R.J.H. Kappert et al., to be published.

[93] K. Brot et al., to be published.

[94] T.B. Massalski (Ed.), *Binary Alloy Phase Diagrams*, vol. 2. (Am. Soc. Metals, Ohio, 1986).

[95] Tb-Ni and Gd-Ni alloys were kindly supplied by K.H.J. Buschow, Philips Research Laborotories, Eindhoven, The Netherlands.

[96] J.C. Fuggle, F.U. Hillebrecht, R. Zeller, Z. Zolnierek, P.A. Bennet and Ch. Freiburg, Phys. Rev. B **27**, 2145 (1982).

[97] R.A. de Groot, F.M. Müller, P.G. van Engen, and K.H.J. Buschow, Phys. Rev. Lett. **50**, 2024 (1983).

4. Finite Temperature Magnetism[†]

An important development in the theoretical treatment of finite temperature magnetism during the past decade, has been the assumption that the (local) exchange splitting of electronic energy bands, and hence the local magnetic moment, in itinerant-electron magnetic systems does not reduce to zero at the critical temperature T_c when the macroscopic magnetization becomes zero. Direct experimental evidence for this view, however, has remained scarce. Our purpose, with the investigation we report here, is to provide additional support for the view of persisting magnetic moments above T_c in itinerant-electron, or band-magnetic systems.

4.1. Introduction

With this investigation we aim at drawing conclusions on the behaviour of the local exchange splitting *versus* temperature in a series of binary alloys. The exchange splitting is an important parameter in the itinerant electron description of metallic ferromagnets, which was conceived by Stoner[1] more than fifty years ago, and subsequently developed by Stoner and Wohlfahrt.[2] Due to the fact that Stoner successfully defined the condition for the occurrence of a magnetic ground state, and at the same time provided a mechanism that supports non-integral magnetic moments, the Stoner-Wohlfahrt theory still remains the basis for our present understanding of 3*d*-transition metal ferromagnetism at low temperatures.

Nevertheless there are severe limitations to the Stoner model, especially in its use to compute finite temperature properties. In the Stoner model the local magnetic moment reduces proportionally to the spontaneous magnetization when approaching the critical temperature T_c. However, the T_c calculated by Stoner theory, i.e., the Stoner temperature, is 5–10 times higher than found from experiment.[3] Moreover, the near-perfect Curie-Weiss behaviour of the magnetic susceptibility found in nearly all itinerant magnetic systems cannot be derived from Stoner theory.[4] Also, there is evidence from neutron scattering[5,6] (since contested[7,8]) that seems to indicate the existence of spin waves, and therefore of magnetic moments, above T_c.

A fundamental reason for Stoner theory, in its bare form, to fail at higher temperatures is the neglect of low-energy collective modes as elementary excitations. Several models, developed in the seventies and eighties, specifically incorporate these

[†]This Chapter has been accepted for publication in Phys. Rev. B.

modes. The result is that the phase transition is no longer solely determined by spin-flip (Stoner) excitations, with energies of the order of the exchange splitting, i.e., 0.5–2 *e*V. Rather, the phase transition is driven by thermal excitation of a large number of spin waves, which are only of the order of 50 m*e*V. This also implies that above the phase transition there still may be magnetic moments, even though they no longer exhibit long range order. These moments could, however, exhibit some degree of short range magnetic order, and this seems to be the main point of debate between the various new models. Limiting cases are the "local band theory" (LBT),[9-12] assuming strong short range magnetic order, on a range of 20 Å, above T_c, and the "disordered local moment" (DLM) theory,[13-15] that assumes no short range order in the paramagnetic phase. Both theories assume only transverse fluctuations of the magnetic moment, i.e., spin waves. Moriya[4] has also taken into account longitudinal fluctuations and has had considerable success in describing weakly ferromagnetic metals, like $ZnZr_2$, where long-wavelength spin fluctuations appear to be responsible for the main effects, implying strong short range correlations. However, the controversy as to the amount of short range magnetic order has persisted, despite much experimental[16-21] and theoretical[22-27] work.

Persistence of a moment and of local magnetic order above T_c has to be associated with a persisting exchange splitting of the electronic energy bands, which may be observed more or less directly by (spin-polarized) photoemission[28-31] and inverse photoemission.[21,32-34] Most of the experimental work in this area has until now focussed on direct resolution of the $\boldsymbol{k}$-dependent exchange splitting in single crystals of Fe and Ni. At low temperature these experiments actually show the spin-split electronic states, especially when the photoelectron spin is resolved explicitly.[34] Such experiments can give information on the variation of the exchange splitting through $\boldsymbol{k}$-space. However, the interpretation of the results obtained at elevated temperatures is complicated by phonon assisted transitions which cause a larger part of the Brillouin zone to be sampled at elevated temperatures.

In view of the difficulties of (spin and $\boldsymbol{k}$-resolved) work with single crystals and the paucity of data, we have tried to open up a new experimental approach to the problem. We have studied random alloy systems — where crystal momentum and $\boldsymbol{k}$-conservation do not have the same relevance as in ordered systems — of magnetic 3*d*-transition metal impurities in Pd and Pt. These systems are indeed itinerant electron magnets, as can be judged from the Rhodes-Wohlfahrt plot [Ref. 4, page 131], altough in view of the fact that the magnetic moments are spatially quite localized to the impurity sites, they can also be classified as being close to the local moment limit [Ref. 4, page 130]. The critical temperatures for these systems are given in Table 4.1. We have used angle-integrated photoemission at the Cooper minimum in the Pd 4*d* or Pt 5*d* cross section in order to isolate the electronic structure effects at the magnetic impurity site.[37,38] Finally, we have performed these measurements both at liquid nitrogen temperature and at room temperature in

Table 4.1: Critical temperatures T_c (taken from Ref. 35) and reduced temperatures $\tau = T/T_c$ for all measured alloys. The relative contribution of the impurity to the photoemission signal in the Cooper minimum at 130 *eV* is given in the last column, and is calculated from atomic cross sections given in Ref. 36.

		T_c	τ(80 K)	τ(300 K)	imp. cont.
PdNi	(5 at.%)	80 K	~1	3.8	0.45
PdNi	(10 at.%)	150 K	0.53	2.0	0.63
PdCo	(4 at.%)	170 K	0.47	1.8	0.35
PdFe	(10 at.%)	225 K	0.36	1.3	0.53
PtFe	(10 at.%)	170 K	0.47	1.8	0.50

order to compare the electronic structure of the impurity below and above T_c. The results will show that the changes are very small indeed. In order to establish some semi-quantitative upper limit to the changes in the exchange parameter, consistent with these small changes, we then proceed to analyze the data with a generalized Clogston-Wolff model described earlier.[39]

4.2. Experimental Details

The polycrystalline alloys PdCo (4 at.%), PdNi (5 and 10 at.%), PdFe (10 at.%) and PtFe (10 at.%) were prepared by arc melting. X-ray diffraction was used to check that the samples were single phase. All samples were verified to be ferromagnetic [Table 4.1] at liquid nitrogen temperature and to be paramagnetic at room temperature, with the exception of PdNi (5 at.%), which was found to be paramagnetic at both temperatures.

The samples were mounted on a copper block attached to a cryostat. The cryostat consisted of a hollow tube mounted on a rotatable manipulator. Low temperatures were obtained by filling the cryostat with liquid nitrogen. Temperature was monitored by a chromel-alumel thermocouple attached to the sample block.

The photoemission experiments were carried out at the HE-TGM2 beamline at BESSY (Berliner Elektronenspeicherring-Gesellschaft für Synchrotronstrahlung). All experiments were performed at 130 *eV* photon energy with a resolution of typically 0.6 *eV* (fwhm). The spectra were taken at normal incidence, collecting electrons with take-off angles up to ~40° with respect to the surface normal.

The samples were cleaned by scraping *in situ* before each measurement. The pressure was about 1×10^{-10} mbar during room temperature measurements, and dropped to about 5×10^{-11} mbar when the cryostat was cooled. For low temperature measurements, samples were scraped after cooling down. Prolonged measurements

were done in several runs with repeated scraping before each run.

After each run the spectrum was carefully checked for reproducibility. Enough spectra were taken to ensure that the peak intensity in the summed spectrum would be of the order of 100,000 counts.

Absolute normalization of the spectra was not possible. For each sample, we normalized the spectra to the integrated intensity of the valence band, after subtracting an inelastic loss background, so that at a chosen point below the valence band the intensity went to zero.

4.3. Results and Interpretation

The valence band photoemission spectra of the disordered alloys PdNi (5 and 10 at.%), PdCo (4 at.%), PdFe (10 at.%) and PtFe (10 at.%) are presented in Fig. 4.1. The dotted curves were recorded at liquid nitrogen temperature (~80 K). Room temperature curves are shown as full lines wherever they differed significantly from the low temperature spectra.

As to the gross features of the spectra, we note that in general the states at the bottom of the valence band in these materials contribute proportionally less to the spectra because the single-particle photoemission matrix elements are lower[40] and because the high binding energy regions contribute proportionally more to the satellite regions.[41–43] The width of the single particle region of the spectrum is ~6 eV, which corresponds to the width of the Pd (Pt) host bands. About 30–60% of the spectral intensity in this region is derived from the host and its shape is similar to that of pure Pd (Pt). Because of the Cooper minimum effect, up to ~60% of the intensity is derived from the impurity [Table 4.1]. The shape of the impurity contribution also tends to reflect many features of the host because of the strong hybridization between impurity and host states.[38,44] However, this contribution also reflects the effective atomic energy levels of the impurities, and hence the exchange splitting of spin up and spin down levels.[38,44]

Below the single particle region (and partly overlapping it) we see a large signal due primarily to inelastically scattered electrons. This region also contains the contributions from satellites and many-body excitations.[41–43] In general, this region shows little structure. Exceptions are the weak features at ~8 and ~11 eV in the PdNi alloy spectra. These could be confused with peaks from a (very low) level of CO contamination.[45] We found the intensity of these peaks to be remarkably constant between scraping sessions and not to increase significantly with exposure to the vacuum. We are thus inclined to attribute them to many-body satellites intrinsic to the PdNi system and not to CO. However, because their intensity is constant, their presence is not relevant to the central theme of this work.

For all systems, the difference between room temperature and 80 K spectra, magnified 5 times, is presented in Fig. 4.1. It is clear from these data that the

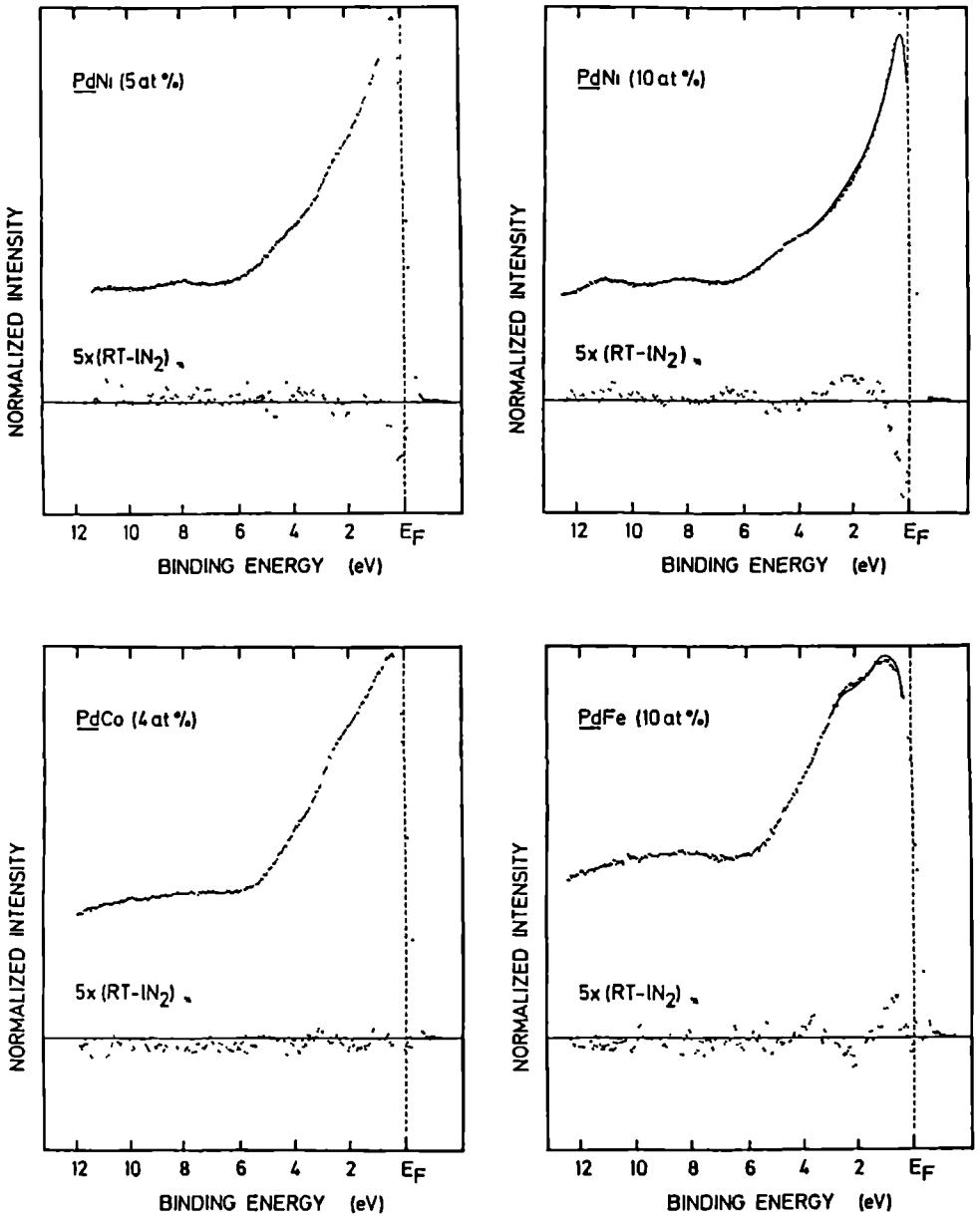

Figure 4.1: Valence band photoemission spectra of PdFe, PdCo, PdNi (5 and 10%) and PtFe, taken at 130 eV photon energy. The upper dotted curves represent the spectra taken at liquid nitrogen temperature. Solid lines represent the room temperature spectra. The difference between these spectra, magnified 5 times, is presented by the lower dotted curve.

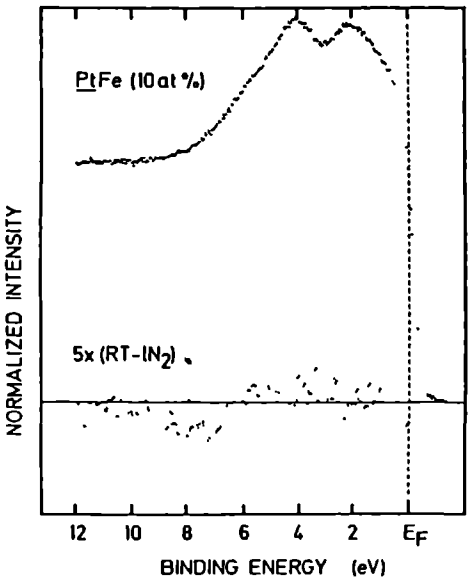

Figure 4.1: *Continued.*

differences between room temperature and 80 K spectra are small, especially in the high binding energy region. The most pronounced changes in the photoemission signal are found at the Fermi level Of the investigated systems, only PdCo and PtFe do not show any significant structure at all in the difference spectra.

We will discuss in detail below the nature and origin of the changes found in these spectra. First, however, we want to stress how small the changes are. This is extremely relevant because in all cases the contribution of the impurity 3*d*-states to these spectra is of the order of ~50% [Table 4.1]. In the dilute limit of Pd-(Pt-)based alloys, we already expect a strong redistribution of the local impurity density of states with small changes in the local magnetic moment or the effective exchange splitting, as will be discussed below. A large change of the local moment thus would have been immediately noticeable and it must therefore be concluded that the impurity moments in these systems persist almost unchanged above T_c.

The largest changes were found in the PdNi (10 at.%) spectrum. The spectrum at room temperature exhibits less intensity at the Fermi level than the 80 K spectrum. A little more spectral weight is found around ~2 *e*V below E_F as compared to the low temperature spectrum. The PdNi (5 at.%) difference spectrum resembles that of the PdNi (10 at.%), but the structure at the Fermi level is smaller by a factor of ~2, in agreement with the different stoichiometries of these alloys.

The changes observed in the PdFe spectra are opposite to those of PdNi. Here the intensity of the room temperature spectrum near the Fermi level is higher than in the 80 K spectrum, while at higher binding energy (~2 *e*V) the intensity is lower. These

changes are very weak and similar to those caused by exposure to residual gases in the vacuum chamber for periods longer than an hour. It is therefore possible that the differences observed are associated with contamination of the sample, despite the severe precautions taken.

4.4. Discussion

Magnetic transition metal impurities in Pd (Pt) can be described by a majority band and a minority band, self-consistently separated in energy by the combined effects of the (mostly intra-atomic) exchange interaction, and the hybridization with the host d-bands. From the calculated local density of states (LDOS) for a single Fe impurity in Pd[46,47] [see also Fig. 4.2(a)], it follows that the minority spin states are pushed above the Fermi level by the hybridization with the Pd d-band. This happens because the effective energy level of the Fe minority spin states is situated above the Pd d-band centroid. The calculations show the Fe majority states to be situated in the host d-band, the largest weight of the majority states being at 2–5 eV binding energy.

For Ni in Pd (Pt),[46,47] the situation is slightly different. The calculated DOS for Ni in Pd shows that most of the minority states are situated at the top of the valence band. The Ni majority states are calculated to have their largest weight at 0–2 eV binding energy. For Co, the theoretical results are intermediate between Fe and Ni.[46,47] The large photoemission intensity at the Fermi level for Ni and Co in Pd is thus mainly due to minority states.

To show the sensitivity of the photoemission spectrum on the (local) magnetic structure we will present results of calculations using a generalized Clogston-Wolff (CW) model.[39] In this model the impurity is characterized by the energy difference $\Delta_{\uparrow(\downarrow)}$ between the host d-band centroid and the impurity spin-up (down) state, and a renormalization of the impurity-host hybridization potential. A CW calculation with $\Delta_{\uparrow(\downarrow)}$ and the relative hybridization as fitparameters to an *ab initio* self-consistent KKR calculation[46,47] provides a suitable basis for data interpretation.

For Fe in Pd, the impurity-host interaction reduced to 75% of the Pd-Pd hybridization yields the best agreement.[44] The effective impurity levels are found at $\Delta_{\uparrow} = -1.06$ eV for the majority spin level, and $\Delta_{\downarrow} = 1.99$ eV for the minority spin level,[44] corresponding to an effective exchange splitting $\Delta_{ex} = \Delta_{\downarrow} - \Delta_{\uparrow} = 3.05$ eV. The resulting local density of states for majority states (full curve) and minority states is shown in the bottom panel of Fig. 4.2.

As in the *ab initio* calculation, we observe the Fe majority spin states to be well separated from the minority spin states. The impurity-host hybridization has resulted in the Fe majority spin LDOS reflecting the shape of the Pd host d-band, while the minority spin states have been pushed above the Fermi level and are dominated by a single peak.

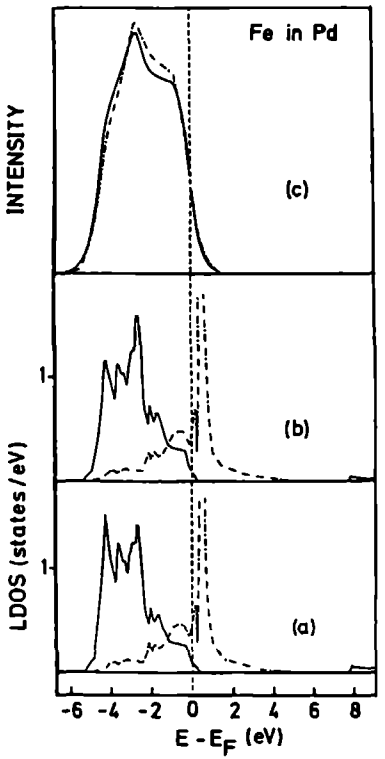

Figure 4.2: Fe impurity in Pd. (a): LDOS on Fe site obtained from a Clogston-Wolff (CW) model calculation fitted to an *ab initio* KKR calculation. (b): LDOS on Fe site obtained from a CW calculation with the local magnetic moment reduced to 99% of the value of (a). (c): The occupied part of the LDOS on Fe, broadened to simulate instrumental (Gaussian, fwhm 0.6 eV) and lifetime (Lorentzian, fwhm 0.1 $(E - E_F)$ eV) effects. Single electron matrix elements[40] are taken into account by multiplying with a sloping line of 15%/eV. Full curve: broadened LDOS obtained from (a). Dash-dotted curve: broadened DOS obtained from (b).

Reducing the magnetic moment at the Fe site by 1%, while keeping the local number of d-electrons constant, we obtain the LDOS shown in the middle panel of Fig. 4.2. This corresponds to a reduction of the local exchange splitting by ~5%. Although the minority spin LDOS hardly changes, significant changes can be seen to occur in the majority spin part of the LDOS, on shifting the weight of the majority spin band towards the Fermi level. We may already conclude from comparison of Figs. 4.2(a) and 4.2(b) with the experimental results, that there is only a weak temperature dependence of the magnetic moment at the Fe site, and of the local exchange splitting. However, if we can simulate other experimental effects, such as instrumental and lifetime broadening, binding energy dependence of the photoemission matrix elements (ME) and inelastic losses, we may further quantify this statement. To this end we have broadened the occupied part of the LDOS from Figs. 4.2(a) and 4.2(b) to simulate instrumental and lifetime broadenings, and multiplied the LDOS by a sloping line to simulate ME effects [Fig. 4.2(c)]. We are aware of the limitations of this procedure, but it does show that even after taking into account these effects (plus the fact that ~50% of the photoemission signal still originates from Pd) large changes in the local exchange splitting at the Fe site would

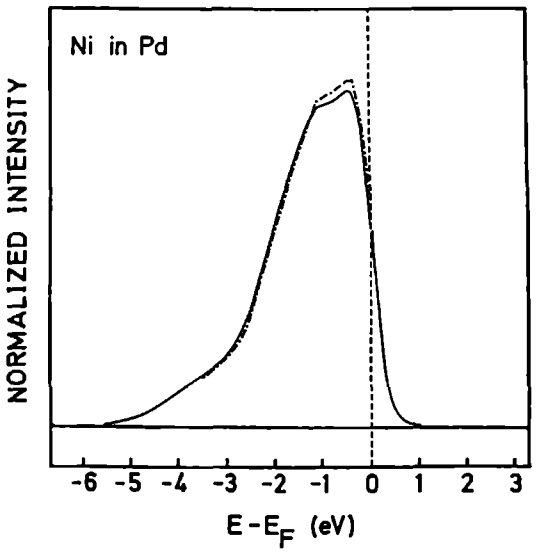

Figure 4.3: Full curve: CW calculation for a Ni impurity in Pd. LDOS on Ni site, broadened as in Fig. 4.2(c). Dash-dotted curve: as for the full curve, but with the local magnetic moment reduced to 98%.

still be recognizable. We must conclude that the changes in local moment at the Fe site in PdFe are less than ~1%, corresponding to changes in the local exchange splitting smaller than ~5%, over the temperature range studied.

Similar conclusions can be drawn for Co in Pd and Fe in Pt. For Ni in Pd the situation is different. Based on the CW calculation Ni is expected to be the least sensitive to changes in the local moment, as is shown in Fig. 4.3, because the exchange splitting is much smaller. The local moment in pure Ni in the DLM-model[14] is expected to decrease ~30% over the temperature range of the experiment, whereas the local moment in pure Fe is expected to decrease by only ~5%. We observe the largest changes for the PdNi system, but they are different to those calculated. If the observed changes are of magnetic nature, we would expect an increase of the spectral intensity at E_F going to higher temperatures, whereas we observe a decrease. Thus the effects observed in the PdNi systems are a puzzle to us, but here too the conclusion remains that temperature-induced changes in the effective atomic moment and the exchange splitting are small.

4.5. Concluding Remarks

In this work we have reported a study of the temperature dependence of photoemission spectra of Pd and Pt with magnetic impurities. The spectra were taken in the Pd (Pt) Cooper minimum so that typically ~50% of the signal originated from the impurity, in order to optimally observe changes in the local exchange splitting at the impurity site. The temperature dependence of the spectra was very weak. Com-

parison with model calculations indicates that the changes observed are inconsistent with changes larger than ~5% in the local exchange splitting. Thus our results are certainly incompatible with a collapse of the local magnetic moment on the impurity site at T_c when the long-range magnetic order goes to zero.

4.6. References

[1] E.C. Stoner, Proc. R. Soc. London **A154**, 656 (1936).

[2] E.P. Wohlfarth, Rev. Mod. Phys. **25**, 211 (1953).

[3] O. Gunnarson, J. Phys. F **6**, 587 (1976).

[4] T. Moriya, *Spin Flucuations in Itinerant Electron Magnetism*, vol. 56 of *Series in Solid-State Sciences*. (Springer Verlag, Berlin, 1985).

[5] H.A. Mook, J.W. Lynn and R.M. Nicklow, Phys. Rev. Lett. **30**, 556 (1973).

[6] J.W. Lynn, Phys. Rev. B **11**, 2624 (1975).

[7] G. Shirane, Y.J. Uemura O. Steinvoll and J. Wicksted, J. Appl. Phys. **55**, 1887 (1984).

[8] J. Callaway, Phys. Lett. **112A**, 67 (1985).

[9] V. Korenman, J.L. Murray and R.E. Prange, Phys. Rev. B **16**, 4032 (1977).

[10] V. Korenman, J.L. Murray and R.E. Prange, Phys. Rev. B **16**, 4048 (1977).

[11] V. Korenman, J.L. Murray and R.E. Prange, Phys. Rev. B **16**, 4058 (1977).

[12] H. Capellmann, Z. Phys. B **34**, 29 (1979).

[13] J. Staunton, B.L. Gyorffy, A.J. Pindor, G.M. Stocks and H. Winter, J. Magn. Magn. Mat. **45**, 15 (1984).

[14] A.J. Pindor, J. Staunton, G.M. Stocks and H. Winter, J. Phys. F **13**, 979 (1983).

[15] H. Hasegawa, J. Phys. Soc. Jpn. **46**, 1504 (1979).

[16] C.S. Fadley, in *Electron Spectroscopy*, edited by D.A. Shirley. (North-Holland Publishing, Amsterdam, 1972).

[17] R.E. Kirby, E. Kisker, F.K. King and E.L. Garwin, Sol. St. Commun. **56**, 425 (1985).

[18] R. Clauberg, E. Haines and R. Feder, J. Magn. Magn. Mat. **54-57**, 622 (1986).

[19] C. Rau and H. Kuffner, J. Magn. Magn. Mat. **54-57**, 767 (1986).

[20] J.F. van Acker, Z.M. Stadnik, J.C. Fuggle, H.J. Hoekstra, K.H.J. Buschow and G. Stroink, Phys. Rev. B **37**, 6827 (1988).

[21] M. Donath, Appl. Phys. A **49**, 351 (1989), and references therein.

[22] E.M. Haines, Sol. St. Commun. **69**, 561 (1989).

[23] H. Capellmann and V. Vieira, Sol. St. Commun. **43**, 747 (1982).

[24] D.M. Edwards, J. Magn. Magn. Mat. **36**, 213 (1983).

[25] R. Clauberg, E. Haines and R. Feder, Z. Phys. B **62**, 31 (1985).

[26] H. Hasegawa and F. Herman, J. Physique **49**, 1677 (1988).

[27] W. Nolting, W. Borgieł V. Dose and Th. Fauster, Phys. Rev. B **40**, 5015 (1989).

[28] D.E. Eastman, F.J. Himpsel and J.A. Knapp, Phys. Rev. Lett. **40**, 1514 (1978).

[29] H. Hopster, R. Raue, G. Güntherodt, E. Kisker, R. Clauberg and M. Campagna, Phys. Rev. Lett. **51**, 829 (1983).

[30] E. Kisker, K. Schröder, W. Gudat and M. Campagna, Phys. Rev. B **31**, 329 (1985).

[31] K.-P. Kämper, W. Schmidt and G. Güntherodt, J. Physique **49**, 39 (1988).

[32] J. Unguris, A. Seiler, R.J. Celotta, D.T. Pierce, P.D. Johnson and N.V. Smith, Phys. Rev. Lett. **49**, 1047 (1982).

[33] H. Scheidt, M. Glöbl, V. Dose and J. Kirschner, Phys. Rev. Lett. **51**, 1688 (1983).

[34] D.T. Pierce, Surf. Sci. **189**, 710 (1987), and references therein.

[35] J.A. Mydosh and G.J. Nieuwenhuys, in *Ferromagnetic Materials*, edited by E.P. Wohlfahrt, vol. 1. (North-Holland, Amsterdam, 1980).

[36] J.J. Yeh and I. Lindau, At. Data and Nucl. Data Tables **32**, 1 (1985).

[37] J.W. Cooper, Phys. Rev. **128**, 681 (1962).

[38] J.F. van Acker, P.W.J. Weijs, J.C . Fuggle, K. Horn, W. Wilke, H. Haak, H. Saalfield, H. Kuhlenbeck, W. Braun. G.P. Williams, D. Wesner, M. Strongin, S. Krummacher and K.H.J. Buschow, Phys. Rev. B **38**, 10463 (1988).

[39] W. Speier, J.F. van Acker and R. Zeller, Phys. Rev. B **41**, 2753 (1990).

[40] W. Speier, J.C. Fuggle, P. Durham, R. Zeller, R.J. Blake and P. Sterne, J. Phys. C **21**, 2621 (1988), and references therein.

[41] A. Liebsch, Phys. Rev. Lett. **43**, 1431 (1979).

[42] A. Liebsch, Phys. Rev. B **23**, 5203 (1981).

[43] J.C. Fuggle, F.U. Hillebrecht, R. Zeller, Z. Zolnierek, P.A. Bennet and Ch. Freiburg, Phys. Rev. B **27**, 2145 (1982), and references therein.

[44] J.F. van Acker, to be published.

[45] D.E. Eastman and J.K. Cashion, Phys. Rev. Lett. **27**, 1520 (1971).

[46] A. Oswald. Ph.D. thesis, KFA Jülich, 1985.

[47] A. Oswald, R. Zeller and P.H. Dederichs, Phys. Rev. Lett. **56**, 1419 (1986).

A. Surface Mössbauer Spectroscopy[†]

We report in this chapter the operating experience with a system designed to investigate the feasability of depth-selective conversion electron Mössbauer spectroscopy (DCEMS) or, more precisely, surface Mössbauer spectroscopy (SMS). The reason to develop such a system is obvious. In recent years the study of magnetism at and near surfaces has enjoyed increasing interest [see also Ch. 1]. Being the main representative of magnetic materials as well as being the most convenient Mössbauer isotope it seems only natural to try and exploit the Mössbauer effect in ^{57}Fe to obtain information on surface-related magnetic properties.

In relation to other techniques used to investigate surface magnetism, like spin-polarized (inverse) photoemission, low-energy electron diffraction, etc., the question rises as to the practical *applicability* and also *compatibility* of DCEMS or SMS in such a "surface spectroscopy environment". This means, for instance, that it is highly desirable to be able to perform DCEMS/SMS under the same circumstances as, or even *in situ* with, the other techniques, i.e., without the use of protective capping layers, but also without having to resort to very-high-activity radioactive sources, to obtain comparable data acquisition times.

A.1. Introduction

Mössbauer spectroscopy rests on the observation that in solids there is a finite probability that the γ-photon emitted by a nucleus does not lose recoil energy. This effect was first observed by R.L. Mössbauer,[1] a nuclear physicist, in 1957/58 in experiments aimed at determining the lifetime of an excited state of ^{191}Ir.

Until that time the yield in resonance fluorescence of γ-rays by nuclei was limited by the fact that in the emission and absorption of a photon by a particle energy as well as momentum have to be conserved. For relatively low photon energies the momentum which is transferred to the particle is usually negligible, hence resonance absorption by, for instance, transitions of core electrons can be readily observed. However, for nuclear transitions in the keV to MeV region the recoil energy related to the momentum transfer amounts up to several meV. In view of the relatively long lifetimes of excited nuclear states and hence narrow linewidths of the order of 10^{-8} eV this prevents resonance absorption to be observed.

[†]Parts of this Chapter have been published in Rev. Sci. Instrum. **60**, 708 (1989).

To overcome this problem of "detuning" in a resonance experiment various methods had been employed, all aimed at broadening the effective linewidths of the emission and absorption lines. One method was to add to the photon energy a Doppler shift by mechanical movement of the source or absorber. Alternatively, increasing the temperature would broaden the lines by thermal motion of the nuclei. In both cases the resonance fluorescence yield increased.

The realization that a nucleus bound in a solid can only dissipate energy by creating or annihilating quantized lattice vibrations, or phonons, leads to the observation that whenever the recoil energy is smaller then, or comparable to, the threshold energy for creating a phonon a certain fraction of the emitted photons will not suffer any energy loss. This is called recoilless or recoil-free emission and absorption. The threshold energy for phonon creation or annihilation is related to the Debye temperature of a particular solid. Hence, the recoil-free fraction for γ-ray emission or absorption is inversely proportional to the ratio of the actual temperature and the Debye temperature, as well as to the photon energy. The discovery of Mössbauer consisted of the observation that the resonance fluorescence yield increased instead of decreased with decreasing temperature.

If recoil-free emission or absorption takes place, the linewidth is just the natural linewidth related to the excited-state lifetime by the uncertainty principle. Shortly after the discovery of the Mössbauer effect it was realized that the linewidths associated with the nuclear transitions (10^{-8} eV) are smaller than the splittings induced by the hyperfine interaction between the nucleus and magnetic or electric fields,[2] i.e., Zeeman splitting and quadrupole splitting. The small energy shifts, of the order of 10^{-7} eV, of the hf-split lines with respect to the unperturbed line can easily be provided by means of a mechanically-induced Doppler shift of the order of several mm/s. Therefore, the effect provides unique energy-resolving power to study this interaction just by measuring the resonance absorption as a function of the relative motion of source and absorber.

Moreover, when it was discovered that the hf interaction contains also information on the chemical environment of the nucleus,[2] i.e., isomer shift, it was clear that the effect could be of great use in many areas of natural sciences. An overview of the applications of Mössbauer spectroscopy to various problems can be found in many textbooks and reviews.[3,4]

In practice, the effect has been employed mainly in transmission geometry, measuring the resonance absorption as a function of the relative source-absorber velocity. This mode, applied to thin absorbers, provides bulk information. However, also other modes of detection have been developed, the most important of which for our purposes is conversion electron detection.

Following the absorption of a photon the nucleus will decay back to the ground state, with a characteristic time-constant. This can occur either by re-emission of the photon or by transferring the nuclear excitation energy by internal conversion

to the *s*-electrons of the atom (which have a finite density at the nucleus). These electrons then get an energy large enough for them to be emitted from the solid with a characteristic kinetic energy determined by the nuclear transition energy and their binding energy. Following the emission of these core electrons also Auger processes can take place. The emitted electrons can be detected integrally (CEMS),[5] or differentially (DCEMS)[6,7] by energy-selection. This last mode offers, in principle, the possibility to perform non-destructive depth-profiling exploiting the relatively low (and energy-dependent) escape depth of hot electrons in solids.[8]

The first attempts at DCEMS date already from 1961.[9] After some more attempts over the years[10–12] the first demonstration of a sharp depth resolution was given in 1980.[13] However, all these experiments suffered from very low signal intensities limiting the practical applicability of the method. Along with the developments on the experimental side the matter was also taken up by theoreticians. This resulted in a better insight into the actual attainable depth resolution using the 7.3 k*e*V conversion electrons of ^{57}Fe, especially related to the spectrometer resolution.[14–16] This then showed that a very high energy resolution is not required — 1–3% suffices — and that in view of the low countrates in a DCEMS experiment the luminosity (the product of transmission and useable sample area) is by far more important. Another conclusion that could be drawn from the theoretical results was that to obtain real surface sensitivity one has to resort either to artificially layered samples with the surface preferentially enriched in ^{57}Fe, or, if one also wants to measure on real surfaces, to use lower-energy electrons, i.e., the 600 *e*V *LXY* Auger electrons or even the very-low-energy (<15 *e*V) secondary electrons.[17] It is in this context that we decided to build a DCEMS/SMS machine with possible application as an additional tool in our surface spectroscopy group, in addition to existing PES/IPES, AES and LEED facilities.

A.2. Design Considerations

We present here details of a high-transmission spectrometer for Mössbauer spectroscopy with energy resolution of the conversion electrons. We also discuss the potential of such devices for depth-selective surface analysis.

The recoil-free resonant absorption of γ rays by Mössbauer nuclei is followed by their de-excitation, which takes place by either the re-emission of γ rays, or x rays, or internal conversion electrons accompanied by Auger electrons. Most of the Mössbauer experiments involve the detection of γ rays transmitted through an absorber, which has provided a wealth of information relating to the bulk properties of solids.[4] However, a second mode exists involving the detection of electrons. This method has the advantage of smaller backgrounds, and since the escape depth of the emitted electrons is much smaller than that of γ rays and x rays, the method is much more surface sensitive.[18] For the most widely used ^{57}Fe Mössbauer isotope,

the surface layer probed is about 250 nm thick if all the electrons are detected with no attempt at energy resolution, and use of this mode has also yielded a wealth of information.[18] However, the inelastic mean free path of electrons in the solid state is small,[8] being of the order of $15\sqrt{E}$Å if the electron kinetic energy E is measured in keV, and the amount of energy lost in the average inelastic collision is typically 15–20 eV. Thus, if the conversion or Auger electrons are energy selected to restrict detection to the "no-loss" electrons, the surface sensitivity can be greatly enhanced.[19]

This apparently simple experiment has only been exploited to a limited extent until now because of the enormous loss in integrated signal intensity as a result of the energy selection. Restriction of the conversion electrons to a 1% band pass is likely to reduce the total signal by a factor of about 100, even if the electron energy analyzer transmits 100% of the electrons emitted in a 4π solid angle. Indeed, a typical analyzer for x-ray photoelectron spectroscopy, with an energy resolution of about 0.01% and a transmission of about 0.1% of 4π, would reduce the signal by a factor of nearly 10^6. Because the average electron energy-loss per collision is so high, the crucial factor in choice of an electron analyzer for Mössbauer spectroscopy is in fact the transmission, and not the energy resolution. This is especially true for studies of the first monolayer(s) of a surface without the influence of contamination.

Various types of electrostatic analyzers have been used (a list is given in Ref. 19; the latest electrostatic Mössbauer system is described in Ref. 20), and the highest transmission (13% of 4π) is probably that of a spherical spectrometer constructed by Yang *et al.*[21] The energy resolution of all constructed electrostatic spectrometers is comparable, although their transmission differs significantly. There are, however, few reports in the literature which allow one to assess the rate of data acquisition and the feasibility of, for instance, true depth profiling experiments using energy-selective conversion electron Mössbauer spectroscopy. It is this need which we attempt to treat here. The Mössbauer system constructed is an ultra-high vacuum system with a spherical electrostatic analyzer similar to that of Yang *et al.*[21] and with the possibility of performing measurements between liquid nitrogen and room temperatures. We will illustrate its use with spectra from ^{57}Fe-enriched Fe samples and discuss the limitations of such measurements.

A.3. System Description

The operating principles of an electrostatic spherical analyzer have been demonstrated a long time ago.[22,23] The main result is the calibration equation

$$E_0 = e\Delta V/(R_0/R_1 - R_1/R_0),$$

where E_0 is the pass energy and ΔV is the potential difference between the inner and outer spheres, whose radii are, respectively, R_1 and R_0. When these radii are

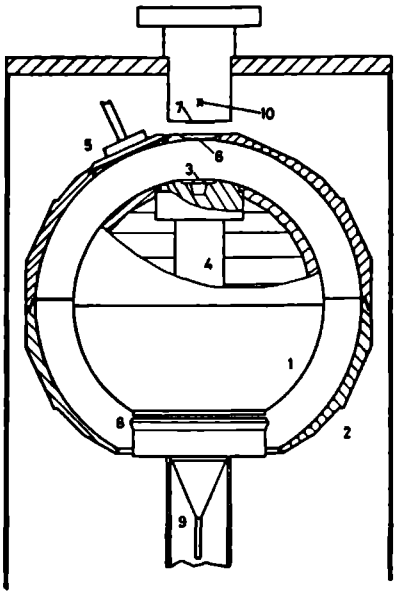

Figure A.1: Schematic view of the electrostatic spherical analyzer: (1) inner sphere, (2) outer sphere, (3) sample holder, (4) cold finger, (5) sample access port, (6) Al window, (7) Be window, (8) adjustable slit, (9) channeltron, (10) Mössbauer source position.

chosen properly, i.e., not too small and sufficiently separated, the resolution R and the transmission T depend only on the exit angle χ of the analyzer. An angle $\chi = 0$ would correspond to electron orbits traversing the full 180°. For a point source these relations are: $R \equiv \Delta E/E = (\chi/4)^2$ and $T = \chi/4$ (fraction of 4π). The maximum escape angle α of the electrons relative to the surface plane is given by: $\sin\alpha = \chi/2$.

The main limitation on the choice of construction parameters is the overall size of the spectrometer, which has to fit into an ultra-high vacuum (UHV) system. We chose, therefore, $R_0 = 150.5$ mm and $R_1 = 116.0$ mm. The optimum exit angle then is $\chi = 30° = 0.52$ rad. This means that the analyzer constant $e\Delta V/E_0$ is 0.527. The theoretical limits on R and T (for a point source) are $R = 1.7\%$ and $T = 13\%$ of 4π. The maximum escape angle for the electrons to be detected is $\alpha = 15° = 0.26$ rad. This means at the same time that the effective probing depth relative to perpendicular escape angles is smaller by a factor of 0.26, which is important for surface analysis. For a disc source with a radius of 5 mm the actual resolution reduces to $R = 2.1\%$.[21]

A schematic view of the spherical analyzer is presented in Fig. A.1. As can be seen, both the inner and the outer sphere are almost completely closed to assure high uniformity of the dispersive electric field. The spheres were preformed of non-magnetic austenitic stainless steel RVS316Ti[24] and then further worked to reduce weight and increase sphericity. The inner sphere is made of two halves that were first welded together with a rather deep weld and only then turned on a lathe to the required sphericity. This procedure, though not common practice in UHV work,

resulted in a connection without any detectable leaks. Also, this weld was tested to be non-magnetic. The sphere can be filled with liquid nitrogen. The sample to be investigated is placed at the pole of this sphere on a copper sample holder to prevent radiation from the Mössbauer source hitting any stainless steel parts, with consequent emission of electrons from Fe in the steel. By means of a massive copper "cold finger" extending into the liquid nitrogen reservoir, the sample can be cooled to 77 K.

The outer sphere, whose top is demountable, has a "window" at the top to let the radiation from the Mössbauer source reach the sample. To minimize field inhomogeneities, this window is covered with a thin aluminium foil. The same holds for the sample access port in this sphere. Normally this port is closed with a lid. To change samples and for *in situ* sample preparation, this lid can be retracted and the sample can be picked up from its measurement position.

The slit at the exit of the analyzer is moveable and can be adjusted to obtain the optimum resolution or to increase the transmission (at the cost of resolution). The inner sphere has a small lip at this point. This is to prevent entrance into the electron counter of low energy (secondary) electrons that might skim over the surface of the sphere. The slit can be set at a variable potential to improve the field pattern at the exit stage of the analyzer. Behind the slit a single channel electron multiplier with a very wide (50-mm-diam) entrance cone[25] is mounted to detect the electrons.

The Mössbauer source is mounted on a transducer outside the UHV system for ease and safety of operation. A vacuum-tight beryllium window[26] welded to a UHV flange allows the radiation to pass. The source-to-sample distance is chosen to be 7 cm. A shorter distance, even with the source penetrating the outer sphere of the analyzer, would have been possible and would have increased the radiation intensity at the sample. Apart from field inhomogeneities, a shorter distance would cause distortion of the usual Lorentzian lineshape in the Mössbauer spectra due to geometric effects,[27] which, however, one might find acceptable in view of the intensity problems described later.

The spherical analyzer is mounted in a custom-built bakeable UHV system (Varian) pumped with 120-ℓ/s ion getter pumps and a 1000-ℓ/s liquid-nitrogen-cooled Ti sublimation pump to a base pressure of about 10^{-10} mbar. The high voltages applied to the outer sphere, the slit, and the sample can be controlled by a microprocessor system that is also used as a multichannel analyzer and controller for the Mössbauer spectrometer. Velocity calibration is achieved using a Michelson interferometer.[28]

A.4. System Operation

The ion pumps used introduced unacceptable noise at the shielded channeltron due to charged particle emission, which could only slightly be reduced by inserting a

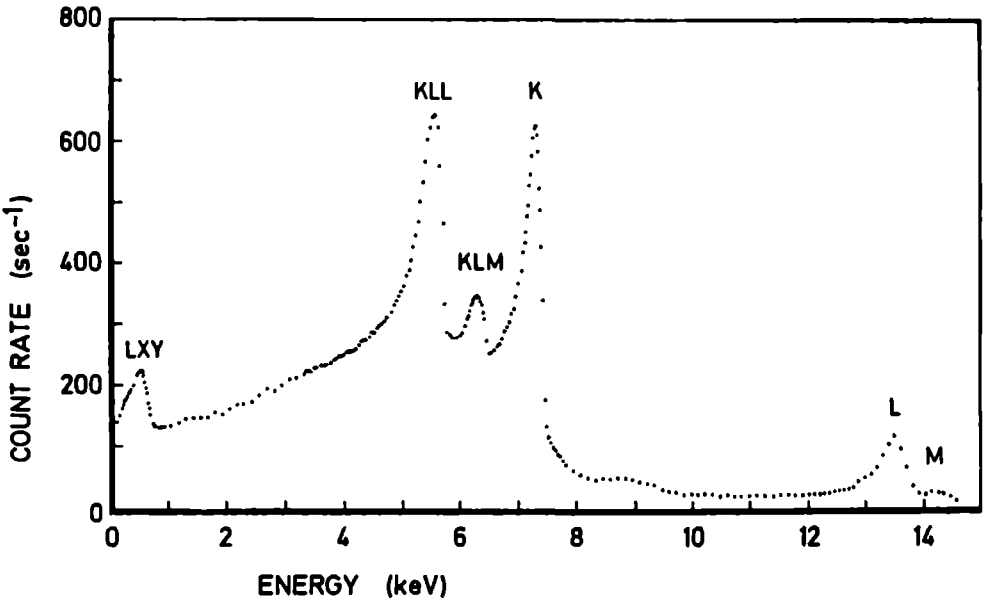

Figure A.2: Energy spectrum of electrons emitted from a ^{57}Co β-source ($^{57}CoCl_2$ electrodeposited on Al), showing the K, L, and M conversion electrons, as well as the KLL and other Auger electrons.

mesh or a baffle on a small potential between the pumps and the analyzer. With the ion pumps on, the noise was typically 500 c/s at 10^{-7} mbar and 50 c/s at 10^{-9} mbar. Therefore, during measurements the ion pumps were switched off and only the Ti sublimation pump was used. Occasional pumping with the ion pumps, with the measurement interrupted, was sufficient to keep the level of light residual inert gases that are not pumped by the sublimation pump low.

In order to measure the energy spectrum of internal conversion and Auger electrons emitted in the decay of the 14.4-keV state of ^{57}Fe, a 60-μCi source, prepared by electrodeposition of $^{57}CoCl_2$ on an aluminum plate, was placed at the sample position. The spectrum is shown in Fig. A.2. All expected conversion and Auger peaks are visible down to the smallest energies. The energy resolution of the 7.3-keV K-conversion peak is 3.5%, which is somewhat larger than the expected value. This could be related to the finite thickness of the source or, alternatively, to contamination of the source surface. The experimental analyzer constant is 0.51 and is close to the expected value of 0.527. Note the high inelastic background level just above the LXY Auger peak.

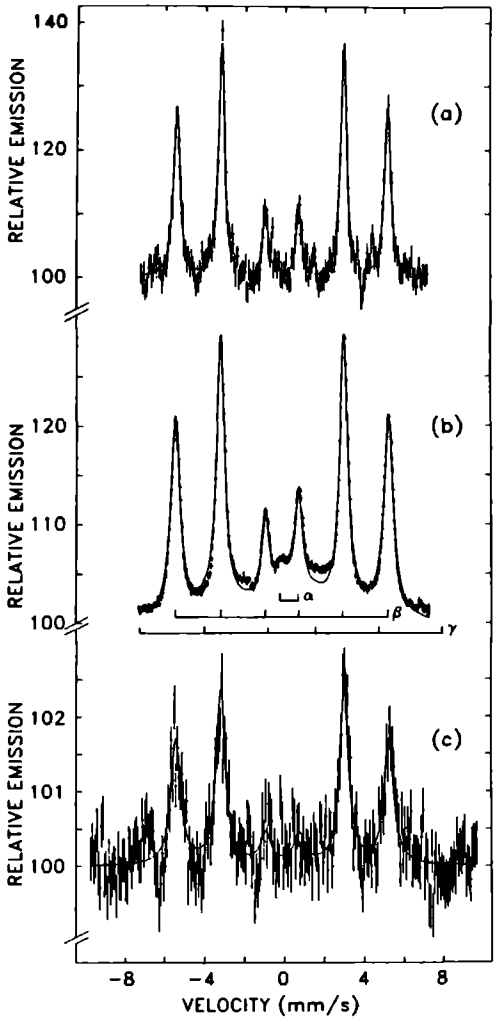

Figure A.3: ^{57}Fe Mössbauer spectra of a 100-nm Fe film enriched in ^{57}Fe to 95% on an Al substrate [(a)], and of a 12.7-μm Fe foil enriched in ^{57}Fe to 95% [(b) and (c)]. The spectra (a) and (b) were measured using Fe K-conversion electrons, and for spectrum (c) the LXY Auger electrons were used. The solid line is a least-squares computer fit, as described in the text. The vertical bars indicate statistical error. The pattern designated β is that of α-Fe. The α and γ patterns are due to α-Fe_2O_3 and Fe_3O_4, respectively.

To test the performance of the system, ^{57}Fe Mössbauer spectra of two samples were recorded at room temperature. The first was a 100-nm Fe film (enriched to 95% in ^{57}Fe) on an Al substrate prepared in ultra-high vacuum (during the evaporation the pressure rose to 10^{-8} mbar). This sample had been exposed to air for many weeks, so that one would expect it to be covered with an oxide layer. The Mössbauer spectrum of this sample [Fig. A.3(a)] measured with a 10-mCi ^{57}Co(Rh) source and with the spectrometer set at the K-conversion electron energy shows only the six-line Zeeman pattern due to α-iron, which is surprising in view of the sample history. The fitted parameters [isomer shift (relative to the source) $\delta = -0.104(2)$ mm/s and

hyperfine magnetic field $H = 329.5(0.9)$ kOe] correspond indeed to α-Fe.[29] It should be stressed that the baseline corresponds to only 3890 counts and the effect is high.

The second sample was in the form of a 12.7 μm Fe foil (enriched in ^{57}Fe to 95%). It was cleaned in UHV by Ar sputtering and then transferred, via air, to the Mössbauer spectrometer. Control x-ray photoelectron (XPS) measurements of this sample indicated that it was covered with about 10–15 Å of Fe oxides during the Mössbauer experiment. The foil Mössbauer spectrum measured with a 60-mCi ^{57}Co(Rh) source and with the spectrometer set at the K-conversion electron energy [Fig. A.3(b)] clearly shows the presence at the surface not only of Fe metal but also of Fe oxide contaminants. To determine these contaminants, the Mössbauer spectrum was fitted to three subspectra: two Zeeman patterns [patterns β and γ in Fig. A.3(b)] characterized by parameters δ_i and H_i ($i = 1, 2$) and one doublet [pattern α in Fig. A.3(b)] characterized by parameters δ_3 and quadrupole splitting Δ. Their values are: $\delta_1 = -0.106(3)$ mm/s, $H_1 = 330.4(0.8)$ kOe, $\delta_2 = 0.621(35)$ mm/s, $H_2 = 470.6(5.5)$ kOe, $\delta_3 = 0.265(33)$ mm/s, and $\Delta = 0.913(102)$ mm/s. The first set of parameters corresponds to α-Fe.[29] The second set of parameters is compatible with that of Fe_3O_4.[30] The parameters of the doublet correspond to ferric iron ions and are most probably due to the presence of small Fe_2O_3 particles at the surface.[31] We thus conclude that the surface of the second sample is covered with iron oxides, most probably Fe_3O_4 and Fe_2O_3. However, the signal due to oxides is only a few percent of the total.

The spectrum of the second sample measured with an electron energy set at 550 eV (LXY-Auger peak in Fig. A.2) is shown in Fig. A.3(c). In spite of its relatively low signal-to-noise ratio, there is clearly no contribution from the oxides, and the parameters of the observed Zeeman pattern [$\delta = -0.102(6)$ mm/s, $H = 331.0(1.3)$ kOe] are due to α-Fe. This is a very surprising result, since by using LXY-Auger electrons one would expect an enhancement of the oxide contribution to the spectrum (see also Sec. A.5).

A.5. Discussion

We have constructed and operated an instrument for Mössbauer spectroscopy based on the principle of energy selection of the conversion electrons in order to assess the potential of this technique. We find, as expected, that the low intensity of the spectrum is a severe problem. Count rates at the peak KLL-Auger or K-conversion energies were typically 0.08 counts per second with (a) 95% enriched ^{57}Fe samples, (b) a 50-mCi source, and (c) a 70-mm source-sample distance.

The count rates might realistically be improved by a factor of 3–4 by increasing the activity of the Mössbauer source and by a further factor of about 4 if the source-sample distance were reduced to 35 mm. The latter is, of course, at the cost of broadening of the Mössbauer spectrum due to the finite sample size and geometric

factors. Such increases would not be sufficient to compensate for the decrease by a factor of about 50 in the signal from natural Fe in, for instance, steels due to the low abundance of ^{57}Fe (2.14%). We thus conclude that the applications of a spectrometer such as ours to commercial steels or other real surfaces have limited potential, unless more effective detection methods can be conceived, e.g., use of position sensitive detectors.

A surprising feature of the spectra shown in Fig. A.3 is the low intensity of features due to oxides. The electrons analyzed have low take-off angles α with respect to the surface. At the K-conversion energy the electron inelastic mean free path is of the order of 50 Å and the mean escape depth of the electrons is $50 \sin \alpha$ Å. Even if we assume an unreastically high mean take-off angle of about 20°, the mean inelastic escape depth is less than 20 Å. The first sample [Fig. A.3(a)] had been exposed to air for a considerable time and should have been heavily oxidized (it would not fit into our XPS spectrometer for a definitive test). The second sample was shown by XPS to be covered by an oxide film of about 15 Å thick, so that nearly half of the signal was expected to arise from oxides, instead of only a few percent, as observed [Fig. A.3(b)]. We also observe no enhancement of the surface oxide contribution when the Mössbauer effect is monitored using the low energy LXY Auger electrons [Fig. A.3(c)].

Our failure to observe a Mössbauer signal commensurate with the amount of oxide layers on Fe samples is in agreement with the results of Belozerskii *et al.*[32] However, Staniek *et al.*[33] certainly did observe a spectral contribution from surface oxides, and variation of the surface oxide signal strength with chemical history of the sample clearly has to be further investigated. We see two possible explanations for the low intensity from the surface oxides. First, the top oxide layer may be non-resonant, i.e., the recoil-free fraction of this layer could be close to zero at room temperature for some oxides. This could be a result of, for instance, very small oxide crystallite size and weak coupling to the mass of the bulk material. Alternatively, the Mössbauer signal could be smeared out due to extreme chemical and morphological disorder in the surface layer. Whilst the second explanation may not be so attractive because Mössbauer spectra of disordered systems have been measured, little is known about the degree of disorder in ultra-thin surface oxide layers, and it may be extremely high.

It is clearly of fundamental interest that the Mössbauer signal from thin oxide layers and bulk Fe is variable and not directly related to the concentration of Fe atoms in the environments. However, this variability would be disastrous for any applications in surface analysis and non-destructive depth profiling.

Finally, we note that one of the potentially most appealing features of Mössbauer spectroscopy with conversion electrons was the possibility to use the different information depths for Fe KLL and LXY Auger electrons. However, we find that the LXY Auger peak excited by resonant absorption of γ rays has only approximately

15–20% of the intensity in the peaks due to the Fe KLL Auger, or the K-conversion electrons. Furthermore, this LXY peak sits on a background due to KLL and K electrons which were created deep in the solid and lost most of their energy during transport to the surface. This background, which will resonate with the signal due to the bulk, is more intense than the LXY signal itself. It reduces the surface contribution of the signal at the LXY energy by a factor of about 2.5. Clearly, exploitation of the LXY surface sensitivity requires a difference spectrum between the signal at the LXY energy and at slightly higher energies, which further exacerbates the problem of the low signal strength.

In view of the factors discussed above, we perceive the future of Mössbauer spectroscopy based on energy selection of the conversion electrons to lie in fundamental studies of surface magnetism and chemical bonding at well defined surfaces, of the sort attempted by Korecki and Gradmann.[20] For these studies it will be necessary to take all possible measures to maximize the signal. It will also be necessary to improvise good, *in situ* sample preparation facilities. Finally, great care will be necessary to ensure the best possible vacuum because of the very long counting times.

A.6. References

[1] R.L. Mössbauer, Z. Phys. **151**, 124 (1958).

[2] D.C. Kistner and A.W. Sunyar, Phys. Rev. Lett. **4**, 412 (1960).

[3] U. Gonser, *Mössbauer Spectroscopy*, vol. 5 of *Topics in Applied Physics*. (Springer Verlag, Berlin, 1975).

[4] P. Gütlich, R. Link and A. Trautwein, *Mössbauer Spectroscopy and Transition Metal Chemistry*, vol. 3 of *Inorganic Chemistry Concepts*. (Springer Verlag, Berlin, 1978).

[5] K.R. Swanson and J.J. Spijkerman, J. Appl. Phys. **41**, 3155 (1970).

[6] H. Bokemeyer, K. Wohlfahrt, E. Kankeleit and D Eckhardt, Z. Phys. A **274**, 305 (1975).

[7] J.P. Schunck, J.M. Friedt and Y. Llabador, Revue Phys. Appl. **10**, 121 (1975).

[8] M.P Seah and W.A. Dench, Surf. Interf. An. **1**, 2 (1979).

[9] E. Kankeleit, Z. Phys. **164**, 442 (1961).

[10] Z. Bonchev, A. Jordanov and A. Minkova, Nucl. Instrum. Methods **70**, 36 (1969).

[11] M. Bäverstam, T. Ekdahl, C. Bohm, B. Ringström, V. Stefansson and D. Liljequist, Nucl. Instrum. Methods **115**, 373 (1974).

[12] M. Bäverstam, T. Ekdahl, C. Bohm, D. Liljequist and B. Ringström, Nucl. Instrum. Methods **118**, 313 (1974).

[13] T. Shigematsu, H.-D. Pfannes and W. Keune, Phys. Rev. Lett. **45**, 1206 (1980).

[14] J. Itoh, T. Toriyama, K. Saneyoshi and K. Hisatake, Nucl. Instrum. Methods **205**, 279 (1983).

[15] D. Liljequist and M. Ismail, Phys. Rev. B **31**, 4131 (1985)

[16] D. Liljequist, M. Ismail, K Saneyoshi, K. Debusmann, W. Keune, R.A. Brand and W. Kiauka, Phys. Rev. B **31**, 4137 (1985).

[17] J.S. Zabinski and B.J. Tatarchuk, Nucl. Instrum. Methods **B31**, 576 (1988).

[18] W. Keune, Hyp. Inter. **27**, 111 (1986).

[19] T. Toriyama, K. Asano, K. Saneyoshi and K. Hisatake, Nucl. Instrum. Methods **B4**, 170 (1984).

[20] J. Korecki and U. Gradmann, Hyp. Inter. **28**, 931 (1986).

[21] T.-S. Yang, B. Kolk, T. Kachnowski, J. Trooster and N. Benczer-Koller, Nucl. Instrum. Methods **197**, 545 (1982).

[22] R.H. Ritchie, J.S. Cheka and R.D. Birkhoff, Nucl. Instrum. Methods **6**, 157 (1960).

[23] R.D. Birkhoff, J.M. Kohn, H.B. Eldridge and R.H. Ritchie, Nucl. Instrum. Methods **8**, 313 (1960).

[24] Technische Handelsonderneming "Muysert B.V.", Postbus 35, 2860 AA Berg Ambacht, The Netherlands.

[25] Model 4716, Galileo Electron Optics Corp.

[26] Electrofusion Corporation, 25 Constitution Drive, Menlo Park, CA 940425, USA.

[27] J.J. Bara and B.F. Bogacz, Mössb. Eff. Ref. Data J. **3**, 154 (1980).

[28] B.F. Otterloo, Z.M. Stadnik and A.E.M. Swolfs, Rev. Sci. Instrum. **54**, 1575 (1983).

[29] J.G. Stevens, in *Handbook of Spectroscopy*, edited by J.W. Robinson, vol. III, p. 403–528. (CRC, Boca Raton, FL, 1981).

[30] B.J. Evans and Lu-San Pan, J. Appl. Phys. **61**, 4352 (1987).

[31] W. Kündig, H. Bömmel, G. Constabaris and R.H. Lundquist, Phys. Rev. **142**, 327 (1966).

[32] G.N. Belozerskii, C. Bohm, T. Ekdahl and D. Liljequist, Nucl. Instrum. Methods **192**, 539 (1982).

[33] S. Staniek, T. Shigematsu, W. Keune and H.-D. Pfannes, J. Magn. Magn. Mat. **35**, 347 (1983).

SUMMARY

Magnetism is one of the every-day physical phenomena that, in spite of many years of research, is still not completely understood. Great progress in the understanding of magnetism, which has been known in literature for almost 3000 years, was made in the first quarter of the twentieth century with the development of quantum theory. A long standing argument since then among physicists has been the question to what extent the electrons responsible for the macroscopic magnetic phenomena can be regarded as either localized to the atoms in the solid, or delocalized and contributing to, e.g., electric conduction as well. This argument, between local moment magnetism and itinerant electron magnetism, is strongly related to the question from which starting point a theoretical description of magnetism on a microscopic scale can and should be made, i.e., starting from atomic or molecular states or starting from a band description. The advent of modern spectroscopic techniques, such as photoemission, that gave direct access to the electronic structure of these materials, has had a large influence in this argument and now it seems to be settled, classifying, e.g., transition metals as itinerant magnets and, e.g., rare earth metals and transition metal oxides as local moment magnets. Nevertheless, at the same time it has been realized that in many respects itinerant magnets fit a local moment description quite well. Also, new questions have emerged from the application of modern spectroscopies, such as which are the important many-body interactions, what is the microscopic origin of the magnetic-to-paramagnetic phase transition, and also, because of the surface sensitivity of these spectroscopies, how the surface influences the magnetic properties with respect to the bulk [Chapter 1].

In order to clarify these questions it is vital to get as much experimental data on a system as possible. For this purpose various modern techniques are at the experimentalists disposal. Especially the development of such a powerful technique as spin polarized photoemission as attracted much attention during the last decades, as it should have. Yet, one should keep in mind that, on one hand, not all problems can be solved with this technique and that, on the other hand, not all problems require such an advanced approach. This is illustrated in Ch. 4, where it is shown that it is very well possible to make a statement on the behaviour of, e.g., the exchange splitting in a magnetic material with ordinary, i.e., spin integrated photoemission.

One of the open questions is if and how, on an atomic scale, the magnetization vanishes in going to the paramagnetic state. The successful Stoner theory of itiner-

ant electron magnetism predicts that above the critical temperature the electronic structure no longer shows features from the magnetic state, i.e., even locally all spin directions are equivalent. Experimental data, however, has given some evidence that still some local magnetic order might exist and new theories have been developed in recent years to support this view. We present photoemission data of a specific class of magnetic materials, that show quite elegantly, and almost quantitatively, that in these systems indeed local magnetic moments persist in the paramagnetic state [Chapter 4].

It will be obvious that not all problems may be tackled in this way and therefore spin polarized photoemission will surely maintain its prominent position. It should, however, be realized that the occupied electronic states, which are probed by photoemission, are only part of the story. For many material properties, like conduction, the excitation spectrum, *and* magnetism, the unoccupied states are also of importance. Up to a few years ago these could, however, only be probed by spin integrated inverse photoemission. The most prominent result of this work, therefore, is that this situation now has been straightened out and that also the unoccupied states can be probed in a spin resolved fashion by the newly developed system for spin resolved inverse photoemission. The technical aspects of this BISCEPS apparatus are described in this thesis in some detail [Chapter 2].

We demonstrate this new technique by applying it to the "prototype" itinerant electron ferromagnet nickel. By comparison with very recent model calculations we also give an indication of how BISCEPS might be useful in solving some of the fundamental questions concerning electronic structure and magnetism, i.e., the influence of many-body intercations [Chapter 3, Sect. 1]. More closely related to the effects of surfaces and interfaces on magnetic properties is the study of thin layers of gadolinium, which is the prototype local-moment ferromagnet, on a nickel substrate. Only initial results are presented [Chapter 3, Sect. 2].

The conclusion of this work is that, even today, there are many unresolved questions concerning the phenomenon of magnetism. At the same time, however, there are also many unexplored and promising ways to a possible answer. The words of E.C. Stoner, quoted in the beginning of this thesis, are still very much true.

SAMENVATTING

Magnetisme is één van die alledaagse fysische verschijnselen, die nog steeds niet volledig begrepen zijn, ondanks het feit dat het fenomeen magnetisme al bijna 3000 jaar geleden voor het eerst beschreven werd. Pas in het begin van deze eeuw werd hierin vooruitgang geboekt door de ontwikkeling van de quantum theorie. Er ontwikkelde zich echter allengs een meningsverschil met betrekking tot de vraag tot op welke hoogte de electronen, die voor de magnetische verschijnselen verantwoordelijk zijn, beschouwd mogen worden als gelokaliseerd rond het atoom, of dat zij gedelokaliseerd zijn en, b.v., ook bijdragen aan de electrische geleiding. Dit dispuut, tussen de kampen van het zgn. lokaal moment magnetisme en het itinerant magnetisme, heeft ook te maken met de vraag waarmee een theoretische beschrijving van magnetisme moet en kan beginnen. Hetzij met atomaire of moleculaire toestanden hetzij met een bandbeschrijving. Voor de uitkomst van dit dispuut is de opkomst van moderne spectroscopische technieken, die direct toegang gaven tot de electronische structuur van deze materialen, van groot belang geweest. Het pleit lijkt nu te zijn beslecht en, b.v., overgangsmetalen worden beschouwd als itinerante magneten en zeldzame-aardmetalen en overgangsmetaaloxiden als lokaal-moment magneten. Tegelijkertijd is men zich echter gaan realiseren dat itinerante systemen in veel opzichten wel degelijk met lokale momenten beschreven kunnen worden. Er zijn echter ook nieuwe vragen gerezen, zoals: welke veel-deeltjes wisselwerkingen zijn belangrijk, wat is de oorzaak van de magnetische fase-overgang, en wat is de invloed van het oppervlak op de magnetische eigenschappen [Hfdst. 1].

Om op deze vragen een antwoord te kunnen geven is het belangrijk om een systeem experimenteel zo volledig mogelijk te karakteriseren. Hiertoe stonden en staan de experimentator verscheidene moderne technieken ter beschikking. Met name de ontwikkeling van een krachtige techniek als spin-opgeloste fotoëmissie heeft, terecht, de laatste decennia veel aandacht gekregen. Toch is het goed om niet uit het oog te verliezen dat, enerzijds, niet alle problemen met deze techniek opgelost kunnen worden, en dat, anderzijds, niet voor alle problemen een dergelijk geavanceerde methode gebruikt hoeft te worden. Ter illustratie van deze laatste bewering laat Hfdst. 4 zien dat men ook met gewone, d.w.z., spin-geïntegreerde fotoëmissie heel goed in staat kan zijn om, b.v., uitspraken te doen over het gedrag van de zgn. exchange opsplitsing in magnetische materialen.

Eén van de openstaande vragen is namelijk of, en zo ja, op welke manier de

magnetisatie op atomair niveau verdwijnt bij de overgang naar de paramagnetische toestand. De succesvolle Stoner theorie voor itinerant magnetisme voorspelt dat boven de kritische temperatuur niets meer herinnert aan de magnetische toestand, m.n., dat er zelfs lokaal geen onderscheid meer is tussen verschillende spinrichtingen. Uit experimentele gegevens is echter gebleken dat er wel degelijk enige lokale magnetische orde zou kunnen zijn. Gedurende de laatste jaren zijn er tevens nieuwe theorieën ontwikkeld die deze verschijnselen proberen te verklaren. Wij presenteren fotoëmissie metingen aan een bepaalde klasse van magnetische materialen die op elegante wijze, bijna kwantitatief, aantonen dat deze materialen inderdaad lokaal een magnetisch moment blijven houden in de paramagnetische toestand [Hfdst. 4].

Uiteraard kunnen niet alle vragen op een dergelijke wijze aangepakt worden en zal spin-opgeloste fotoëmissie zijn/haar prominente positie blijven behouden. Daarnaast moet men zich echter realiseren dat de bezette electronische toestanden, die met fotoëmissie afgetast worden, slechts een deel van het verhaal vormen. Voor vele materiaaleigenschappen, zoals geleiding, het excitatiespectrum *en* magnetisme is de structuur va de onbezette toestanden ook van belang. Tot voor enige jaren konden deze echter, m.b.v. inverse fotoëmissie, alleen spingeïntegreerd gemeten worden. Het voornaamste resultaat van het onderhavige werk is dan ook dat deze situatie nu is rechtgetrokken en ook de onbezette toestanden spin-opgelost kunnen worden afgetast met het nieuw ontwikkelde systeem voor spin-opgeloste inverse fotoëmissie. De technische aspecten van dit zgn. BISCEPS systeem worden in dit proefschrift uitgebreid besproken [Hfdst. 2].

De techniek wordt tevens gedemonstreerd aan de hand van metingen aan nikkel: het "prototype" van itinerante magnetische systemen. We vergelijken deze metingen met recente modelberekingen om te laten zien hoe BISCEPS van nut kan zijn bij het oplossen van fundamentele vragen met betrekking tot de electronische structuur en magnetisme, m.n. wat betreft de invloed hierop van veel-deeltjes wisselwerkingen [Hfdst. 3, Sectie 1]. Het onderzoek aan dunne lagen gadolinium, het prototype van een lokaal moment systeem, op een nikkel substraat gaat meer in op de effecten van oppervlakken en grensvlakken op magnetisme. Hiervan kunnen echter alleen voorlopige resultaten gepresenteerd worden [Hfdst. 3, Sectie 2].

De conclusie, die uit dit werk getrokken kan worden is dat er, ook vandaag nog, vele vragen zijn op te lossen rond het verschijnsel magnetisme, maar tevens dat er nog vele niet of nauwelijks beproefde veelbelovende wegen zijn naar een mogelijke oplossing. Het citaat van E.C. Stoner voorin dit proefschrift is nog onverkort geldig.

Curriculum Vitae

Harry R. Borsje

Geboren	:	8 juli 1962 te Rotterdam
Opleiding	:	ongedeeld VWO aan het Elzendaal College te Boxmeer, van 1974 tot 1980
		kandidaats en doctoraal Natuurkunde aan de Katholieke Universiteit Nijmegen, van september 1980 tot september 1985
Onderzoek	:	doctoraalonderzoek in de Vaste Stof Fysica aan de Katholieke Universiteit Nijmegen onder leiding van prof.dr. P. Wyder, van februari 1984 tot september 1985
		promotieonderzoek in de Fysische Chemie aan de Katholieke Universiteit Nijmegen, in dienst van de Stichting voor Fundamenteel Onderzoek der Materie (FOM), onder leiding van prof.dr. J.C. Fuggle, van september 1985 tot maart 1990
Huidige werkkring	:	post-doc in de Mesoscopische Fysica bij het Delfts Instituut voor Micro-Electronica en Submicrontechnologie (DIMES), in dienst van de Stichting voor Fundamenteel Onderzoek der Materie (FOM)

Experimental Investigations of Surface Magnetism

Harry R. Borsje